

Quantum Monte-Carlo Studies of Generalized Many-body Systems

by

Jørgen Høgberget

THESIS
for the degree of
MASTER OF SCIENCE

(Master in Computational Physics)



Faculty of Mathematics and Natural Sciences
Department of Physics
University of Oslo

June 2013

Preface

blah blah

Contents

| | | |
|----------|---|-----------|
| 1 | Introduction | 11 |
| I | Theory | 13 |
| 2 | Scientific Programming | 15 |
| 2.1 | Programming Languages | 15 |
| 2.1.1 | High-level Languages | 15 |
| 2.1.2 | Low-level Languages | 16 |
| 2.2 | Object Orientation | 17 |
| 2.2.1 | Inheritance | 18 |
| 2.2.2 | Pointers, Typecasting and Virtual Functions | 20 |
| 2.2.3 | Polymorphism | 21 |
| 2.2.4 | Const Correctness | 23 |
| 2.2.5 | Accessibility levels and Friend classes | 23 |
| 2.2.6 | Example: PotionGame | 24 |
| 2.3 | Structuring the code | 28 |
| 2.3.1 | File Structures | 28 |
| 2.3.2 | Class Structures | 29 |
| 3 | Quantum Monte-Carlo | 31 |
| 3.1 | Modeling Diffusion | 31 |

| | | |
|-------|--|----|
| 3.1.1 | Stating the Schrödinger Equation as a Diffusion Problem | 31 |
| 3.1.2 | Solving the Diffusion Problem | 34 |
| 3.1.3 | Isotropic Diffusion | 34 |
| 3.1.4 | Anisotropic Diffusion: Fokker-Planck | 35 |
| 3.1.5 | The connection between anisotropic- and isotropic diffusion models | 36 |
| 3.2 | Diffusive Equilibrium Constraints | 38 |
| 3.2.1 | Detailed Balance | 39 |
| 3.2.2 | Ergodicity | 39 |
| 3.3 | The Metropolis Algorithm | 39 |
| 3.4 | The Process of Branching | 42 |
| 3.5 | The Trial Wave Function | 44 |
| 3.5.1 | Many-body Wave Functions | 44 |
| 3.5.2 | Choice of Trial Wave function | 47 |
| 3.5.3 | Calculating Expectation Values | 49 |
| 3.5.4 | Normalization | 49 |
| 3.5.5 | Selecting Optimal Variational Parameters | 50 |
| 3.6 | Gradient Descent Methods | 51 |
| 3.6.1 | General Gradient Descent | 51 |
| 3.6.2 | Stochastic Gradient Descent | 52 |
| 3.6.3 | Adaptive Stochastic Gradient Descent | 53 |
| 3.7 | Variational Monte-Carlo | 57 |
| 3.7.1 | Motivating the use of Diffusion Theory | 57 |
| 3.7.2 | Implementation | 59 |
| 3.7.3 | Limitations | 59 |
| 3.8 | Diffusion Monte-Carlo | 60 |
| 3.8.1 | Implementation | 60 |
| 3.8.2 | Sampling the Energy | 60 |
| 3.8.3 | Limitations | 62 |
| 3.8.4 | Fixed node approximation | 62 |

| | | |
|----------|---|-----------|
| 3.9 | Estimating the One-body Density | 63 |
| 3.9.1 | Estimating the Exact Ground State Density | 64 |
| 3.9.2 | Radial Densities | 65 |
| 3.10 | Estimating the Statistical Error | 66 |
| 3.10.1 | The Variance and Standard Deviates | 66 |
| 3.10.2 | The Covariance and correlated samples | 67 |
| 3.10.3 | The Deviate from the Exact Mean | 67 |
| 3.10.4 | Blocking | 69 |
| 3.10.5 | Variance Estimators | 69 |
| 4 | Generalization and Optimization | 71 |
| 4.1 | Underlying Assumptions and Goals | 71 |
| 4.1.1 | Assumptions | 71 |
| 4.1.2 | Generalization Goals | 72 |
| 4.1.3 | Optimization Goals | 72 |
| 4.2 | Specifics Regarding Generalization | 73 |
| 4.2.1 | Generalization Goals (i)-(vii) | 73 |
| 4.2.2 | Generalization Goal (vi) and Expanded bases | 74 |
| 4.2.3 | Generalization Goal (viii) | 75 |
| 4.3 | Optimizations due to a Single two-level Determinant | 75 |
| 4.4 | Optimizations due to Single-particle Moves | 76 |
| 4.4.1 | Optimizing the Slater ratios | 76 |
| 4.4.2 | Optimizing the Inverse | 78 |
| 4.4.3 | Optimizing the Padé Jastrow factor Ratio | 78 |
| 4.5 | Optimizing the Padé Jastrow Derivative Ratios | 79 |
| 4.5.1 | The Gradient | 79 |
| 4.5.2 | The Laplacian | 80 |
| 4.6 | Tabulating Recalculated Data | 81 |
| 4.6.1 | The relative distance matrix | 81 |
| 4.6.2 | The Slater related matrices | 82 |

| | | |
|-----------|---|------------|
| 4.6.3 | Avoiding spin tests | 82 |
| 4.6.4 | The Padé Jastrow gradient | 83 |
| 4.6.5 | The single-particle Wave Functions | 84 |
| 4.7 | CPU Cache Optimization | 86 |
| 4.7.1 | Disadvantage of Generalizing the code | 87 |
| 4.7.2 | Consequences | 87 |
| II | Results | 89 |
| 5 | Results | 91 |
| 5.1 | Optimization Results | 91 |
| 5.2 | Validating the code | 93 |
| 5.2.1 | Calculation for non-interacting particles | 93 |
| 5.3 | Results for Quantum Dots | 97 |
| 5.3.1 | FIXED NODE TESTS | 97 |
| 5.3.2 | One-body Densities | 100 |
| 5.3.3 | Lowering the frequency | 100 |
| 5.4 | Results for Atoms | 107 |
| 5.4.1 | Ground State Energies | 107 |
| 5.4.2 | The Noble-Gases | 107 |
| 5.4.3 | Alkaline Earth Metals | 109 |
| A | Dirac Notation | 113 |
| B | DCViz: Visualization of Data | 115 |
| B.1 | Basic Usage | 115 |
| C | Auto-generation with SymPy | 121 |
| C.1 | Usage | 121 |
| C.1.1 | Doing Symbolic Algebra | 121 |
| C.1.2 | Exporting C++ and Latex Code | 122 |
| C.1.3 | Calculating Derivatives | 122 |

| | |
|--|------------|
| C.2 Using the auto-generation Script | 124 |
| D Harmonic Oscillator Orbitals | 125 |
| E Hydrogen Orbitals | 133 |
| Bibliography | 139 |

1

Introduction

blah blah

Part I

Theory

2

Scientific Programming

The introduction of the computer around World War II had a major impact on the mathematical fields of science. Previously unsolvable problems were now solvable. The question was no longer whether or not it was possible, but rather to what precision and with which method. The computer spawned a new branch of physics, *computational physics*, redefining the limits of our understanding of nature. The first major result of this synergy between science and computers came with the infamous atomic bombs *Little Boy* and *Fat Man*, a product of *The Manhattan Project* leaded by *J. Robert Oppenheimer* [1].

2.1 Programming Languages

Programming is the art of writing computer programs. A program is a list of instructions for the computer often referred to as *code*. It is in many ways similar to human-to-human instructions; for instance, different programming languages may be used to write instructions, such as *C++*, *Python* or *Java*, as long as the recipient is able to translate it. The instructions may be translated *a priori* of execution, i.e the code is *compiled*, or it may be translated *run-time* by an *interpreter*.

The native language of the computer is *binary*: Ones and zeros, i.e. high - or low voltage. Every character, number, color, etc. is on the lowest level represented as a sequence of binary numbers referred to as *bits*. Programming languages, in other words, serve as a bridge between the binary language of computers and a more manageable language for everyday programmers.

The closer the programming language at hand is to pure processor (CPU) instructions¹, the lower the *level* of the language is. This section will introduce high- and low level languages, focusing on *C++* and *Python*, as these were the most used languages throughout this thesis.

2.1.1 High-level Languages

Scientific programming involves an array of different tasks, all from pure visualization and organization of data to efficient memory allocation and processing. For less CPU-intensive tasks, the runtime of the program is so small that efficiency becomes irrelevant, leaving languages which prefer simplicity and structure over efficiency the optimal tool for the job. These languages are referred to as *high-level*

¹The CPU is the part of the computer responsible for flipping bits.

*languages*².

High-level codes are often short and structured designed with a specific aim such as analyzing raw data, administrating input and output from different tools, creating a *Graphical User Interface* (GUI), or gluing together different programs which are meant to be run sequentially or in parallel. These short specific codes are referred to as *scripts*, and hence high-level languages designed for these tasks often are referred to as *scripting languages*[2, 3].

Examples of high-level languages are Python, Ruby, Perl, Visual Basic and UNIX shells. Excellent introductions to these languages are found throughout the World Wide Web.

Python

Named after the infamous *Monty Python's flying circus*, Python is an easy to learn open source interpreted programming language invented by Guido van Rossum around 1990 designed for optimized development time through very clean and rigorous coding syntax [4, 3].

To demonstrate the simplicity of Python, let us have a look at a simple implementation and execution of the following expression

$$S = \sum_{i=1}^{100} i = 5050.$$

```
1 print sum(range(101))
```

```
~$ python Sum100Python.py
5050
```

For details regarding the basics of Python, I suggest reading Ref. [4], or more advanced topics in Ref. [2].

2.1.2 Low-level Languages

Scientific programming involves solving complex equations. Complexity does not necessarily imply that the equations themselves are hard to understand; frankly, this is often not the case. In most cases of e.g. linear algebra, the problem can be boiled down to solving $\mathbf{Ax} = \mathbf{b}$, however, the complexity lies in the dimensionality of the problem at hand. Matrix dimensions range as high as millions. With each element being a double precision number (8 bytes or 64 bits), it is crucial that we have full control of the memory, and execute operations as efficiently as possible.

This is where lower level languages excel. Hiding few to none of the details, the power is in the hand of the programmer. This, however, comes at a price: More technical concepts such as memory pointers, declarations, compiling, linking, etc. makes the development process slower than that of a higher-level language.

Requesting access to an uninitialized element outside the bounds of an allocated array, Python will provide a detailed error message with proper traceback, whereas the compiled C++ code would crash

²There are different definitions of the distinction between high- and low-level languages. Languages such as *assembly* is extremely complex and close to machine code, leaving all machine-independent languages as high-level ones. However, for the purpose of this thesis I will not go into assembly languages, and keep the distinction at a higher level.

runtime leaving nothing but a “segmentation fault” for the user. However, when the optimized program ends up running for days, the extra time spent in development pays off.

In addition, several options to optimize compiled machine code are available by having the compiler rearrange the way instructions are sent to the processor. Details regarding memory latency optimization will be discussed in section 4.7.

C++

C++ is a programming language developed by Bjarne Stroustrup in 1983. It serves as an extension to the original *C* language, adding *object oriented* features, that is, classes etc. [5]. The following code is a C++ implementation of the sum in Eq. 2.1.1:

```

1 //Sum100C++.cpp
2 #include <iostream>
3
4 int main(){
5
6     int S = 0;
7     for (int i = 1; i <= 100; i++){
8         S += i;
9     }
10
11    std::cout << S << std::endl;
12
13    return 0;
14 }
```

```

~$ g++ Sum100C++.cpp -o sum100C++.x
~$ ./sum100C++.x
5050
```

Notice that, unlike Python, C++ requests an explicit declaration of *S* as an integer variable. This in turn tells the compiler the exact amount of memory needed to store the variable, opening up the possibility of efficient memory optimization.

Even though this is an extremely simply example, it illustrates the difference in coding styles between high- and low-level languages. The next section will cover the basics needed to understand object orientation in C++, and how it can be used to develop larger generalized coding frameworks.

2.2 Object Orientation

The concept of classes and objects were introduced for the first time in the language *Simula 67*, developed by the Norwegian scientists Ole-Johan Dahl and Kristen Nygaard at the Norwegian Computing Research Center [5]. Object orientation quickly became the state-of-the-art in programming, and has since enjoyed great success in numerous computational fields.

Object orientation ties our everyday intuition into the programming language: Our brains are object oriented in the sense that we tend to focus around *objects* of *classes*, e.g. an animal of a certain species. This fact renders object oriented codes extremely readable compared to what is possible with standard functions and variables. In addition to simple object structures, which in some sense can be achieved with standard C *structs*, classes provide functionality such as *inheritance* and accessibility control. These concepts will be the focus for the rest of the chapter.

2.2.1 Inheritance

Consider the abstract idea of a keyboard: A board and keys (obviously). In object orientation terms, the *superclass* of keyboards describe a board with keys. It is *abstract* in the sense that no specific information regarding the formation or functionality of the keys is needed in order to define the concept of a keyboard.

On the other hand, there exist different specific kinds of keyboards, e.g. computer keyboards or musical keyboards. Although quite different in design and function, they both relate to the same concept of a keyboard described previously: They are both *subclasses* of the same superclass, inheriting the basic concepts, but overloading the abstract parts with specific implementations.

The following examples will assume a basic knowledge of programming concepts such as constructors and functions. Consider the following Python implementation of a keyboard superclass

```

1 class Keyboard():
2
3     #Set member variables keys and the number of keys
4     #A subclass will override these with their own representation
5     keys = None
6     nKeys = 0
7
8     #Constructor (function called when creating an object of this class)
9     #Sets the number of keys and calls the setup function,
10    #ensuring that no object of this abstract class can be created.
11    def __init__(self, nKeys):
12        self.nKeys = nKeys
13        self.setupKeys()
14
15    def setupKeys(self):
16        raise NotImplementedError("Override me!")
17
18    def pressKey(self, key):
19        raise NotImplementedError("Override me!")
20
21    def releaseKey(self, key):
22        raise NotImplementedError("Override me!")

```

This class does not function on its own, and is clearly an abstract class meant for sub-classing. Potential subclasses are e.g. computer - and musical keyboards. An easy way to visualize this inheritance relation is by drawing an *inheritance diagram* as in figure 2.1. A python implementation of these subclasses are given on the next page.

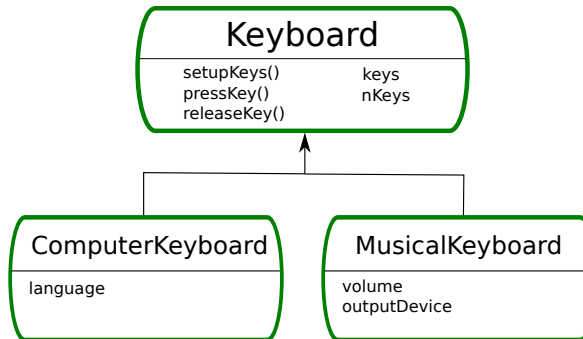


Figure 2.1: Inheritance diagram for a Keyboard superclass. Class members are listed below the class name.

```

1 #The (keyboard) specifies inheritance from Keyboard
2 class ComputerKeyboard(Keyboard):
3
4     def __init__(self, language, nKeys):
5
6         self.language = language
7
8         #Use the superclass contructor to set the number of keys
9         super(ComputerKeyboard, self).__init__(nKeys)
10
11
12     def setupKeys(self):
13
14         if self.language == "Norwegian":
15             "Set up norwegian keyboard style"
16             elif ...
17
18
19     def pressKey(self, key):
20         return self.keys[key]
21
22
23
24 #Dummy import for illustration purposes
25 from myDevices import Speakers
26
27 class MusicalKeyboard(Keyboard):
28
29     def __init__(self, nKeys, volume):
30
31         #Set the ouput device to speakers implemented elsewhere
32         self.outputDevice = Speakers()
33         self.volume = volume
34
35         super(ComputerKeyboard, self).__init__(nKeys)
36
37
38     def setupKeys(self):
39         lowest = 27.5 #Hz
40         step = 1.06 #Relative increase in Hz (neighbouring keys)
41
42         self.keys = [lowest + i*step for i in range(self.nKeys)]
43
44
45     def pressKey(self, key):
46
47         #returns harmonic wave with frequency and amplitude
48         #representing key pressed and volume level.
49         output = ...
50         self.outputDevice.play(key, output)
51
52
53     #Fades out the playing tune
54     def releaseKey(self, key):
55         self.outputDevice.fade(key)

```

It is clear from looking at the superclass that two keyboard are at least different in the way their keys are set up. Not overriding the `setupKeys()` function would cause the generic superclass constructor to call the function which would raise an exception and close the program. These kinds of superclass member functions which requires an implementation in order for the object to be constructed are referred to as *pure virtual functions*³. The other two functions does not necessarily have to be implemented, and are thus referred to as *virtual* functions. These topics will be discussed in more detail in the next section.

³We could simply choose not to call the superclass constructor in the given example, however, let's assume for the sake of proving a point that we can't.

2.2.2 Pointers, Typecasting and Virtual Functions

A pointer is a hexadecimal number representing a memory address where some *type* of object is stored, e.g. a `int` at `0x7fff0882306c` (`0x` simply implies hexadecimal). Higher level languages like Python handles all the pointers and typesetting automatically. In low-level languages like C++, however, you need to control everything. This is commonly referred to as *type safety*.

Memory addresses are *global*, that is, they are shared throughout the program. This implies that changes done to a pointer to an object, e.g. `Keyboard* myKeyboard`, are applied everywhere the object is in use. This is particularly handy (or dangerous) when passing a pointer as an argument to a function, as changes applied to the given object will cause the object to remain changed after exiting the function. Passing non-pointer arguments would only change a local copy of the object which is destroyed upon exiting the function. The alternative would be to pass the reference to the object, e.g. `&myObject`, which passes the address just as in the case of pointers.

Creating a pointer to a keyboard object in C++ can be done in several ways, e.g.

```
1 MusicalKeyboard* myKeyboard1 = new MusicalKeyboard(...);
2 Keyboard* myKeyboard2 = new Keyboard(...);
```

the second which is identical to

```
1 Keyboard* myKeyboard2 = (Keyboard*) myKeyboard1;
```

For reasons which will be explained in Section 2.2.3, the second expression is extremely handy. Technically, the subclass object is *type cast* to the superclass type. This is allowed since *any subclass is type-compatible with a pointer to its superclass*. Any standard functions implemented in the subclass will not be directly callable from outside the object itself, and identical functions will be overwritten by the corresponding superclass functions, unless the functions are *virtual*. Flagging a function as virtual in the superclass will then tell the compiler not to overwrite this particular function when a subclass object is typecast to the superclass type.

Python does not support virtual functions in the same strict sense as C++, since typecasting does not make sense in a dynamically (automatically) typed language. The following example should bring some clarity to the current topic.

```
1 #include <iostream>
2 using namespace std;
3
4 class superClass{
5 public:
6     // virtual = 0 implies pure virtual
7     virtual void pureVirtual() = 0;
8     virtual void justVirtual() {cout << "superClass virtual" << endl;}
9     void notVirtual()           {cout << "superClass notVirtual" << endl;}
10 };
11
12 class subClass : public superClass{
13 public:
14     void pureVirtual() {cout << "subClass pure virtual override" << endl;}
15     void justVirtual() {cout << "subClass standard virtual override" << endl;}
16     void notVirtual() {cout << "subClass non virtual" << endl;}
17 };
18
19 //Testfunc is set to retrieve a superClass pointer, then calls all the functions.
20 void testFunc(superClass* someObject){
21     someObject->pureVirtual(); someObject->justVirtual(); someObject->notVirtual();
22 }
```

```

1 int main(){
2
3     cout << "-Calling subClass object of type superClass*" << endl;
4     superClass* object = new subClass(); testFunc(object);
5
6     cout << endl << "-Calling subClass object of type subClass*" << endl;
7     subClass* object2 = new subClass(); testFunc(object);
8
9     cout << endl << "-Directly calling object of type subclass*" << endl;
10    object2->pureVirtual(); object2->justVirtual(); object2->notVirtual();
11
12    return 0;
13 }
```

```

~$ ./virtualFunctionsC++.x
-Calling subClass object of type superClass*
subclass pure virtual override
subclass standard virtual override
superclass notVirtual

-Calling subClass object of type subClass*
subclass pure virtual override
subclass standard virtual override
superclass notVirtual

-Directly calling object of type subclass*
subclass pure virtual override
subclass standard virtual override
subclass non virtual
```

As introduced in the keyboard example, the superclass in this case has a pure virtual function. Creating an object of the superclass would raise an error in the compilation, claiming that the superclass is abstract. Implemented subclasses must overload pure virtual functions in order to compile.

From the first standard output block it is clear that creating subclass objects of superclass type will indeed overload non-virtual functions, and keep the virtual ones. The second block is as expected identical to the first block, since the function on input typecasts the subclass type into a superclass type, rendering the two examples identical. The third block does not involve typecasting; the subclass functions are called whether they are virtual in the superclass or not.

2.2.3 Polymorphism

The previous example involved a concept referred to as *polymorphism*, a concept tightly connected to virtual functions and type casting. Because of the virtual nature of the superclass' functions, the function `testFunc()` does not a priori know its exact task. All it knows is that the received object has three functions (see the previous example). Exploiting this property is referred to as polymorphism.

Using polymorphism, codes can be written in an organized and versatile fashion. To further illustrate this, consider the following example from the Quantum Monte Carlo code developed in this thesis:

```

1 class Potential {
2 protected:
3     int n_p;
4     int dim;
5
6 public:
7     Potential(int n_p, int dim);
8
9     //Pure virtual function
10    virtual double get_pot_E(const Walker* walker) const = 0;
11
12 };
13
14 class Coulomb : public Potential {
15 public:
16     Coulomb(GeneralParams &);

17     //Returns the sum 1/r_i
18     double get_pot_E(const Walker* walker) const;

19 };
20
21
22 class Harmonic_osc : public Potential {
23 protected:
24     double w;
25
26 public:
27     Harmonic_osc(GeneralParams &);

28     //return the sum 0.5*w*r_i^2
29     double get_pot_E(const Walker* walker) const;

30 };
31
32 ...
33
34
35 ...
36
37 ...

```

Assume an object `Potential*` `potential` is sent to an energy function. Since `get_pot_E()` is virtual, the potential can take any form. Is it therefore possible to write a code for a general potential while maintaining excellent readability. Moreover, the code can quite easily be adapted to handle any combination of any potential by storing the potential objects in a vector and simply accumulate the contributions:

```

1 //Simple compiler definition to clean up the code
2 #define potvec std::vector<Potential*>
3
4 class System {
5 protected:
6
7     double get_potential_energy(const Walker* walker) const;
8     potvec potentials;
9
10 ...
11 };
12
13 double System::get_potential_energy(const Walker* walker) const {
14     double potE = 0;
15
16     //Iterates through all loaded potentials and accumulate energies.
17     for (potvec::iterator pot = potentials.begin(); pot != potentials.end(); ++pot) {
18         potE += (*pot)->get_pot_E(walker);
19     }
20
21     return potE;
22 }

```

2.2.4 Const Correctness

In the previous Potential code example, function declarations with the `const` flag were used. As mentioned in the section on pointers, passing pointers to functions are dangerous business. If an object is flagged with `const` on input, e.g. `void f(const x)`, the function itself cannot alter the value of `x`. If it does, the compiler will abort. This property is referred to as *const correctness*, and serve as a safeguard guaranteeing that nothing will happen to `x` as it passes through `f`. This is practical in situations where major bugs will arise if changes are made to the object.

If you declare a member function itself with `const` on the right hand side, e.g. `void class::f(x) const`, no changes may be applied to class members inside this specific function. For instance, in the potential energy functions, all that is requested is to evaluate a function at a given set of coordinates; there is no need to change anything, hence the `const` correctness in the previous example.

In other words: `const` correctness works as a safeguard preventing changes to values which should remain unchanged. A change in such a variable is then followed by a compiler error instead of unforeseen consequences.

2.2.5 Accessibility levels and Friend classes

Upon declaration of a C++ class, each member needs to be related to an *accessibility level*. The three accessibility levels in C++ are

- (i) **Public:** The variable or function may be accessed from anywhere the object is available.
- (ii) **Private:** The variable or function may be accessed only from within the class itself.
- (iii) **Protected:** As for private, but also accessible from subclasses of the class.

As an example, for any standardized application (`app`), the `app::execute_app()` function needs to be public, i.e. accessible from the main file (executing applications from the constructor directly is generally considered bad coding). On the other hand, `app::dump_progress()` should be controlled by the application itself, and should be private or protected in case the application has subclasses.

There is one exception to the rule of protected and private variables. In certain situations where a class needs to access private variables from another class, but going full public would lead to undesired situations, the latter class can *friend* the first class. This implies that the first class has access to the second class' private members.

In the QMC code developed in this thesis, the distribution is calculated by a class `Distrubution`. In order to achieve this, the protected members of `QMC` needs to be made available to the `Distrubution` class. This is implemented in the following fashion:

```

1 class QMC {
2     protected:
3
4         arma::mat dist; //!< Matrix holding positional data for the distribution.
5         int last_inserted; //!< Index of last inserted positional data.
6
7         ...
8
9     public:
10    ...
11
12     //Gives Distribution access to protected members of QMC.
13     friend class Distribution;
14
15 };
16
17 void Distribution::finalize() {
18
19     //scrap out all the over-allocated space (DMC)
20     qmc->dist.resize(qmc->last_inserted, dim);
21
22     if (dim == 3) {
23         generate_distribution3D(qmc->dist, qmc->n_p);
24     } else {
25         generate_distribution2D(qmc->dist, qmc->n_p);
26     }
27
28     qmc->dist.reset();
29
30 }
31
32 }
```

Codes could be developed without using `const` flags and with solely public members, however, in that case it is very easy to put together a very disorganized code, with pointers going everywhere and functions being called in all sorts of contexts. This is especially true if there are several developers on the same project.

Clever use of accessibility levels will make codes easier to develop in an organized intuitive way, forcing an organized implementation of a framework involving several classes. Put in other words: If you have to break an accessibility level to implement a desired functionality, there probably exists a better way to implement it.

2.2.6 Example: PotionGame

To conclude this section on object orientation, consider the following code for a player vs. player game:


```

1 #potionClass.py
2
3 class Potion:
4
5     def __init__(self, amount):
6         self.amount = amount
7         self.setName()
8
9     def applyPotionTo(self, player):
10        raise NotImplementedError("Member function applyPotion not implemented.")
11
12     #This function should be overwritten
13     def setName(self):
14         self.name = "Undefined"
15
16
17 class HealthPotion(Potion):
18
19     #Constructor is inherited
20
21     #Calls back to the player object's functions to change the health
22     def applyPotionTo(self, player):
23         player.changeHealth(self.amount)
24
25     def setName(self):
26         self.name = "Health Potion (%d)" % self.amount
27
28
29 class EnergyPotion(Potion):
30
31     def applyPotionTo(self, player):
32         player.changeEnergy(self.amount)
33
34     def setName(self):
35         self.name = "Energy Potion (%d)" % self.amount

```

The `Player` class keeps track of everything a player needs of personal data, such as the name, health- and energy levels, potions etc. Bringing another player into the game is now simply done by creating another `Player` object. A player holds a number of `Potion` objects in a list. These objects are subclass implementations which overwrites the virtual function which described the potion's effect on a given player object. This subclass hierarchy of potions makes it incredibly easy to implement new ones.

The power of object orientation shines through in this simple example. The readability is very good, and does not falter if numerous potions or players are brought to the table.

In this section the focus has not been solely on scientific computing, but rather on the use of object orientation in general. The interplay between e.g. potions and players in the current example resembles the interplay between the QMC solver and the potentials introduced previously. Whether games or scientific programs are at hand, the methods used in the programming remain the same.

On the following page, a game is constructed using the `Player` and `Potion` classes.

```

1 #potionGameMain.py
2
3 from potionClass import *
4 from playerClass import *
5
6 def roundOutput(n, *players):
7     header= "Round %d: " % n
8     print header.replace('0', 'start')
9     for player in players:
10         print " %s (hp/e=%d/%d):" % (player.name, player.health, player.energy)
11         player.displayPotions()
12         print
13
14
15 Sigve = Player('Sigve');
16 Sigve.addPotion(EnergyPotion(10));
17
18 Jorgen = Player('Jorgen')
19 Jorgen.addPotion(HealthPotion(20)); Jorgen.addPotion(EnergyPotion(20))
20
21 Karl = Player('Karl')
22 Karl.addPotion(HealthPotion(20))
23
24 #Initial output
25 roundOutput(0, Sigve, Jorgen, Karl)
26
27 #Round one: Each player empties their arsenal
28 Sigve.attack(Jorgen); Sigve.attack(Karl); Sigve.usePotion(0); Sigve.attack(Karl)
29 print
30
31 Karl.usePotion(0); Karl.attack(Sigve)
32 print
33
34 Jorgen.attack(Karl); Jorgen.usePotion(1); Jorgen.attack(Sigve)
35 print
36
37 roundOutput(1, Sigve, Jorgen, Karl)
38 #Round one end.
39 ...

```

```

Round start:
Sigve (hp/e=100/100):
Energy Potion (10)

Jorgen (hp/e=100/100):
Health Potion (20)
Energy Potion (20)

Karl (hp/e=100/100):
Health Potion (20)

Sigve hit Jorgen for 36 using 55 energy
Sigve: Insufficient energy to attack.
Sigve consumes Energy Potion (10).
Sigve hit Karl for 39 using 55 energy

Karl consumes Health Potion (20).
Karl hit Sigve for 42 using 55 energy

Jorgen hit Karl for 30 using 55 energy
Jorgen consumes Energy Potion (20).
Jorgen hit Sigve for 35 using 55 energy

Round 1:
Sigve (hp/e=23/0):
No potions aviable

Jorgen (hp/e=64/10):
Health Potion (20)

Karl (hp/e=51/45):
No potions aviable

```

2.3 Structuring the code

Structuring a code is another source of compromises. If the code is short and has a direct purpose, e.g. to calculate the sum from Eq. (2.1.1), structure is not an issue at all (given that reasonable variable names are provided). However, if the code is more complex and the methods used are specific implementations of a more general case, e.g. potentials, code structuring becomes very important. For details about the structuring of the code used in this thesis, see the Doxygen documentation provided in Ref. [6].

2.3.1 File Structures

Not only does the potion game example demonstrate clean object orientation, but also standard file structuring by splitting the different classes and the main application into separate files. In a small code like the potion game, the gain of transparency is not immense, however, when the class structures span thousands of lines (20000 lines in the case of the QMC library), having a good structure is crucial to the development process, the code's readability and the management in general.

Developing codes in scientific scenarios often involves large frameworks. For example, when coding molecular dynamics, several collision models, force models etc. are implemented alongside the main solver. In the case of Markow Chain Monte Carlo methods, different diffusion models (sampling rules) may be selectable. Even though these models are implemented object oriented using polymorphism, the code still gets messy when the amount of classes gets large.

In these scenarios, it is common to gather the implementations of the different classes in separate files (as for the potion game). This would be for purely cosmetic reasons if the process of writing the code was linear, however, empirical evidence suggests otherwise: At least half the time is spent debugging, going back and forth between files.

A standard way to organize code is to have all the source code gathered in a *src* folder, with one folder per distinct class. Subclasses should appear as folders inside the superclass folder. Figure 2.2 shows an example setup for the framework of an object oriented code.

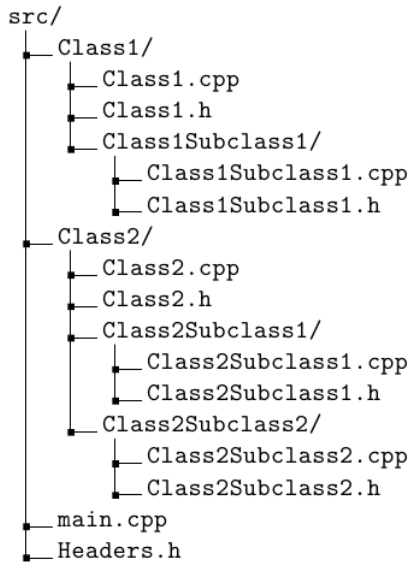


Figure 2.2: An illustration of a standard way to organize source code. The file endings represent C++ code.

Another gain by this type of structuring is that through tools such as Make, QMake, etc., only the actually changed files will be recompiled once changes are made to the code. This will save a lot of time in the development process once the total compilation time starts to span several minutes.

2.3.2 Class Structures

In scientific programming, the simulated process often has a physical or mathematical interpretation. Examples are e.g. atoms in molecular dynamics and bose-einstein condensates, random walkers in diffusion processes, etc. Implementing classes representing these quantities will shorten the gap between the mathematical formulation of the problem and the implementation.

In addition we have estimates such as energy, entropy and temperature, all of which are calculated based on equations from statistical mechanics, quantum mechanics, or similar. Having class methods representing these calculations will again shorten the gap. There is no question what is done when the `system.get_potential_energy` method is called, however, if some random loop appears in the main solver, an initial investigation is required in order to understand the flow of the code.

As described in Section 2.2.3, abstracting e.g. the potential energy function into a system object opens up the possibility of generalizing the code to any potential without altering the main solver. Structure is in other words vital if readability and versatility is desired.

Planning the code structure comes in as a key part of any large coding project. For details regarding the planning of the code used in this thesis, see Section 4.1.

3

Quantum Monte-Carlo

Quantum Monte-Carlo is the method of solving Schrödinger's equation using statistical simulations, i.e. Monte-Carlo simulations. The statistical nature of Quantum Mechanics makes Monte-Carlo methods the perfect tool for accurate simulations. As we will see, the Schrödinger equation resembles a *diffusion equation* in complex time. It is therefore from a mix of diffusion theory and Quantum Mechanics that the Quantum Monte-Carlo methods originate.

In this chapter *Dirac Notation* will be used. See Appendix A for an introduction.

3.1 Modeling Diffusion

Like any phenomena involving a density function, or distribution, Quantum Mechanics can be modeled by diffusion. In Quantum Mechanics, the distribution is given by $|\psi(\vec{r}, t)|^2$, the Wave function squared. The diffusing elements of interest are the particles making up our system. The idea is to have an ensemble of *Random Walkers* in which each walker represents a position in space (and time for time-dependent studies). Averaging values over the paths of the ensemble will yield average values corresponding to the probability distribution governing the movement of individual walkers.

Such random movement is referred to as a *Brownian motion*, named after the British Botanist R. Brown, originating from his experiments on plant pollen dispersed in water. *Markov chains* are a subtype of Brownian motion, where a walker's next move is independent of previous moves. This is the stochastic process in which Quantum Monte Carlo is described.

The purpose of this section is to motivate the use of diffusion theory in Quantum Mechanics, and to derive the sampling rules needed in order to model Quantum Mechanical distributions by diffusion of random walkers correctly. I will be using natural units, that is \hbar , m_e , etc. are all set to unity, in order to simplify the expressions.

3.1.1 Stating the Schrödinger Equation as a Diffusion Problem

Consider the time-dependent Schrödinger Equation for an abstract many-body wave function¹ $\Phi(x, t)$ with an arbitrary energy shift E'

¹See Section 3.5.1 for details about many-body wave functions.

$$-\frac{\partial \Phi(x, t)}{i\partial t} = (\widehat{\mathbf{H}} - E')\Phi(x, t). \quad (3.1)$$

The formal solution given a time-independent Hamiltonian is given by separation of variables in $\Phi(x, t)$ (see ref. [7] for more details regarding assumptions etc.). This corresponds to using the standard time-evolution operator. Further expanding $\Phi(x, t = t_0)$ in the eigenstates of $\widehat{\mathbf{H}}$, $\Psi_k(x)$, yields the following solution

$$\Phi(x, t) = e^{-i(\widehat{\mathbf{H}} - E')(t - t_0)}\Phi(x, t = t_0) \quad (3.2)$$

$$= \sum_{k=0}^{\infty} C_k \Psi_k(x) e^{-i(E_k - E')(t - t_0)} \quad (3.3)$$

$$C_k = \langle \Psi_k(x) | \Phi(x, t = 0) \rangle$$

The real form of this equation is obtained through a Wick rotation in time ($it \rightarrow \tau$), which basically means that the time-evolution operation is substituted by a *projection operation*. To illustrate this, look at the solution of the real equation with E' chosen to be the ground state energy of $\widehat{\mathbf{H}}$, and t_0 chosen to be zero

$$\Phi(x, \tau) = \sum_{k=0}^{\infty} C_k \Psi_k(x) e^{-(E_k - E_0)\tau} \quad (3.4)$$

$$= C_0 \Psi_0(x) + \sum_{k=1}^{\infty} C_k \Psi_k(x) e^{-\delta E_k \tau}, \quad (3.5)$$

where $\delta E_k = E_k - E_0 > 0$ for $k \geq 1$. Observe that as τ increase, the excited states of $\widehat{\mathbf{H}}$ will be exponentially damped, hence the name projection operation. Note however, that no real-time solutions can be achieved by solving this equation; only in the limit $\tau \rightarrow \infty$ will the solution match that of the Schrödinger Equation.

The approach of Quantum Monte Carlo is to split the evolution of τ into small sequential steps $\delta\tau$, and use the latest calculated energy, the *trial energy*, E_T , as an approximation to the ground state energy. The error introduced by this approximation will be discussed in Section 3.8. Either way, restating Eq. (3.4) in terms of sequential steps yields

$$\Phi(x, n\delta\tau) = \left[\prod_{i=1}^n e^{-(\widehat{\mathbf{H}} - E_T)\delta\tau} \right] \Phi(x, t = 0) \quad (3.6)$$

$$= \sum_{k=0}^{\infty} C_k \Psi_k(x) e^{-(E_k - E_T)n\delta\tau} \quad (3.7)$$

which remains exact for an infinite amount of infinitely small time steps. In practice, a balance is sought between the *number of cycles*, n , and the time step. This restatement might seem redundant, however, it is the key which opens up the possibility to model the solution by discretized diffusion of particles in Quantum Mechanical potentials.

In order to simulate the effect of the exponential operator in Eq. (3.6) on our initial state, consider the following rewriting

$$\hat{\mathbf{P}}(n, \delta\tau) \equiv \left[\prod_{i=1}^n e^{-(\hat{\mathbf{H}} - E_T)\delta\tau} \right] \quad (3.8)$$

$$= e^{-(\hat{\mathbf{H}} - E_T)\delta\tau} e^{-(\hat{\mathbf{H}} - E_T)\delta\tau} \cdots e^{-(\hat{\mathbf{H}} - E_T)\delta\tau} \quad (3.9)$$

$$= \int_{x_1} \int_{x_2} \cdots \int_{x_n} |x_n\rangle \langle x_n| e^{-(\hat{\mathbf{H}} - E_T)\delta\tau} |x_{n-1}\rangle \langle x_{n-1}| e^{-(\hat{\mathbf{H}} - E_T)\delta\tau} |x_{n-2}\rangle \\ \times \cdots \langle x_2| e^{-(\hat{\mathbf{H}} - E_T)\delta\tau} |x_1\rangle \langle x_1| dx_1 \cdots dx_n \quad (3.10)$$

where complete sets of position basis states are introduced (see appendix A). The state from Eq. (3.6) are then given by

$$\Phi(x, n\delta\tau) = \langle x| \hat{\mathbf{P}}(n, \delta\tau) |\Phi(t=0)\rangle \quad (3.11)$$

$$= \int_{x_1} \int_{x_2} \cdots \int_{x_{n-1}} \langle x| e^{-(\hat{\mathbf{H}} - E_T)\delta\tau} |x_{n-1}\rangle \langle x_{n-1}| e^{-(\hat{\mathbf{H}} - E_T)\delta\tau} |x_{n-2}\rangle \\ \times \cdots \langle x_2| e^{-(\hat{\mathbf{H}} - E_T)\delta\tau} |x_1\rangle \Phi(x_1, t=0) dx_1 \cdots dx_{n-1} \quad (3.12)$$

The final state x_n are replaced by x due to the fact that $\langle x|x_n\rangle = \delta(x = x_n)$, which makes the x_n integral vanish. The final state is achieved by summing through all possible *paths* represented by integrals over the position variables x_i . This is the path integral formalism of Quantum Mechanics. More information about this formalism can be found in ref. [8]. Integrating out a degree of freedom, that is, *evolving* from x_i to x_{i+1} is given by

$$\Phi(x_{i+1}, i\delta\tau + \delta\tau) = \int_{x_i} \langle x_{i+1}| e^{-(\hat{\mathbf{H}} - E_T)\delta\tau} |x_i\rangle \Phi(x_i, i\delta\tau) dx_i \quad (3.13)$$

$$\equiv \int G(x_{i+1}, x_i; \delta\tau) \Phi(x_i, i\delta\tau) dx_i \quad (3.14)$$

where the *Green's Function*, $G(x_{i+1}, x_i; \delta\tau)$ serves as the transition probability.

This is still not a practical way of solving the equations. By finding the Green's function we might as well find the solution directly. However, if we split the Hamiltonian into the kinetic, $\hat{\mathbf{T}}$ and the potential part, $\hat{\mathbf{V}}$, we can split the Green's function into two well known processes. This splitting is known as the *short time approximation*.

$$\langle x| e^{-(\hat{\mathbf{H}} - E_0)\delta\tau} |y\rangle = \langle x| e^{-(\hat{\mathbf{T}} + \hat{\mathbf{V}} - E_T)\delta\tau} |y\rangle \\ = \langle x| e^{-\hat{\mathbf{T}}\delta\tau} e^{-(\hat{\mathbf{V}} - E_T)\delta\tau} |y\rangle + \frac{1}{2} [\hat{\mathbf{V}}, \hat{\mathbf{T}}]\delta\tau^2 + \mathcal{O}(\delta\tau^3) \\ \simeq \langle x| e^{-\hat{\mathbf{T}}\delta\tau} e^{-(\hat{\mathbf{V}} - E_T)\delta\tau} |y\rangle \quad (3.15)$$

, that is, we split the Green's Function into two processes which are well known, respectively diffusion and branching

$$G_{\text{Diff}} = e^{-\hat{\mathbf{T}}\delta\tau} \quad (3.16)$$

$$G_B = e^{-(\hat{\mathbf{V}} - E_T)\delta\tau} \quad (3.17)$$

Once a diffusion model is selected, for each cycle, the Green's functions are used to propagate the ensemble of walkers making up our distribution into the next time step. The final distributions of walkers will correspond to that of the direct solution of the Schrödinger Equation, given that the time step is sufficiently small, and we simulate long enough. These constraints will be covered in more detail later.

Incorporating only the effect of Eq.(3.16) results in a method called *Variational Monte Carlo*. Including the branching term as well results in *Diffusion Monte Carlo*. These methods will be discussed in sections 3.7 and 3.8. In either of these methods, diffusion is a key process. In practice, we choose a diffusion model where closed form expressions for the Green's Functions exists. Two examples of this will be presented in the following section.

3.1.2 Solving the Diffusion Problem

Different diffusion models may be applied to the problem introduced in the previous section. All models should in theory be able to produce the same result, however, systematic errors of specific implementations may vary depending on the choice of diffusion model. Two of the most common choices in Quantum Monte-Carlo is *Isotropic diffusion* and *Fokker-Planck Anisotropic Diffusion*.

3.1.3 Isotropic Diffusion

Isotropic diffusion is a process in which diffusing particles sees all possible directions as an equally probable path. Eq. (3.18) is an example of this. This is the simplest form of a diffusion equation, the case with a linear *diffusion constant*, D , and no drift terms.

$$\frac{\partial P(\vec{r}, t)}{\partial t} = D \nabla^2 P(\vec{r}, t) \quad (3.18)$$

In the Quantum Monte Carlo case, the value of the diffusion constant is $D = \frac{1}{2}$, that is, the term scaling the Laplacian in the Schrödinger Equation. The closed form expression for the Green's function is a Gaussian distribution with variance $2D\delta t$ [9]

$$G_{\text{Diff}}^{\text{ISO}}(i \rightarrow j) \propto e^{-(x_i - x_j)^2 / 4D\delta t}. \quad (3.19)$$

These equations describe the diffusion process theoretically, however, in order to achieve specific sampling rules for our walkers, we need a connection between the time-dependence of the total distribution and the time-dependence of an individual walker's components in configuration space. This connection is given in terms of a stochastic differential equation called *The Langevin Equation*.

The Langevin Equation for Isotropic Diffusion

The Langevin Equation is a stochastic differential equation used in physics to relate the time dependence of a distribution to the time-dependence of the degrees of freedom in the system. For the simple isotropic diffusion described previously, solving the Langevin equation using a Forward Euler approximation for the time derivative results in the following relation:

$$\begin{aligned} x_{i+1} &= x_i + \xi, & \text{Var}(\xi) &= 2D\delta t, \\ & & \langle \xi \rangle &= x_i, \end{aligned} \quad (3.20)$$

where ξ is a normal distributed number whose variance match that of the Green's function in Eq. (3.19). This relation is in agreement with the isotropy of Eq. (3.18) in the sense that the displacement is symmetric around the current position.

3.1.4 Anisotropic Diffusion: Fokker-Planck

Anisotropic diffusion, in contrast to isotropic diffusion, does not count all directions as equally probable. An example of this is diffusion according to the *Fokker-Planck Equation*, that is, diffusion with a drift term, $\vec{F}(\vec{r}, t)$, responsible for pushing the walkers in the direction of configurations with higher probabilities.

$$\frac{\partial P(\vec{r}, t)}{\partial t} = D \nabla \cdot \left[(\nabla - \vec{F}(\vec{r}, t)) P(\vec{r}, t) \right] \quad (3.21)$$

As will be derived in details in Section 3.1.5, using the Fokker-Planck equation does not violate the original Schrödinger equation, but merely substitute the diffusing value of interest. This means that Quantum Mechanical distributions can be modeled by the Fokker-Planck Equation, leading to a more optimized way of sampling in practical situations due to the drift term.

In Quantum Monte Carlo we want convergence to a stationary state. We can use this criteria to deduce expression for the drift term given our Quantum Mechanical distribution. A stationary state is obtained when the left hand side of Eq. (3.21) is zero:

$$\nabla^2 P(\vec{r}, t) = P(\vec{r}, t) \nabla \cdot \vec{F}(\vec{r}, t) + \vec{F}(\vec{r}, t) \cdot \nabla P(\vec{r}, t)$$

The next thing we want to achieve is cancellation in the rest of the terms. In order to obtain a Laplacian term on the right hand side to potentially cancel out the one on the left, the drift term needs to be on the form $F(\vec{r}, t) = g(\vec{r}, t) \nabla P(\vec{r}, t)$. Inserting this yields

$$\nabla^2 P(\vec{r}, t) = P(\vec{r}, t) \frac{\partial g(\vec{r}, t)}{\partial P(\vec{r}, t)} \left| \nabla P(\vec{r}, t) \right|^2 + P(\vec{r}, t) g(\vec{r}, t) \nabla^2 P(\vec{r}, t) + g(\vec{r}, t) \left| \nabla P(\vec{r}, t) \right|^2.$$

Looking at the factors in front of the Laplacian suggests using $g(\vec{r}, t) = 1/P(\vec{r}, t)$. A quick check reveals that this also cancels out the gradient terms, and the resulting expression for the drift term becomes

$$\begin{aligned} \vec{F}(\vec{r}, t) &= \frac{1}{P(\vec{r}, t)} \nabla P(\vec{r}, t) \\ &= \frac{2}{|\psi(\vec{r}, t)|} \nabla |\psi(\vec{r}, t)| \end{aligned} \quad (3.22)$$

In Quantum Monte Carlo, the drift term is called *The Quantum Force*, since it is responsible for pushing the walkers into regions of higher probabilities, analogous to a force in Newtonian mechanics.

Another strength of the Fokker-Planck equation is that even though the equation itself is more complicated, it's Green's function still has a closed form solution. This means that we can evaluate it efficiently. If this was not the case, the practical value would be reduced dramatically. The reason for this will become clear in Section 3.3. As expected, it is no longer symmetric

$$G_{\text{Diff}}^{\text{FP}}(i \rightarrow j) \propto e^{-(x_i - x_j - D\delta\tau F(x_i))^2 / 4D\delta\tau}. \quad (3.23)$$

The Langevin Equation for the Fokker-Planck Equation

The Langevin equation in the case of a Fokker-Planck Equation has the following form

$$\frac{\partial x_i}{\partial t} = DF(x_i) + \eta, \quad (3.24)$$

where η is a so-called *noise term* from stochastic processes. Solving this using the same method as for the isotropic case yields the following sampling rules

$$x_{i+1} = x_i + \xi + DF(x_i)\delta t, \quad (3.25)$$

where ξ is the same as for the isotropic case. We observe that if the drift term is set to zero, we are back in the isotropic case, just as required. For more details regarding the Fokker-Planck Equation and the Langevin equation, see ref. [10], [11] and [12].

3.1.5 The connection between anisotropic- and isotropic diffusion models

To this point, it might seem far-fetched that switching diffusion model to a Fokker-Planck distribution does not violate the original equation, i.e. the Schrödinger equation. Introducing the distribution function $f(x, t) = \Phi(x, t)\Phi(x, t=0) = \Phi(x, t)\Psi_T(x)$, we can restate the (imaginary time) Schrödinger equation as

$$\begin{aligned} -\frac{\partial}{\partial t}f(x, t) &= \Psi_T(x)\left[-\frac{\partial}{\partial t}\Phi(x, t)\right] = \Psi_T(x)\left(\widehat{\mathbf{H}} - E_T\right)\Phi(x, t) \\ &= \Psi_T(x)\left(\widehat{\mathbf{H}} - E_T\right)\Psi_T(x)^{-1}f(x, t) \\ &= -\frac{1}{2}\Psi_T(x)\nabla^2\left(\Psi_T(x)^{-1}f(x, t)\right) + \widehat{\mathbf{V}}f(x, t) - E_Tf(x, t) \end{aligned} \quad (3.26)$$

Expanding the Laplacian term further reveals

$$\begin{aligned} K(x, t) &\equiv -\frac{1}{2}\Psi_T(x)\nabla^2\left(\Psi_T(x)^{-1}f(x, t)\right) \\ &= -\frac{1}{2}\Psi_T(x)\nabla \cdot (\nabla [\Psi_T(x)^{-1}f(x, t)]) \end{aligned} \quad (3.27)$$

$$\nabla [\Psi_T(x)^{-1}f(x, t)] = -\Psi_T(x)^{-2}\nabla\Psi_T(x)f(x, t) + \Psi_T(x)^{-1}\nabla f(x, t) \quad (3.28)$$

combining these two equations and using the product rule numerous time yields

$$\begin{aligned}
K(x, t) &= -\frac{1}{2}\Psi_T(x)\left[\left(2\Psi_T(x)^{-3}|\nabla\Psi_T(x)|^2\right)f(x, t)\right. \\
&\quad -\Psi_T(x)^{-2}\nabla^2\Psi_T(x)f(x, t) \\
&\quad -\Psi_T(x)^{-2}\nabla\Psi_T(x)\cdot\nabla f(x, t)\big) \\
&\quad +\Psi_T(x)^{-1}\nabla^2f(x, t) \\
&\quad \left.-\Psi_T(x)^{-2}\nabla\Psi_T(x)\cdot\nabla f(x, t)\right] \\
&= -\left|\Psi_T(x)^{-1}\nabla\Psi_T(x)\right|^2f(x, t) \\
&\quad +\frac{1}{2}\Psi_T(x)^{-1}\nabla^2\Psi_T(x)f(x, t) \\
&\quad +\Psi_T(x)^{-1}\nabla\Psi_T(x)\cdot\nabla f(x, t) \\
&\quad -\frac{1}{2}\nabla^2f(x, t)
\end{aligned}$$

In order to clean up the messy calculations, we introduce the following identity

$$\begin{aligned}
\nabla\cdot(\Psi_T(x)^{-1}\nabla\Psi_T(x)) &= -\Psi_T(x)^{-2}|\nabla\Psi_T(x)|^2 + \Psi_T(x)^{-1}\nabla^2\Psi_T(x) \\
\left|\Psi_T(x)^{-1}\nabla\Psi_T(x)\right|^2 &= -\nabla\cdot(\Psi_T(x)^{-1}\nabla\Psi_T(x)) + \Psi_T(x)^{-1}\nabla^2\Psi_T(x)
\end{aligned}$$

which inserted into the expression for $K(x, t)$ reveals

$$\begin{aligned}
K(x, t) &= \nabla\cdot(\Psi_T(x)^{-1}\nabla\Psi_T(x))f(x, t) \\
&\quad +\left(\frac{1}{2}-1\right)\Psi_T(x)^{-1}\nabla^2\Psi_T(x)f(x, t) \\
&\quad +\Psi_T(x)^{-1}\nabla\Psi_T(x)\cdot\nabla f(x, t) \\
&\quad -\frac{1}{2}\nabla^2f(x, t)
\end{aligned}$$

Inserting the expression for the Quantum Force $\vec{F}(x) = 2\Psi_T(x)^{-1}\nabla\Psi_T(x)$ and the local kinetic energy $K_L(x) = -\frac{1}{2}\Psi_T(x)^{-1}\nabla^2\Psi_T(x)$ simplifies the expression dramatically

$$\begin{aligned}
K(x, t) &= -\frac{1}{2}\nabla^2f(x, t) + \underbrace{\frac{1}{2}\left[\vec{F}(x)\cdot\nabla f(x, t) + f(x, t)\nabla\cdot\vec{F}(x)\right]}_{\nabla\cdot[\vec{F}f(x, t)]} + K_L(x)f(x, t) \\
&= \frac{1}{2}\nabla\cdot\left[\left(\nabla - \vec{F}(x)\right)f(x, t)\right] + K_L(x)f(x, t)
\end{aligned}$$

Inserting everything back into Eq. (3.26) yields

$$\begin{aligned}
-\frac{\partial}{\partial t}f(x, t) &= -\frac{1}{2}\nabla\cdot\left[\left(\nabla - \vec{F}(x)\right)f(x, t)\right] + K_L(x)f(x, t) + \widehat{\mathbf{V}}f(x, t) - E_Tf(x, t) \\
\frac{\partial}{\partial t}f(x, t) &= \frac{1}{2}\nabla\cdot\left[\left(\nabla - \vec{F}(x)\right)f(x, t)\right] - (E_L(x) - E_T)f(x, t),
\end{aligned} \tag{3.29}$$

which is a Fokker-Planck diffusion equation (Eq. (3.21)) with constant shift representing the shape of the branching in the case Fokker-Planck QMC (see Eq. (3.39)).

Just as in traditional importance sampled Monte-Carlo integrals, optimized sampling is obtained by switching distributions into one which exploits known information about the problem at hand. In case of standard Monte-Carlo integration, we switch sampling distribution to one which are similar to the original integrand, i.e. smoothing out the sampled function, whereas for Quantum Monte-Carlo, we use a function which is constructed with the sole purpose of imitating the exact ground state to suggest moves more efficiently. It is therefore reasonable to call the use of Fokker-Planck diffusion *Importance sampled Quantum Monte-Carlo*.

Introducing diffusion by the Fokker-Planck equation does not violate the Schrödinger equation, it simply alters the physical interpretation of the distribution of walkers. This new function, $\Psi_T(x)$, is referred to as a *trial wave function*, and will be discussed in more detail in Section 3.5.

The QMC energy estimated using the new distribution $f(x, t)$ will still yield the exact energy in the limit of convergence. Consider the following relation

$$\begin{aligned} E_{\text{DMC}} &= \frac{1}{N} \int f(\mathbf{r}, \tau) \frac{1}{\Psi_T(\mathbf{r})} \hat{\mathbf{H}} \Psi_T(\tilde{\mathbf{r}}) d\mathbf{r} \\ &= \frac{1}{N} \int \Phi(\mathbf{r}, \tau) \hat{\mathbf{H}} \Psi_T(\mathbf{r}) d\mathbf{r} \\ &= \frac{1}{N} \langle \Phi(\tau) | \hat{\mathbf{H}} | \Psi_T \rangle \\ N &= \int f(\mathbf{r}, \tau) d\mathbf{r} \\ &= \int \Phi(\mathbf{r}, \tau) \Psi_T(\mathbf{r}) d\mathbf{r} \\ &= \langle \Phi(\tau) | \Psi_T \rangle \\ E_{\text{DMC}} &= \frac{\langle \Phi(\tau) | \hat{\mathbf{H}} | \Psi_T \rangle}{\langle \Phi(\tau) | \Psi_T \rangle} \end{aligned}$$

Assuming the DMC has converged to the exact ground state, i.e. $|\Phi(\tau)\rangle \rightarrow |\Phi_0\rangle$, letting the Hamiltonian work to the left yields

$$\begin{aligned} E_{\text{DMC}} &= E_0 \frac{\langle \Phi_0 | \Psi_T \rangle}{\langle \Phi_0 | \Psi_T \rangle} \\ &= E_0 \end{aligned}$$

3.2 Diffusive Equilibrium Constraints

Upon convergence of a Markov process, the system at hand will reach its most likely state. This is exactly the behavior of a real system of diffusing particles described by statistical mechanics: It will *thermalize*, that is, be in its most likely state given a surrounding temperature. Markov processes are hence beloved by physicists; they are simple, yet realistic.

Once thermalization is reached, average values may be sampled. However, simply spawning a Markov process and waiting for thermalization is an inefficient and unpractical scenario. This may take forever,

and it may not; either way its not optimal. We can introduce rules of acceptance and rejection of transitions purposed by following the solutions of the Langevin Equation (Eq. (3.20) and Eq. (3.25)), but not without constraints. If any of the following conditions break, we have no guarantee that the system will thermalize properly:

3.2.1 Detailed Balance

For Markov processes, detailed balance is achieved by demanding a *Reversible* Markov process. This boils down to a statistical requirement stating that

$$P_i W(i \rightarrow j) = P_j W(j \rightarrow i), \quad (3.30)$$

where P_i is the probability density in configuration i , and $W(i \rightarrow j)$ is the transition probability between states i and j .

3.2.2 Ergodicity

Another requirement is that the sampling must be ergodic, that is, the Markov chain (or simpler: The walker) needs to be able to be able to reach any configuration state in the space spanned by the distribution function. It is tempting to define a brute force acceptance rule where only steps resulting in a higher overall probability is accepted, however, this limits the path of the walker, and hence breaks the ergodicity requirement.

3.3 The Metropolis Algorithm

The Metropolis Algorithm is a simple set of acceptance/rejection rules used in order to make the thermalization more effective. For a given probability distribution function, P , the metropolis algorithm will force sampled points to follow this distribution. I will not go into details about transport theory in this section, but rather start the derivation from the criteria of detailed balance, Eq. (3.30), modeling the transition probability as two-part: $g(i \rightarrow j)$, the probability of selecting configuration j given configuration i , times a probability of accepting the selected move, $A(i \rightarrow j)$:

$$\begin{aligned} P_i W(i \rightarrow j) &= P_j W(j \rightarrow i) \\ P_i g(i \rightarrow j) A(i \rightarrow j) &= P_j g(j \rightarrow i) A(j \rightarrow i) \end{aligned} \quad (3.31)$$

Inserting the probability distribution as the Wave function squared, and the selection probability as our Green's function, then gives us a simple expression:

$$\begin{aligned} |\psi_i|^2 G(i \rightarrow j) A(i \rightarrow j) &= |\psi_j|^2 G(j \rightarrow i) A(j \rightarrow i) \\ \frac{A(j \rightarrow i)}{A(i \rightarrow j)} &= \frac{G(i \rightarrow j)}{G(j \rightarrow i)} \frac{|\psi_i|^2}{|\psi_j|^2} \equiv R_G(j \rightarrow i) R_\psi(j \rightarrow i)^2 \end{aligned} \quad (3.32)$$

Assume now that configuration i has a higher overall probability than configuration j , that is, $A(i \rightarrow j) = 1$. A more effective thermalization is obtained by accepting all these moves. What saves us from

breaking the criteria of ergodicity is the fact that we do not reject the move otherwise. Instead, we insert $A(i \rightarrow j) = 1$ into Eq. (3.32), and thus ensuring detailed balance as well as ergodicity. This yields

$$A(j \rightarrow i) = R_G(j \rightarrow i)R_\psi(j \rightarrow i)^2$$

Concatenating both scenarios yields the following acceptance/rejection rules:

$$A(i \rightarrow j) = \begin{cases} R_G(i \rightarrow j)R_\psi(i \rightarrow j)^2 & R_G(i \rightarrow j)R_\psi(i \rightarrow j)^2 < 1 \\ 1 & \text{else} \end{cases} \quad (3.33)$$

Or more simplistic:

$$A(i \rightarrow j) = \min\{R_G(i \rightarrow j)R_\psi(i \rightarrow j)^2, 1\} \quad (3.34)$$

For the isotropic case, we have a cancellation of the Greens function due to symmetry, $R_G(i \rightarrow j) = 1$, leaving us with the standard Metropolis algorithm:

$$A(i \rightarrow j) = \min\{R_\psi(i \rightarrow j)^2, 1\} \quad (3.35)$$

If we on the other hand use the Fokker-Planck equation, we will not get a cancellation. Inserting Eq. (3.23) into Eq. (3.33) results in the *Metropolis Hastings algorithm*. The ratio of Green's function can be evaluated efficiently by simply subtracting the exponents of the exponentials

$$\begin{aligned} \log R_G^{\text{FP}}(i \rightarrow j) &= \log(G_{\text{Diff}}^{\text{FP}}(j \rightarrow i)/G_{\text{Diff}}^{\text{FP}}(i \rightarrow j)) \\ &= \frac{1}{2}(F(x_j) + F(x_i))(\frac{1}{2}D\delta t(F(x_j) - F(x_i)) + x_i - x_i) \end{aligned} \quad (3.36)$$

$$A(i \rightarrow j) = \min\{\exp(\log R_G^{\text{FP}}(i \rightarrow j))R_\psi(i \rightarrow j)^2, 1\} \quad (3.37)$$

Derived from detailed balance, the Metropolis Algorithm is as a must-have when it comes to Markov Chain Monte Carlo. Besides Quantum Monte Carlo, we have methods such as the *Ising Model* which greatly benefit from these rules [13].

In practice, without the Metropolis sampling, our ensemble of walkers will not span that of the trial wave function. This is due to the fact that the time step used in simulations are finite, and the trial position of the walkers are random. A chart flow describing the implementation of the Metropolis algorithm and the diffusion process in general is given in Fig. 3.1.

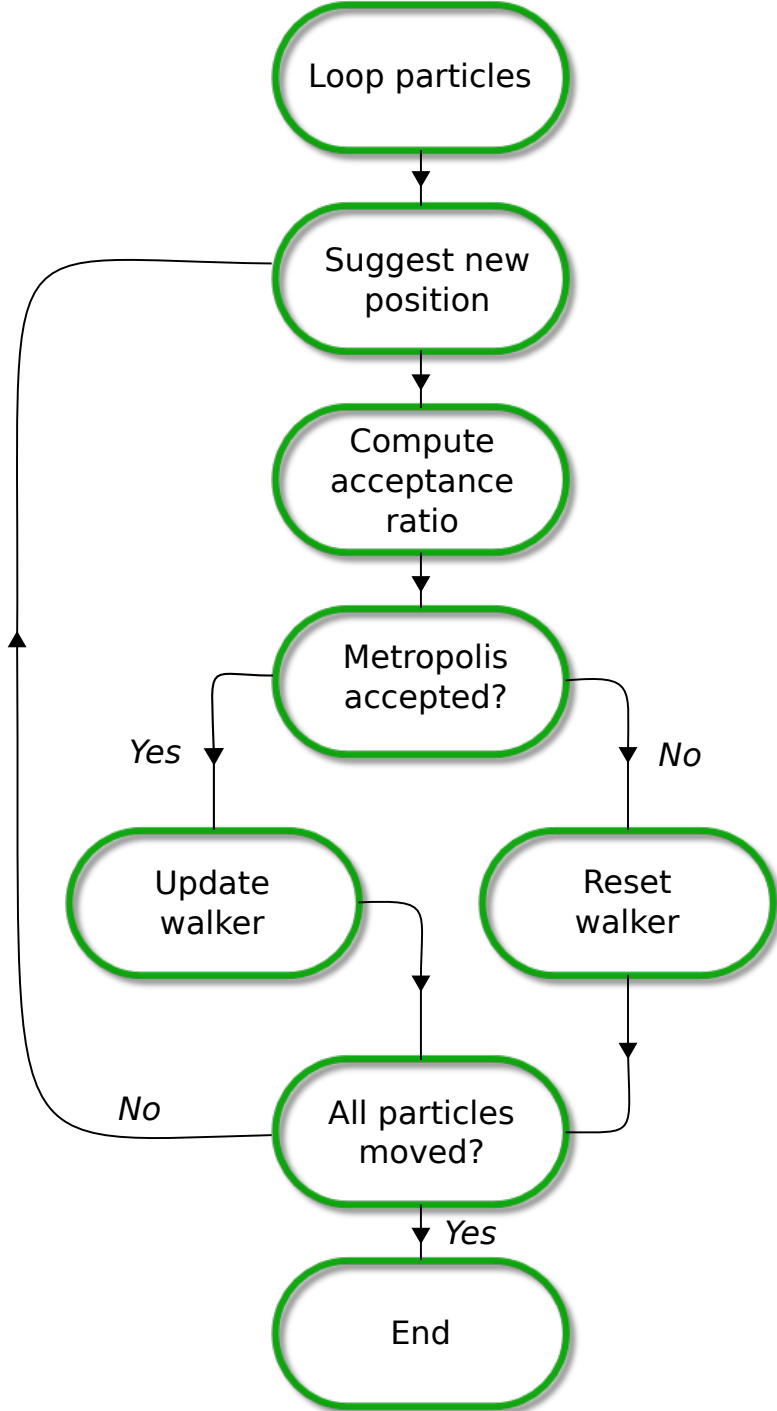


Figure 3.1: Flow chart for iterating a walker through a single time step, i.e. simulation the application of the Green's function from Eq. (3.16) using the Metropolis algorithm. New positions are suggested according to the chosen diffusion model.

3.4 The Process of Branching

The process of branching of Quantum Monte-Carlo is simulated by the creation or destruction of walkers with probability equal to that of the Green's function in Eq. (3.17) [9]. The explicit shapes in case of isotropic diffusion (ISO) and Anisotropic (FP) is

$$G_B^{\text{ISO}}(i \rightarrow j) = e^{-(\frac{1}{2}[V(x_i)+V(x_j)]-E_T)\delta\tau} \quad (3.38)$$

$$G_B^{\text{FP}}(i \rightarrow j) = e^{-(\frac{1}{2}[E_L(x_i)+E_L(x_j)]-E_T)\delta\tau}, \quad (3.39)$$

where $E_L(x_i)$ is the energy evaluated in configuration x_i (see Section 3.5.3 for details).

The Green's function represents a weight of the walker in a current position. When the final estimates are calculated, this weight is factored in to the distribution function. This however, is not a practical way of doing calculations; we cannot calculate a factor for every possible transition. What is done instead is to introduce a birth/death process. If the value is less than one, we have “deaths”, i.e. the walker is removed from the ensemble. “Births” occur when the Green's function is greater than one; the walker is replicated. As for all Green's functions, $G_B(i \rightarrow j) = 1$ implies no change.

The practical implementation becomes simply creating $\lfloor G_B \rfloor - 1$ replicas of the current walker, with $[G_B - \lfloor G_B \rfloor]$ probability of adding one extra on top (I skip the transition indices for now). As an example, a Green's function of $G_B = 3.3$ will have guaranteed three replicas, however, there is a $3.3 - 3 = 0.3$ chance that one additional replica is made. The efficient comparison to do is to define

$$\overline{G}_B = \text{floor}(G_B + a), \quad (3.40)$$

where a is a uniformly distributed number on $[0, 1)$. The chance that $\overline{G}_B = G_B + 1$ is then equal to $[G_B - \lfloor G_B \rfloor]$ as required. The three different scenarios which arise is

- $\overline{G}_B = 1$: No branching, proceed main loop.
- $\overline{G}_B = 0$: The current walker is to be removed from the current ensemble.
- $\overline{G}_B > 1$: Make $\overline{G}_B - 1$ replicas of the current walker.

This process is demonstrated in Fig. 3.2.

There are some programming challenges due to the fact that the number of walkers is not conserved, such as cleaning up dead walkers and stabilizing the population across different nodes. For details regarding this, see the actual code reference at ref. [6]. Isotropic diffusion is in practice never used with branching. From Eq. (3.38) we see that in case of the Coulomb interaction, the branching Green's function would have singularities, leading to large fluctuations in the walker population. This is exactly opposite of the optimal behaviour of the system.

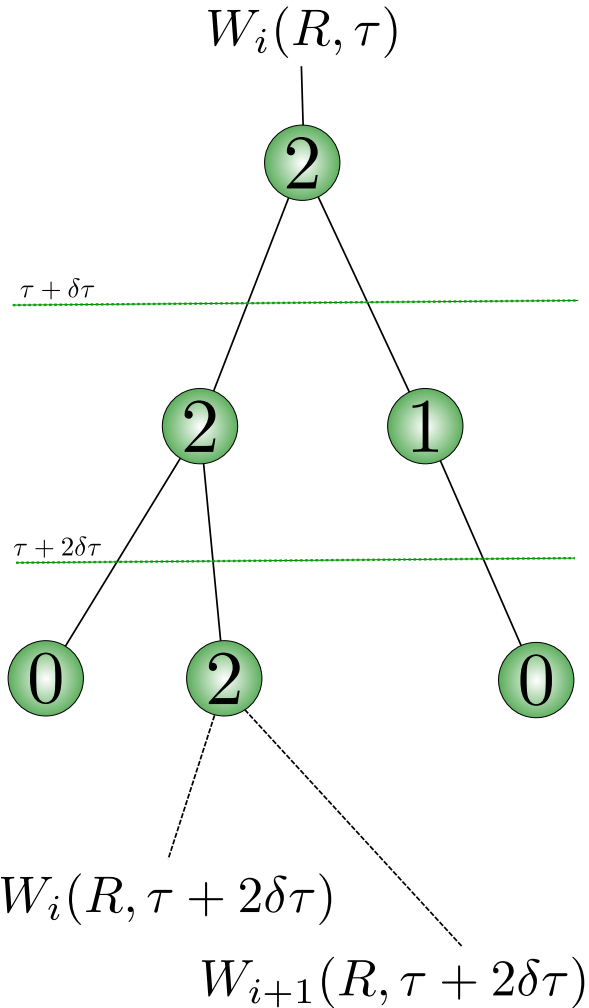


Figure 3.2: Branching illustrated. The initial walker $W_i(R, \tau)$ is branched according to the rules of Section 3.4. The numerical value inside the nodes represents \bar{G}_B from Eq. (3.40). Each horizontal dashed line represent a diffusion step, i.e. a transition in time. Two lines exiting the same node represent identical walkers. After moving through the diffusion process, not two walkers should ever be equal (given that not all of the steps was rejected).

3.5 The Trial Wave Function

Recall Eq. (3.2)-(3.5). The initial condition, $\Phi(\vec{r}, t = 0)$, is in Quantum Monte-Carlo referred to as the trial wave function. Mathematically, we may choose any normalizable wave function, whose overlap with the exact ground state wave function, $\Psi_0(x)$, is non-zero. If the overlap is zero, that is, $C_0 = 0$ in Eq. (3.5), the entire diffusion formalism breaks down, and no final state of convergence can be reached. On the other hand, the opposite scenario implies the opposite behavior; the closer C_0 is to unity, the more rapidly $\Psi_0(x)$ will become the dominant contribution to our distribution.

Before getting into specifics, a few notes on many-body theory is needed. From this point on, all particles are assumed to be identical. For more information regarding basic Quantum Mechanics, I suggest reading ref. [7]. For mathematically rigid derivations of concepts, see ref. [14]. More details regarding many-body theory can be found in ref. [15].

3.5.1 Many-body Wave Functions

Many-body theory arise from the fact that we have *many-body interactions*, e.g. the Coulomb interaction between two particles. If this was not the case, i.e. for non-interacting particles, the full system would decouple into N single particle systems.

Finding the ground state is not surprisingly equivalent to solving the time-independent Schrödinger Equation

$$\hat{\mathbf{H}}\Psi_0(x) = E_0\Psi_0(x), \quad (3.41)$$

where $x \equiv \{x_1, x_2, \dots, x_N\}$. Exact solutions to realistic many-body systems rarely exist, however, like in Section 3.1.1, expanding the solution in a known basis is always legal, which reduces the problem into that of a *coefficient hunt*

$$\Psi_0(x) = \sum_{k=0}^{\infty} C'_k \Phi_k(x). \quad (3.42)$$

Different many-body methods, e.g. *Hartree Fock*² and genetic algorithms, give rise to different ways of hunting down these coefficients, however, certain concepts are necessarily common, for instance truncating the basis at some level, K :

$$\Psi_0(x) = \sum_{k=0}^K \tilde{C}'_k \Phi_k(x). \quad (3.43)$$

The many-body basis elements $\Phi_k(x)$ are constructed using N elements from a basis of single particle wave functions (or *orbitals* for short), $\phi_n(x_i)$, combined in different ways. The process of calculating basis elements often boils down to a combinatoric exercise involving combinations of orbitals.

Imagine electrons surrounding a nucleus, i.e an atom; a single electron occupying state n at a position x_i is then described by the orbital $\phi_n(x_i)$. Each unique³ configuration of electrons will give rise to one

²Hartree-Fock is roughly a basis change from the non-interacting case into a basis which is orthogonal to one-particle excitations. The exact ground state wave function should be orthogonal to all excited states, so it's a fair approximation depending on the dominance of one-particle excitations in the given system.

³Two wave functions are considered equal if they differ by nothing but a phase factor.

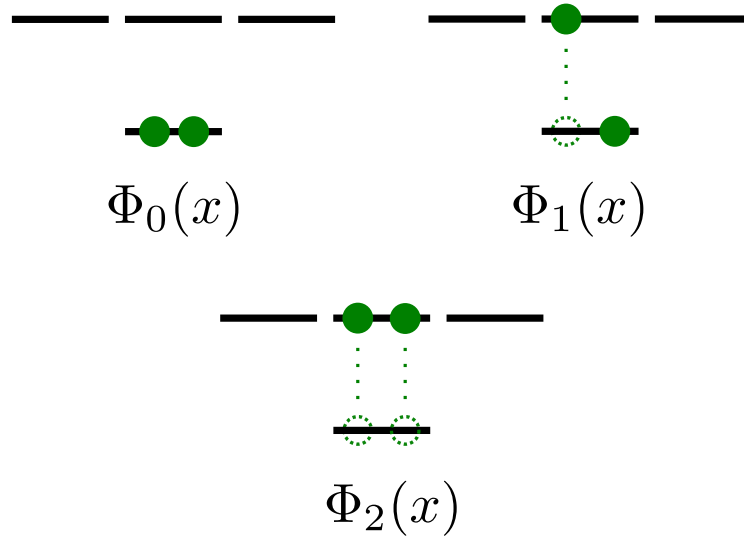


Figure 3.3: Three different electron configurations in an shell structure making up three different $\Phi_k(x)$, i.e. constituents of the many-body basis described in Eq. (3.43). An electron (solid dot) is represented by e.g. the orbital $\phi_{1s}(x_1)$.

unique $\Phi_k(x)$. In other words, the complete basis of $\Phi_k(x)$ is described by the collection of all possible excited states. $\Phi_0(x)$ is the ground state of the atom, $\Phi_1(x)$ has one electron excited to a higher shell, $\Phi_2(x)$ has another, and so on. See Fig. 3.3 for a demonstration of this.

In other words, constructing a single solution of a many-body problem involves three steps:

| | |
|------------|---|
| Step one | Choose a set of orbitals $\phi_n(x_i)$. |
| Step two | Construct $\Phi_k(x)$ from $N \times \phi_n(x_i)$. |
| Step three | Construct $\Psi_k(x)$ from $K \times \phi_k(x)$. |

The last step is well described by Eq. (3.43), but is seldom necessary to perform explicitly; expressions based on the calculated wave functions is given in terms of the constituents and their weights.

Step one in detail

The Hamiltonian for a N -particle system is

$$\hat{\mathbf{H}} = \hat{\mathbf{H}}_0 + \hat{\mathbf{H}}_I, \quad (3.44)$$

where $\hat{\mathbf{H}}_0$ and $\hat{\mathbf{H}}_I$ are respectively the one-body and the many-body term. As an approximation, we truncate the many-body interactions at the Coulomb level. The one-body term consist of the external potential and the kinetic terms for all particles.

$$\hat{\mathbf{H}}_0 = \sum_{i=1}^N \hat{\mathbf{h}}_0(x_i) \quad (3.45)$$

$$\begin{aligned} \hat{\mathbf{H}}_I &\simeq \sum_{i < j=1}^N \hat{\mathbf{v}}(r_{ij}) \\ &= \sum_{i < j=1}^N \frac{1}{r_{ij}} \end{aligned} \quad (3.46)$$

The single particle orbitals are chosen to be the solutions of the non-interacting case (given that they exist)

$$\hat{\mathbf{h}}_0(x_i)\phi_n(x_i) = \epsilon_n\phi_n(x_i). \quad (3.47)$$

If no such choice can be made, choosing an generally suited basis, e.g. free-particle solutions, is the general strategy.

Step two in detail

In the case of *Fermions*, i.e. half-integer spin particles like electrons, protons, etc., $\Phi_k(x)$ is an anti-symmetric function⁴ on the form of a determinant: The *Slater determinant*. The shape of the determinant is given in Eq. (3.48). The anti-symmetry is a direct consequence of the *Pauli Exclusion Principle*: At any given time, two fermions cannot occupy the same state.

Bosons on the other hand, have symmetric wave functions (see Eq. (3.49)), which in many ways are easier to deal with because of the lack of an exclusion principle. In order to keep the terminology less abstract and confusing, from here on, the focus will be on systems of fermions.

$$\begin{aligned} \Phi_0^{\text{AS}}(x_1, x_2, \dots, x_N) &\propto \sum_{\text{P}} (-)^{\text{P}} \hat{\mathbf{P}} \phi_1(x_1) \phi_2(x_2) \dots \phi_N(x_N) \\ &= \left| \begin{array}{cccc} \phi_1(x_1) & \phi_2(x_1) & \cdots & \phi_N(x_1) \\ \phi_1(x_2) & \phi_2(x_2) & \cdots & \phi_N(x_2) \\ \vdots & \vdots & \ddots & \vdots \\ \phi_1(x_N) & \phi_2(x_N) & \cdots & \phi_N(x_N) \end{array} \right| \end{aligned} \quad (3.48)$$

$$\Phi_0^S(x_1, x_2, \dots, x_N) \propto \sum_{\text{P}} \hat{\mathbf{P}} \phi_1(x_1) \phi_2(x_2) \dots \phi_N(x_N) \quad (3.49)$$

Comment to Eq. (3.48) and Eq. (3.49): The permutation operator $\hat{\mathbf{P}}$ is simply a way of writing *in any combination of particles and states*, hence the combinatoric exercise mentioned previously.

⁴Interchanging two particles in an anti-symmetric wave function will reproduce the state changing only the sign.

Dealing with correlations

The contributions to the sum on the right-hand side in Eq. (3.42) for $k > 0$ are often referred to as *correlation* terms. Given that the orbital wave functions are chosen by Eq. (3.47), the existence of the correlation terms, i.e. $C'_k \neq 0$ for $k > 0$, follows as a direct consequence of the many-body interaction, H_I .

As an example, imagine performing an energy calculation with two particles being infinitely close; the Coulomb singularity will cause the energy to blow up. However, if we perform the calculation using the exact wave function, the diverging terms will cancel out; the energy is position independent.

In other words, incorporating the correct correlated wave function will result in a cancellation in the diverging term as we approach singularities, a property which brings us closer to the exact wave function.

These criteria are called *Cusp Conditions*, and serve as a powerful guide when it comes to selecting a trial wave function.

3.5.2 Choice of Trial Wave function

Choosing the trial wave function boils down to optimizing the overlap described in the introduction using a priori knowledge about the system at hand. As discussed previously, the optimal choice of single particle basis is eigenfunctions of the non-interacting case (given that they exist). Starting from Eq. (3.43), the *spatial wave function*, the first step is to make sure the cusp conditions are obeyed.

Introducing the correlation functions $f(r_{ij})$, where r_{ij} is the relative distance between particle i and j , the general *anzats* for the trial wave function becomes

$$\Psi_T(x_1, \dots, x_N) = \left[\sum_{k=0}^K C_k \Phi_k(x_1, \dots, x_N) \right] \prod_{i < j} f(r_{ij}) \quad (3.50)$$

Explicit shapes

Several models for the correlation function exist, however, some are less practical than others. An example given in ref. [9] demonstrates this nicely: Hylleraas presented the following correlation function

$$f(r_{ij})_{\text{Hylleraas}} = e^{-\frac{1}{2}(r_i + r_j)} \sum_k d_k(r_{ij})^{a_k} (r_i + r_j)^{b_k} (r_i - r_j)^{e_k}, \quad (3.51)$$

where all k -subscripted parameters are free. Calculating the helium ground state energy using this correlation function with nine terms yields a four decimal precision. Eight digit precision is achieved by including almost 1078 terms. For the purpose of Quantum Monte-Carlo this is beyond overkill.

A more well suited correlation function is the *Padé Jastrow* function (skipping some redundant indices)

$$\begin{aligned} \prod_{i < j}^N f(r_{ij}) &= \exp(U) \\ U &= \sum_{i < j}^N \left(\frac{\sum_k a_k r_{ij}^k}{1 + \sum_k \beta_k r_{ij}^k} \right) + \sum_i^N \left(\frac{\sum_k a'_k r_i^k}{1 + \sum_k \alpha_k r_i^k} \right). \end{aligned}$$

For systems where the correlations are well behaving, it is custom to drop the second term, and keep only the $k = 1$ term, i.e.

$$f(r_{ij}; \beta) = \exp\left(\frac{a_{ij}r_{ij}}{1 + \beta r_{ij}}\right), \quad (3.52)$$

where β is a variational parameter, and a_{ij} is a spin-dependent constant tuned to obey the cusp condition.

Shifting the focus back to the spatial wave function, in the case of a fermionic system, the evaluation of a $N \times N$ Slater determinant is holding back the effectiveness of many-particle simulations. However, assuming we have a spin-independent Hamiltonian, we can split the spatial wave function into two; one part for each spin eigenvalue. A detailed derivation of this is given in the appendix of ref. [16]. Assuming spin-half particles we get

$$\Psi_T(x_1, \dots, x_N; \beta) = \left[\sum_{k=0}^K C_k \tilde{\Phi}_k(x_1, \dots, x_{\frac{N}{2}}) \tilde{\Phi}_k(x_{\frac{N}{2}+1}, \dots, x_N) \right] \prod_{i < j}^N f(r_{ij}; \beta). \quad (3.53)$$

Since the particles are identical, we are free to say that the first half are spin up, and the second spin down, hence the splitting as above. For simplicity, the spin up determinant will from here on be labeled D^\uparrow , and the spin down one D^\downarrow . Stitching everything together yields the following explicit shape for a spin-independent Hamiltonian using a one-parameter Padé Jastrow function

$$\Psi_T(x_1, \dots, x_N; \beta) = \sum_{k=0}^K C_k D_k^\uparrow D_k^\downarrow \prod_{i < j}^N f(r_{ij}; \beta). \quad (3.54)$$

This shape is referred to as a *Multi-determinant* trial wave function.

Limitations

Depending on the complexity of the system at hand, we need more complicated trial wave functions. However, it is important to distinguish between simply integrating a trial wave function, and performing the full diffusion calculation. As a reminder: Simple integration will not be able to tweak the distribution; what you have is what you get. Solving the diffusion problem, on the other hand, will alter the distribution from that of the trial wave function ($t = 0$) into a distribution closer to the exact wave function by Eq. (3.5).

Because of this fact, our limitations due to the trial wave function is far less than what is the case of standard Monte-Carlo integration. A heavier trial wave function might converge faster, but at the expense of being more CPU-intensive. This means that we are in a position to trade CPU-time per walker for convergence time. For systems of many particles, CPU-time per walker needs to be as low as possible in order to get the computation done in a reasonable amount of time, i.e., the choice of trial wave function needs to be done in light of the system at hand, and the specific aim of the computation.

Single Determinant Trial Wave function

In the case of well-behaving systems, a single determinant converges rapidly enough. This simplicity opens up the possibility of simulating large systems efficiently. This will be referred to as a *single determinant* trial wave function, and serve as a very simple approximation. In order to optimize the overlap with the exact wave function, a variational parameter α is introduced in the spatial part (from Eq. (3.52), we already have β)

$$\Psi_T(x_1, \dots, x_N; \alpha, \beta) = D^\dagger(\alpha) D^\downarrow(\alpha) \prod_{i < j}^N f(r_{ij}; \beta). \quad (3.55)$$

Determining optimal values for the variational parameters will be discussed in Section 3.5.5.

3.5.3 Calculating Expectation Values

The expectation value of an operator $\hat{\mathbf{O}}$ is sampled through *local* values, $O_L(x)$

$$\begin{aligned} \langle \Psi_T | \hat{\mathbf{O}} | \Psi_T \rangle &= \int \Psi_T(x)^* \hat{\mathbf{O}} \Psi_T(x) dx \\ &= \int |\Psi_T|^2 \left(\frac{1}{\Psi_T(x)} \hat{\mathbf{O}} \Psi_T(x) \right) dx \\ &= \int |\Psi_T|^2 O_L(x) dx \end{aligned} \quad (3.56)$$

$$O_L(x) = \frac{1}{\Psi_T(x)} \hat{\mathbf{O}} \Psi_T(x) \quad (3.57)$$

Discretizing the integral (and thus introducing an error) yields

$$\langle \Psi_T | \hat{\mathbf{O}} | \Psi_T \rangle \equiv \langle O \rangle \simeq \frac{1}{n} \sum_{i=1}^n O_L(x_i) \equiv \bar{O}, \quad (3.58)$$

where x_i is a random variable following the distribution of the trial wave function. The *ensemble average*, $\langle O \rangle$ will, given ergodicity, equal the estimated average \bar{O} in the limit $n \rightarrow \infty$, i.e.

$$\langle O \rangle = \lim_{n \rightarrow \infty} \bar{O} = \lim_{n \rightarrow \infty} \frac{1}{n} \sum_{i=1}^n O_L(x_i) \quad (3.59)$$

In the case of the energy estimation, this means that once our walkers hit equilibrium, we can start sampling local values based on their configurations x_i . In the case of energies, we get

$$\langle E \rangle \simeq \frac{1}{n} \sum_{i=1}^n \left(\frac{1}{\Psi_T(x_i)} \left(-\frac{1}{2} \nabla^2 \right) \Psi_T(x_i) + V(x_i) \right) \quad (3.60)$$

3.5.4 Normalization

Every explicit calculation using the trial wave function in Quantum Monte-Carlo involves taking ratios. Ratios implies cancellation of the normalization factors. Eq. (3.33) from the Metropolis section, the Quantum Force in the Fokker-Planck equation, and the sampling of local values describes in the previous section demonstrates exactly this; everything involves ratios.

Not having to normalize our wave functions saves us a lot of CPU-time, but it also relieves us of complicated normalization factors in our single particle basis expressions; any constants multiplying $\phi_n(x_i)$ in Eq. (3.48) and Eq. (3.49), can be taken outside the sum over permutations, and will hence cancel when

the ratio between two wave functions constituting of the same single particle orbitals are computed (note: Single determinant only).

In the case of multi-determinants trial wave functions, the normalization factors from the single particle basis elements will be absorbed by the respective determinant's coefficient C_k , and is hence obsolete in this case as well.

3.5.5 Selecting Optimal Variational Parameters

All practical ways of determining the optimal values of the variational parameters originate from the same powerful principle: *The Variational Principle*. The easiest way of demonstrating the principle is to evaluate the expectation value of the energy, using an approach similar to what used in Eq. (3.5)

$$\begin{aligned} E_0 &= \langle \Psi_0 | \hat{\mathbf{H}} | \Psi_0 \rangle \\ E &= \langle \Psi_T(\alpha, \beta) | \hat{\mathbf{H}} | \Psi_T(\alpha, \beta) \rangle \\ &= \sum_{kl} C_k^* C_l \underbrace{\langle \Psi_k | \hat{\mathbf{H}} | \Psi_l \rangle}_{E_k \delta_{kl}} \\ &= \sum_k |C_k|^2 E_k \end{aligned}$$

Using further that E_0 is the lowest energy eigenvalue, we can, just as done with the time propagator, introduce $E_k = E_0 + \delta E_k$ to simplify the arguments

$$\begin{aligned} E &= \sum_k |C_k|^2 (E_0 + \delta E_k) \\ &= E_0 \underbrace{\sum_k |C_k|^2}_1 + \underbrace{\sum_k |C_k|^2 \delta E_k}_{\geq 0} \\ &\geq E_0 \end{aligned}$$

The conclusion is stunning: No matter how we choose our trial wave function, we will never undershoot the exact ground state energy. This basically means that the problem of choosing variational parameters boils down to a minimization problem in the parameters space (we assume no maximum exist for finite parameter values)

$$\frac{\partial \langle E \rangle}{\partial \alpha_i} = \frac{\partial}{\partial \alpha_i} \langle \Psi_T(\alpha_i) | \hat{\mathbf{H}} | \Psi_T(\alpha_i) \rangle = 0 \quad (3.61)$$

In order to work with Eq. (3.61) in practice, we need to rewrite it in terms of known values. Since our wave function is dependent on the variational parameter, we need to include the expression for the normalization factor before we can expand the expression

$$\begin{aligned}
\frac{\partial \langle E \rangle}{\partial \alpha_i} &= \frac{\partial}{\partial \alpha_i} \frac{\langle \Psi_T(\alpha_i) | \hat{\mathbf{H}} | \Psi_T(\alpha_i) \rangle}{\langle \Psi_T(\alpha_i) | \Psi_T(\alpha_i) \rangle} \\
&= \frac{\left(\langle \Psi_T(\alpha_i) | \frac{\partial}{\partial \alpha_i} \hat{\mathbf{H}} | \Psi_T(\alpha_i) \rangle + \langle \Psi_T(\alpha_i) | \hat{\mathbf{H}} \frac{\partial}{\partial \alpha_i} | \Psi_T(\alpha_i) \rangle \right)}{\langle \Psi_T(\alpha_i) | \Psi_T(\alpha_i) \rangle^2} \langle \Psi_T(\alpha_i) | \Psi_T(\alpha_i) \rangle \\
&- \langle \Psi_T(\alpha_i) | \hat{\mathbf{H}} | \Psi_T(\alpha_i) \rangle \frac{\left(\langle \Psi_T(\alpha_i) | \frac{\partial}{\partial \alpha_i} \right) | \Psi_T(\alpha_i) \rangle + \langle \Psi_T(\alpha_i) | \left(\frac{\partial}{\partial \alpha_i} | \Psi_T(\alpha_i) \rangle \right)}{\langle \Psi_T(\alpha_i) | \Psi_T(\alpha_i) \rangle^2},
\end{aligned}$$

where the product and division rules for derivatives have been applied. The Hamiltonian does not depend on the variational parameters, and hence both terms in the first expansion is equal. Cleaning up the expression yields

$$\begin{aligned}
\frac{\partial \langle E \rangle}{\partial \alpha_i} &= 2 \left(\frac{\langle \Psi_T(\alpha_i) | \hat{\mathbf{H}} \frac{\partial}{\partial \alpha_i} | \Psi_T(\alpha_i) \rangle}{\langle \Psi_T(\alpha_i) | \Psi_T(\alpha_i) \rangle} - \langle E \rangle \frac{\langle \Psi_T(\alpha_i) | \frac{\partial}{\partial \alpha_i} | \Psi_T(\alpha_i) \rangle}{\langle \Psi_T(\alpha_i) | \Psi_T(\alpha_i) \rangle} \right) \\
&= 2 \left(\left\langle E \frac{\partial \Psi_T}{\partial \alpha_i} \right\rangle - \langle E \rangle \left\langle \frac{\partial \Psi_T}{\partial \alpha_i} \right\rangle \right)
\end{aligned} \tag{3.62}$$

Using this expression for the *variational gradient* means we can calculate the derivatives exactly the same way we calculate the energy, and use these derivatives to move in the direction of the variational minimum in Eq. (3.61).

This strategy give rise to numerous ways of finding the optimal parameters, such as using the well known Newton's method, conjugate gradient methods [17], steepest descent (similar to Newton's method), and many more. The method implemented for this thesis is called *Adaptive Stochastic Gradient Descent*, and is an efficient iterative algorithm for seeking the variational minimum.

3.6 Gradient Descent Methods

The direction of a gradient serves as a guide to extremal values. Gradient Descent, also called Steepest Descent, is a family of minimization methods using this property of gradients in order to back trace a local minimum in the vicinity of an initial guess.

3.6.1 General Gradient Descent

Seeking maxima or minima is simply a question of whether the positive or negative direction of the gradient is followed. Imagine a function, $f(x)$, with a minimum residing at $x = x_m$. The information at hand is then

$$\nabla f(x_m) = 0 \tag{3.63}$$

$$\nabla f(x_m - dx) < 0 \tag{3.64}$$

$$\nabla f(x_m + dx) > 0 \tag{3.65}$$

where dx is a infinite decimal displacement.

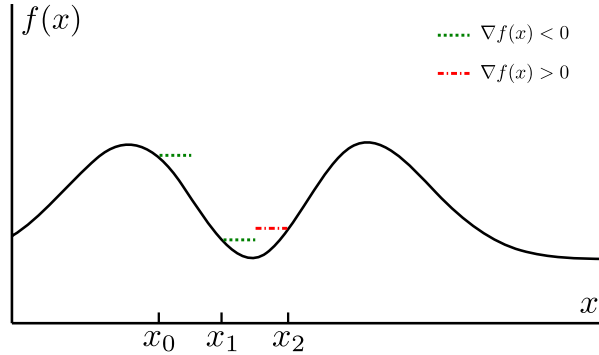


Figure 3.4: Two steps of a one dimensional Gradient Descent process. Steps are taken in the direction of the negative gradient (indicated by dotted lines).

Assume now that we start from an initial position x_0 , and measure the direction of the gradient before we take a step in that direction. From Fig. 3.4 and the previous equations, we see that once we cross the minimum, the gradient changes sign. The brute force way of minimizing is to stop once the gradient changes sign, however, this would require extremely many extremely small steps in order to achieve good precision. The difference equation for the brute force case would be

$$x_{i+1} = x_i - \delta \frac{\nabla f(x_i)}{|\nabla f(x_i)|} \quad (3.66)$$

A better algorithm is to continue iterating even though the minimum is crossed. The brute force scheme breaks down in this case, oscillating between two points, e.g. x_1 and x_2 in Fig. 3.4, because of the constant step length δ . To counter this, a changing step length δ_i is introduced

$$x_{i+1} = x_i - \delta_i \nabla f(x_i) \quad (3.67)$$

All Gradient/Steepest Descent methods is in principle described by Eq. (3.67). Some examples are

- Brute Force I $\delta_i = \delta \frac{1}{|\nabla f(x_i)|}$
- Brute Force II $\delta_i = \delta$
- Monotone Decreasing $\delta_i = \delta/i^2$
- Newton's Method $\delta_i = \frac{1}{\nabla^2 f(x_i)}$

Iterative gradient methods will only reveal one local extrema, depending on the choice of x_0 and δ . In order to find several extrema, multiple unique processes can be run. Calculating the local gradient is simply a finite difference calculation (assuming the analytic expression is not known).

3.6.2 Stochastic Gradient Descent

Minimizing stochastic quantities, such as the variance or expectation values, adds another layer of complications on top of the methods described in the previous section. Assuming a closed form expression for

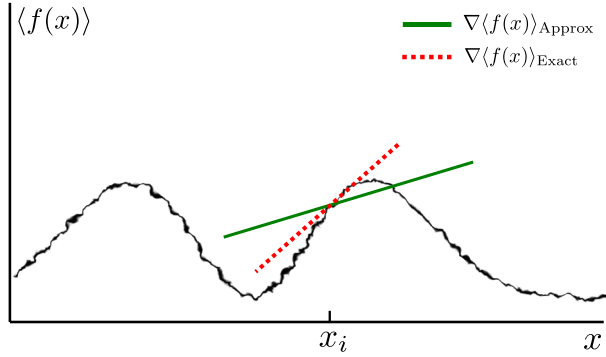


Figure 3.5: A one dimensional plot of an expectation valued function. Smeared lines are representing uncertainties due to rough sampling. The direction of the local gradient (solid green line) at a point x_i is not necessarily a good estimate of the actual analytic gradient (dashed red line).

the stochastic quantity is unobtainable, the gradient needs to be calculated by using e.g. Monte-Carlo sampling. Eq. (3.62) is an example of such a process.

A full precise sampling of the stochastic quantities are expensive and unpractical. Stochastic Gradient methods use different techniques in order to make the sampling more effective, such as multiple walkers, thermalization, and more.

Using a finite difference scheme with stochastic quantities are dangerous, as uncertainties in the values will cause the gradient to become unstable when the variations are (expectedly) low close to the minimum. This is illustrated in Fig. 3.5.

3.6.3 Adaptive Stochastic Gradient Descent

Adaptive Stochastic Gradient Descent (ASGD) has its roots in the mathematics of automated control theory [18]. The automated process, is that of choosing an optimal step length δ_i for the current transition $x_i \rightarrow x_{i+1}$. This process is based on the inner product of the old and the new gradient though a variable

$$X_i \equiv -\nabla_i \cdot \nabla_{i-1} \quad (3.68)$$

The step length from Eq. (3.67) is in ASGD modeled in the following manner

$$\delta_i = \gamma(t_i) \quad (3.69)$$

$$\gamma(t) = a/(t + A) \quad (3.70)$$

$$t_{i+1} = \max(t_i + f(X_i), 0) \quad (3.71)$$

$$f(x) = f_{\min} + \frac{f_{\max} - f_{\min}}{1 - (f_{\max}/f_{\min})e^{-x/\omega}} \quad (3.72)$$

with $f_{\max} > 0$, $f_{\min} < 0$, and $\omega > 0$. Free parameters are a , A , t_0 , however, Ref. [19] suggests $A = 20$ and $t_0 = t_1 = A$ for universal usage.

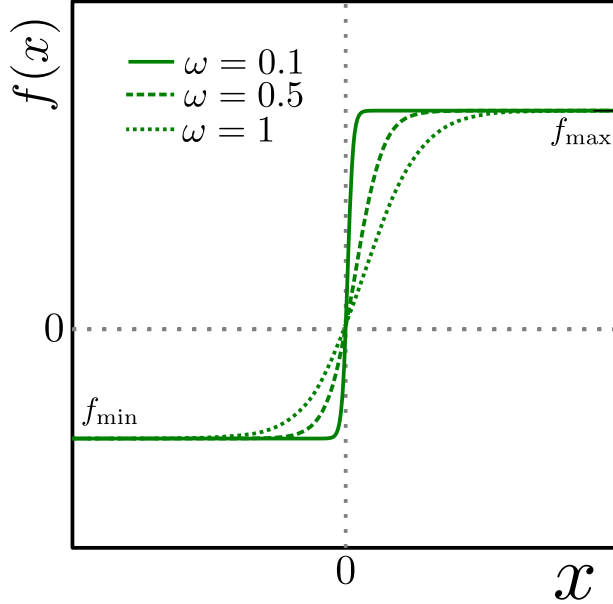


Figure 3.6: Examples of $f(X_i)$ as published in ref. [19]. As $\omega \rightarrow 0$, $f(x)$ approaches a step function.

Notice that the step length increase if t_i decrease and vice-versa. A smaller step length is sought for regions close to the minimum. The function of $f(x)$ is to alter the step length by changing the trend of t . If we are close to the minimum, a smaller step length is sought, and hence t must increase. We know from previous discussion, that if the sign of the gradient change, we have crossed the minimum. Crossing the minimum with ASGD has the following consequence

- Eq. (3.68): The value of X_i will be positive.
- Eq. (3.72): $f(X_i)$ will return a value in $[0, f_{\max}]$ depending on the magnitude of X_i .
- Eq. (3.71): The value of t will increase, i.e. $t_{i+1} > t_i$.
- Eq. (3.70): The step length will decrease.

The second step regarding $f(X_i)$ can be visualized in Fig. 3.6.

Assumptions

- The statistical error in the sampled gradients are distributed with zero mean.

This is shown in ref. [19] to be true; they are normally distributed. The implication is that upon combining gradient estimates for N different processes, the accumulative error will tend to zero quickly.

- The step length $\gamma(t)$ is a positive monotone decreasing function defined on $[0, \infty)$ with maximum at $t = 0$.

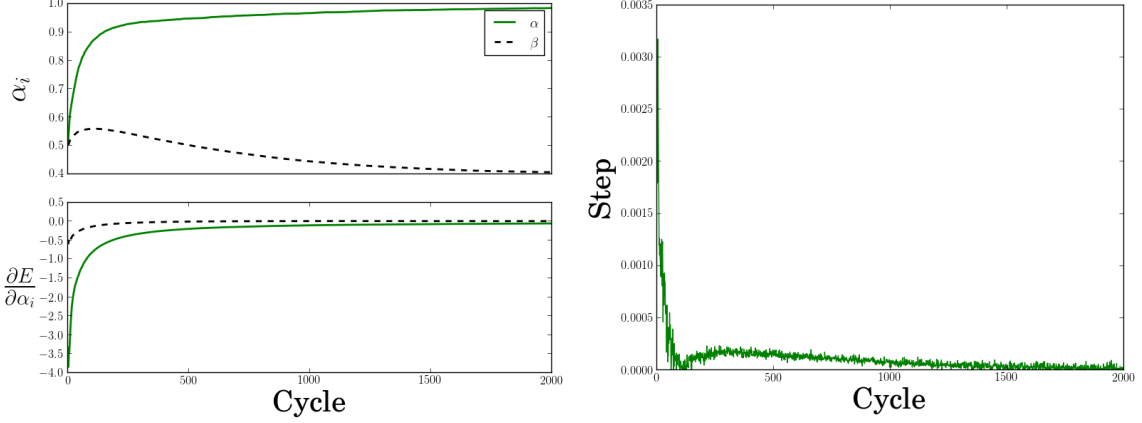


Figure 3.7: Results of Adaptive Stochastic Gradient Descent used on a two-particle Quantum Dot with unit oscillator frequency using 400 cycles pr. gradient sampling and 40 independent walkers. The right figure shows the evolution of the time step. The left figure shows the evolution of the variational parameters α and β introduced in Section 3.5 on top, and the evolution of the gradients on the bottom. The gradients are cycle averaged to reveal the pattern underlying the noise. We clearly see that they tend to zero, β somewhat before α . The step rushes to zero; we get a small rebound in the step after forcing it zero as it attempts to cross to negative values.

With $\gamma(t)$ being as in Eq (3.70), this is easily shown.

- The function $f(x)$ is continuous and monotone increasing with $f_{\min} = \lim_{x \rightarrow \infty} f(x)$ and $f_{\max} = \lim_{x \rightarrow -\infty} f(x)$.

This is exactly the behavior displayed in Fig. 3.6.

These assumptions and several more are described in more detail in ref. [19]. They underline that the shape and flow of the algorithm is in no way random; ASGD is optimizing minimization of stochastic quantities.

Implementation

A flow chart of the implementation is given in Fig. 3.8. For specific details regarding the implementation, i refer to the code [6]. An example of minimization using ASGD is given in Fig. 3.7.

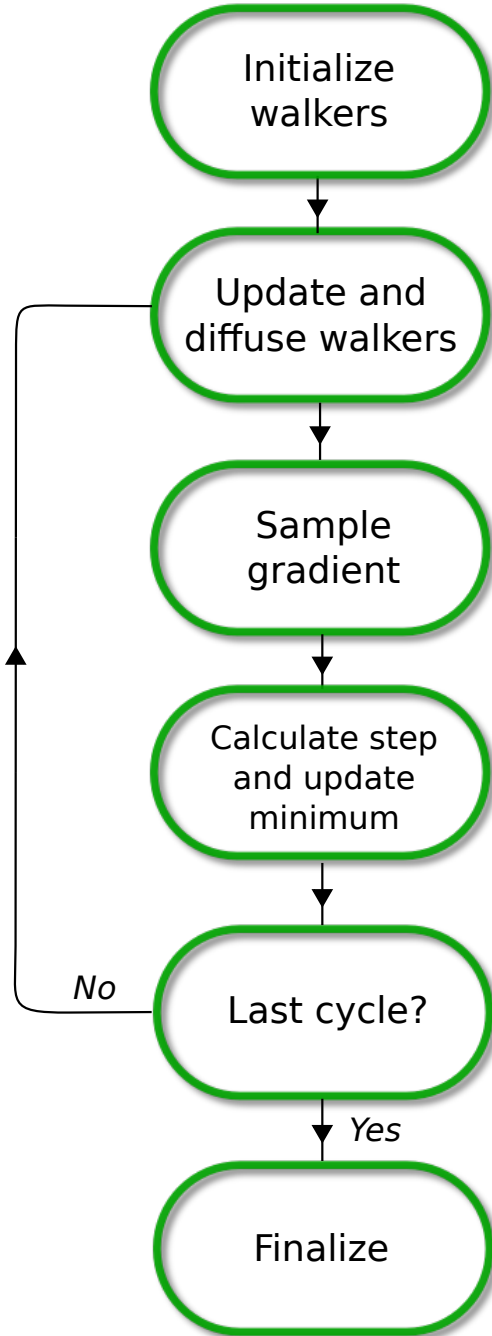


Figure 3.8: Chart flow of ASGD algorithm. Diffusing a walker is done as described in Fig. 3.1. Updating the walkers involves recalculating any values afflicted by updating the minimum. The step is calculated by Eq. (3.70). In case of Quantum Monte-Carlo, the gradient is sampled by Eq. (3.62).

3.7 Variational Monte-Carlo

As briefly mentioned in the derivation of the Quantum Monte-Carlo projection process, neglecting the branching term, i.e. force $G_B = 1$, leaves us with a method called Variational Monte-Carlo (VMC). The naming is due to the fact that the method is variational; it supplies as upper bound for the exact ground state energy (see Section 3.5.5). The better the trial wave function, the better the answer.

Without the branching term, the optimal converged state of the Markov Chain is to span that of the trial wave function. From the flow chart of the VMC algorithm in Fig. 3.9, it is clear that VMC corresponds to nothing but a standard Monte-Carlo integration of the local energy, using the trial wave function for distributing the points.

3.7.1 Motivating the use of Diffusion Theory

The question becomes: Why bother with all the diffusion theory if the result is simply an expectation value? From statistics we know that we may use *any* distribution when calculating an expectation value. Why bother with a trial wave function, thermalization, etc.?

The reason is simple, yet not obvious. The quantity of interest, the local energy, is *dependent on a wave function* $\psi(x)$. It is not necessarily smooth, and even though the wave functions tend to zero at infinities, the local energy is *undefined*; a “0/0” expression (see Eq. (3.73)). This is the case for all the roots of $\psi(x)$. Given an arbitrary distribution $P(x)$, we get

$$\begin{aligned} E_{\text{VMC}} &= \int P(x) \frac{1}{\psi(x)} \hat{\mathbf{H}}\psi(x) dx \\ &\simeq \frac{1}{n} \sum_{i=1}^n \frac{1}{\psi(x_i)} \hat{\mathbf{H}}\psi(x_i), \end{aligned} \quad (3.73)$$

where the points x_i are drawn from the distribution $P(x)$.

We *need* to importance sample the integral with the distribution corresponding to that of the wave function used in the local energy in order to solve the integral in a satisfying manner, that is, avoid sampling close to the roots of $\psi(x)$ without “cheating”. Introducing importance sampling is done by simply switching distributions (we do not need to scale the sampled function, we are computing an expectation value, not an arbitrary integral).

$$P(x) = |\psi(x)|^2$$

Suggesting new positions (diffusion) boils down to be analogous to calling a *random number generator* corresponding to our trial wave function squared distribution. The problem was the roots of $\psi(x)$, however, the distribution of points now share these roots, i.e. the probability of sampling a point where the local energy is undefined equals zero.

$$\psi(x_m) = 0 \implies P(x_m) = 0 \quad (3.74)$$

In other words, the more undefined the energy is at a point, the less probable the point is. That is what we need, and it’s what all the theory of Quantum Monte-Carlo safely delivers that standard Monte-Carlo can not.

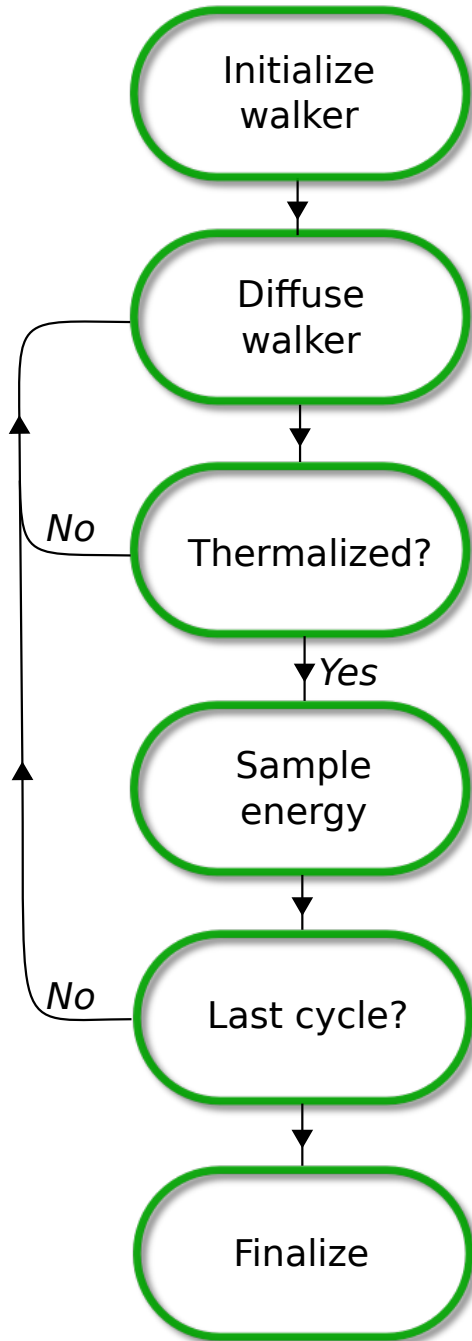


Figure 3.9: Chart flow of the Variational Monte-Carlo algorithm. The second step, *Diffuse Walker*, is the process described in Fig. 3.1. Energies are sampled as described in Section 3.5.3. Thermalization is usually set to a fixed number of cycles.

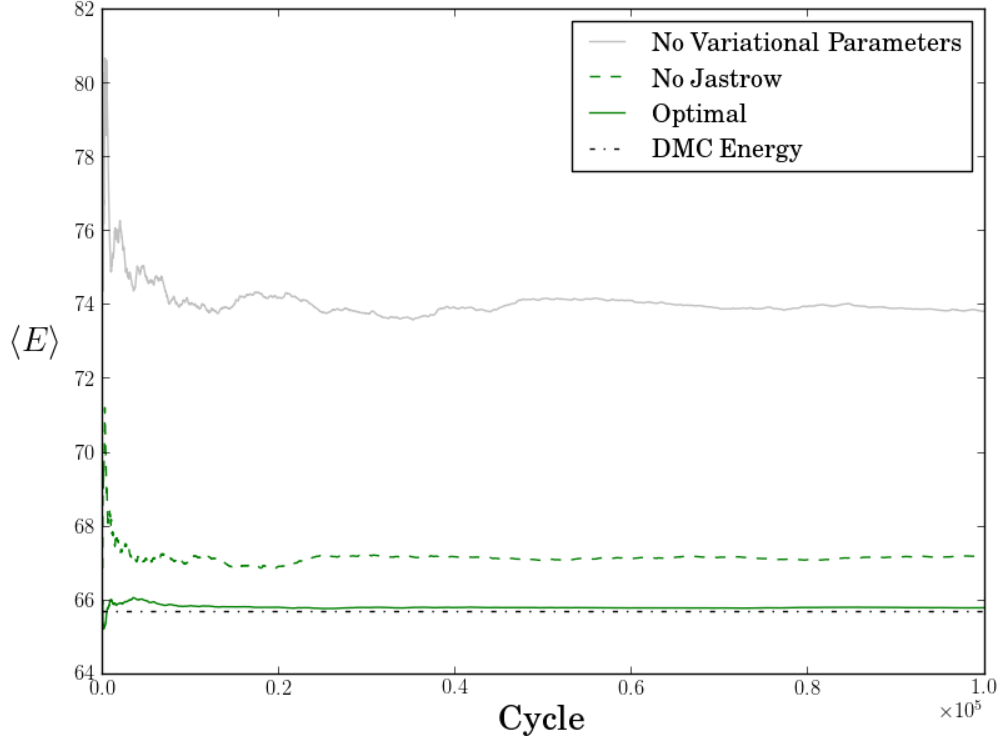


Figure 3.10: Comparison of the VMC energy using different trial wave functions. The DMC energy is believed to be very close to the exact ground state. We see that adding a variational parameter to the trial wave function lowers the energy somewhat, however, when adding the Jastrow factor described in Section 3.5.2 we get very close to the “exact” answer. Lower energy means a better energy when dealing with variational methods. In this example, a 12 particle Quantum Dot is used.

3.7.2 Implementation

Variational Monte-Carlo does not benefit much from an increase of samples (beyond a given point, that is). It is much more important that the system is thermalized, than that the number of walkers are high, or the final amount of samples are huge. It is therefore sufficient to use a single walker pr. VMC process.

The single walker is initialized in a normal distributed manner (with variance $2D\delta\tau$), and released to diffuse according to the process in Fig. 3.1. A flow chart of the VMC algorithm is given in Fig. 3.9. Finalizing the sampling involves scaling energies, calculating the variance, etc.

For details regarding specific implementations, I refer to the code in ref. [6].

3.7.3 Limitations

The only limitation in VMC is the choice of trial wave function. This makes VMC extremely robust; it will *always* produce a result. As the overlap C_0 in Eq. (3.5) approach unity, the VMC energy approaches the exact ground state energy as a monotone decreasing function. Fig. 3.10 described this effect.

3.8 Diffusion Monte-Carlo

Applying the full diffusion framework introduced in the previous sections results in a method known as Diffusion Monte-Carlo (DMC)⁵. Diffusion Monte-Carlo results are often referred to as *exact*, in the sense that it is overall one of the most precise many-body methods. Where other many-body methods run into the *curse of dimensionality* (CPU-time exponentially increasing with number of particles, precision, etc.), DMC with its position basis Quantum Monte-Carlo formalism does not. With DMC, it is simply a matter of evaluating a more complicated trial wave function, or simulating for a longer period, in order to reach convergence to the “exact” ground state in a satisfactory way.

3.8.1 Implementation

DMC is a precise method; more statistics is like water in a desert - you can not get enough of it. In addition, branching is a major part of the algorithm. In other words: DMC uses a large ensemble of walkers to generate enormous amounts of statistics. These walkers are initialized using a VMC calculation, i.e. the walkers are distributed according to the trial wave function at $\tau = 0$.

There are three layers of loops in the DMC method implemented in this thesis. Normally one would only use two: The time-step and walker loops, however, introducing a third *block loop* within the walker loop will boost convergence dramatically. This loop continues until the current walker is either dead, or diffused n_b times. Using this method, “good” walkers will have multiple offspring per cycle, while “bad” walkers will rarely survive the block loop. Perfect walkers will supply a ton of statistics as they surf through all the loops without branching ($G_B \sim 1$).

A flow chart of the DMC algorithm is given in Fig. 3.11.

3.8.2 Sampling the Energy

Unlike VMC, DMC does not weigh all walkers equally. It is therefore necessary to weigh each walker’s contribution to a cumulative energy sampling accordingly, that is, with the branching Green’s function. Let E_k denote the cumulative energy for time-step k , n_w be the number of walkers in our system at time-step k , $\tilde{n}_{b,i}$ be the number of blocks walker i survives, and let $W_i(\vec{r}, \tau)$ represent walker i . Then we have

$$E_k = \frac{1}{n_w} \sum_{i=1}^{n_w} \frac{1}{\tilde{n}_{b,i}} \sum_{l=1}^{\tilde{n}_{b,i}} G_B(W_i(\vec{r}, \tau_k + l\delta\tau)) E_L(W_i(\vec{r}, \tau_k + l\delta\tau)) \quad (3.75)$$

As the formalism required, setting $G_B = n_w = n_b = 1$ reproduce the VMC algorithm.

The new trial energy (remember Eq. (3.7)) is set to be

$$E_T = E_k \quad (3.76)$$

The DMC energy is updated each cycle to be the trailing average of the trial energies

$$E_{\text{DMC}} = \overline{E_T} = \frac{1}{n} \sum_{k=1}^n E_k \quad (3.77)$$

⁵In literature, DMC is also known as *Projection Monte-Carlo*, for reasons described in Section 3.1.1.

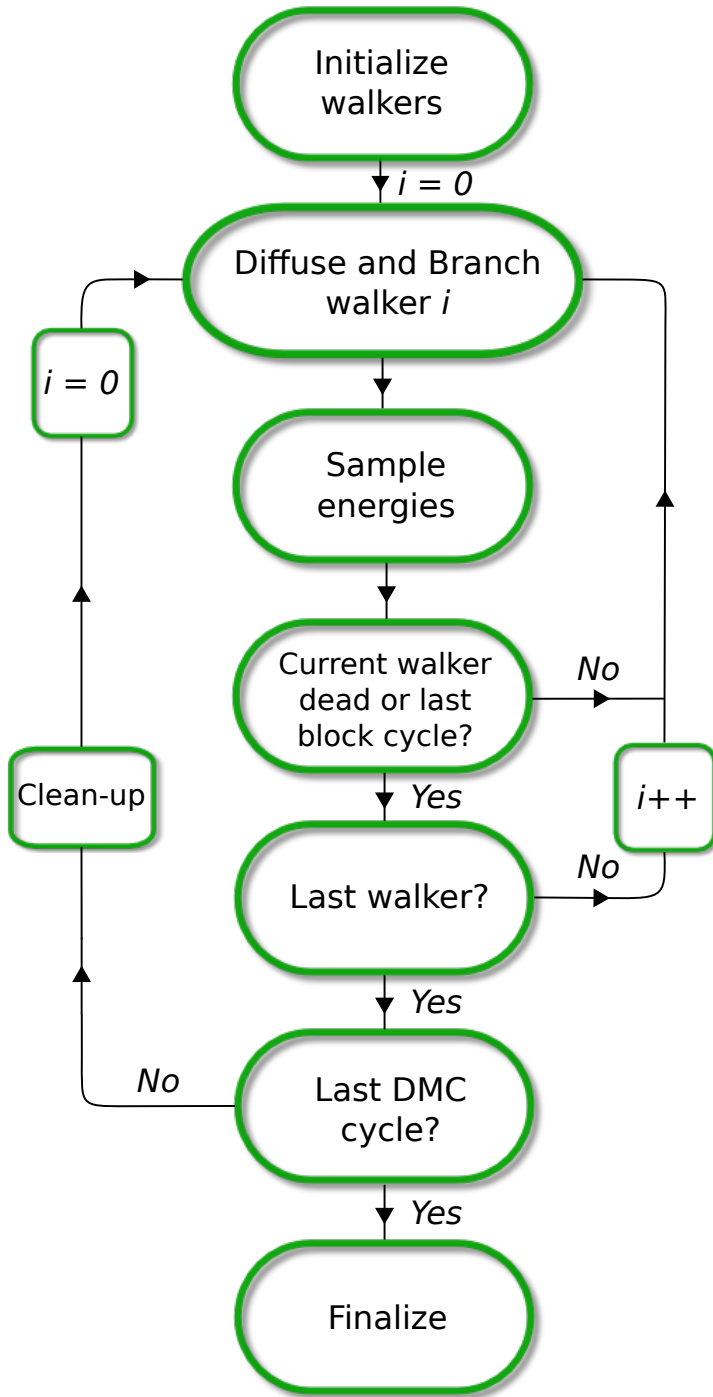


Figure 3.11: Chart flow of the Diffusion Monte-Carlo algorithm. The count variable i is the index of the walker loop. The second step, *Diffuse and Branch Walker*, is the process described in Fig. 3.1 in combination with the branching from Fig. 3.2. Energies are sampled as described in Section 3.8. Thermalization is not done in the same way as VMC (see Fig. 3.9), but rather includes the entire flow with a reduced number of DMC - and block cycles.

3.8.3 Limitations

By introducing the branching term, DMC is a far less robust method compared to VMC. Action must be taken in order to stabilize the iterations through tuning of parameters such as population size, time-step, block size, etc. This is the disadvantage of DMC compared to other many-body methods such as Coupled Cluster, which is far more *Plug and Play*.

Time Step Errors

The error introduced by the short time approximation goes as $\mathcal{O}(\delta\tau^2)$ (see Eq. (3.15)). There is a second error related to the time-step, arising from the fact that not all steps are accepted by the Metropolis algorithm. This introduces an effective reduction in the time step, and is countered by scaling the time step with the acceptance ratio upon calculating G_B . However, DMC is rarely used without importance sampling (Fokker-Planck), which, due to the Quantum Force, has an acceptance ratio ~ 1 . It is therefore common to ignore this problem, and use a sufficiently low time step.

Selecting the Time-step

Studying the branching Green's function in more detail reveals that its magnitude increase exponentially with the spread of the energies

$$G_B \propto \exp(\Delta E \delta\tau) \quad (3.78)$$

As will be shown in Section 3.10.1, the spread in energy samples are higher the worse of an approximation to the ground state our trial wave function becomes. In addition, the magnitude of the spread scales with the magnitude of the energy. Due to finite computer memory, we have N slots dedicated for storing walkers on every node. Too large branching factors may cause the system to max out the memory on one node before the walkers can be redistributed across all the nodes.

The solution is to balance out the increase in ΔE by lowering the time-step accordingly. However, too low a time-step will hinder DMC to evolve walkers. Every time we perform a time-step without having the trial energy close to the exact energy, we introduce an error to the Quantum Monte-Carlo equations (remember the transition from Eq. (3.5) to Eq. (3.7)). It is therefore necessary to have rapid convergence down to a sufficiently low energy level, where the magnitude of the exact energy error matches those of the other systematic errors.

Another source of error is due to the *fixed node approximation*. This approximation will be covered in the next section.

3.8.4 Fixed node approximation

Looking at Eq. (3.49), we notice that by choosing positive phases for our single particle wave functions, the bosonic many body wave function is exclusively positive. For fermions however, the sign change upon permuting a particle pair introduces the possibility that the wave function will have both negative and positive regions, independent of our choice of phases in the single particle wave functions.

As we simulate importance sampled DMC in time, the density of walkers at a given time, $P(x, \tau)$, is given by Eq. (3.5) multiplied by the trial wave function (see the end of Section 3.1.4 for details)

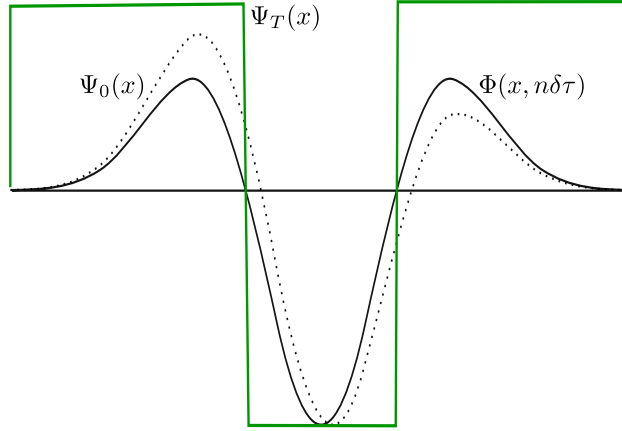


Figure 3.12: An illustration of the fixed node approximation. The dotted line is the exact ground state $\Psi_0(x)$. The distribution of walkers at cycle n , $\Phi(x, n\delta\tau)$, similar in shape with $\Psi_0(x)$, however, sharing nodes with the trial wave function $\Psi_T(x)$ (box-like function for illustration purposes), and thus making it impossible to match the true ground state exactly.

$$P(x, \tau) = \Phi(x, \tau)\Psi_T(x), \quad (3.79)$$

where

$$\lim_{\tau \rightarrow \infty} P(x, \tau) = \Phi_0(x)\Psi_T(x), \quad (3.80)$$

which, if interpreted as a density, should always be greater than zero. In the case of Fermions, this is not guaranteed, as the node structure, i.e. the roots, of the exact ground state and the trial wave function will generally be different.

To avoid this anomaly in the density, $\Phi(x, \tau)$ and $\Psi_T(x)$ have to change sign together⁶. The brute force way of solving this problem is to *fix* the nodes by rejecting a walker's step if the trial wave function changes sign:

$$\frac{\Psi_T(x_i)}{\Psi_T(x_j)} < 0 \implies A(i \rightarrow j) = 0 \quad (3.81)$$

where $A(i \rightarrow j)$ is the probability of accepting the move, as described in Section 3.3. An illustrative example is attempted in Fig. 3.12.

3.9 Estimating the One-body Density

The one-body density is defined as

⁶It should be mentioned that more sophisticated methods exist for dealing with the sign problem, some of which splits the distribution of walkers into a negative and a positive region.

$$\rho_\Phi(\mathbf{r}_1) = \iint_{\mathbf{r}_2 \mathbf{r}_3} \dots \int_{\mathbf{r}_N} |\Phi(\mathbf{r}_1 \mathbf{r}_2 \dots \mathbf{r}_N)|^2 d\mathbf{r}_2 \dots d\mathbf{r}_N. \quad (3.82)$$

Due to the indistinguishable nature of the particles, the integral above corresponds to projecting every degree of freedom into a single configuration. In a Monte-Carlo simulation, estimating this quantity is done by collecting snapshots of the position data. These snapshots serve as samples to a histogram where each set of Cartesian coordinates (independent of particle number) give rise to one count on the grid.

3.9.1 Estimating the Exact Ground State Density

The one-body density of the trial wave functions is in other words trivial; create a histogram of sampled VMC positions. The challenge is estimating the one-body density of the exact wave function, given a set of DMC data. As described in Section 3.1.4, the distribution of walkers are designed to span $f(\mathbf{r}, \tau) = \Phi(\mathbf{r}, \tau)\Psi_T(\mathbf{r})$, which does not correspond to the ground state distribution unless the trial wave function is indeed the exact ground state.

In other words: We need a method to transform a given estimate from the *mixed estimate* (using $f(\mathbf{r}, \tau)$) into the *pure estimate* using the ground state distribution $|\Phi_0(\mathbf{r})|^2$. This is done by using a third estimate obtained from VMC, the *variational estimate*, which is the estimate sampled from $|\Psi_T(\mathbf{r})|^2$. It is shown in ref. [9] that the relation is

$$\begin{aligned} \langle A \rangle_0 &= \frac{\langle \Phi_0 | \hat{\mathbf{A}} | \Phi_0 \rangle}{\langle \Phi_0 | \Phi_0 \rangle} \simeq 2 \frac{\langle \Phi_0 | \hat{\mathbf{A}} | \Psi_T \rangle}{\langle \Phi_0 | \Psi_T \rangle} - \frac{\langle \Psi_T | \hat{\mathbf{A}} | \Psi_T \rangle}{\langle \Psi_T | \Psi_T \rangle} + \mathcal{O}(\Delta^2) \\ &= 2\langle A \rangle_{\text{DMC}} - \langle A \rangle_{\text{VMC}} + \mathcal{O}(\Delta^2) \end{aligned} \quad (3.83)$$

where $\Delta \equiv \Phi_0(\mathbf{r}) - \Psi_T(\mathbf{r})$. Expressed in terms of *density operators*, the expectation values becomes

$$\begin{aligned} \langle A \rangle_0 &= \text{tr}(\hat{\rho}_0 \hat{\mathbf{A}}) \\ \langle A \rangle_{\text{VMC}} &= \text{tr}(\hat{\rho}_{\text{VMC}} \hat{\mathbf{A}}) \\ \langle A \rangle_{\text{DMC}} &= \text{tr}(\hat{\rho}_{\text{DMC}} \hat{\mathbf{A}}) \end{aligned}$$

where tr denotes the *trace* (sum of eigenvalues. Read more in ref. [8]). Inserting these equation into Eq. (3.83) yields

$$\begin{aligned} \text{tr}(\hat{\rho}_0 \hat{\mathbf{A}}) &\simeq 2\text{tr}(\hat{\rho}_{\text{DMC}} \hat{\mathbf{A}}) - \text{tr}(\hat{\rho}_{\text{VMC}} \hat{\mathbf{A}}) + \mathcal{O}(\Delta^2) \\ &\simeq \text{tr}\left((2\hat{\rho}_{\text{DMC}} - \hat{\rho}_{\text{VMC}}) \hat{\mathbf{A}}\right) + \mathcal{O}(\Delta^2) \end{aligned} \quad (3.84)$$

which leads to the conclusion that the mixed density can be transformed in the following manner

$$\hat{\rho}_0 \simeq 2\hat{\rho}_{\text{DMC}} - \hat{\rho}_{\text{VMC}} \quad (3.85)$$

In other words, combining the one-body densities from DMC and VMC according to Eq. (3.85) will give a good view of the exact one-body density.

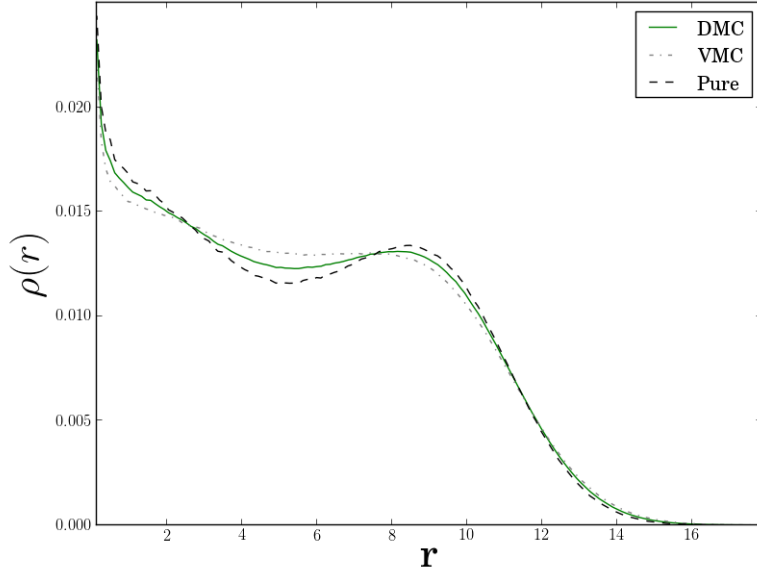


Figure 3.13: An example radial one-body density of a 12-particle Quantum Dot with $\omega = 0.1$. The one-body density is flat in for VMC in comparison to DMC. The pure density calculated from Eq. (3.85) transforms the mixed density $f(\mathbf{r}, \tau) = \Phi(\mathbf{r}, \tau)\Psi_T(\mathbf{r})$ from DMC into $|\Phi(\mathbf{r}, \tau)|^2$ with very small errors. The density diverges close to zero due to a “ $\frac{0}{0}$ ” expression (see Eq. (3.88)).

3.9.2 Radial Densities

In the case of symmetric wave functions, like in the case for Helium and Quantum Dots, the radial one-body density is obtained by integrating out the angular dependencies of the one-body density. This corresponds to weighing all angular directions equally in a brute force average and should only be applied to angular symmetric systems.

Calculating the integral in two and three dimensions yields

$$\begin{aligned} I_{3D} &= \iint \rho(r_1, \theta_1, \phi_1) r_1^2 \sin \theta_1 d\theta_1 d\phi_1 \\ &= r_1^2 \rho(r_1) \end{aligned} \quad (3.86)$$

$$\begin{aligned} I_{2D} &= \int \rho(r_1, \phi_1) r_1 d\phi_1 \\ &= r_1 \rho(r_1) \end{aligned} \quad (3.87)$$

In practice, this integral is calculated by creating a histogram $H(r)$ of sampled radii. Transforming this histogram into the radial one-body density $\rho(r_1)$ is according to Eq. (3.86) and Eq. (3.87) done in the following manner

$$\rho(r_1) = \frac{H(r_1)}{r_1^{(d-1)}} \quad (3.88)$$

where d denotes the number of dimensions. An example radial one-body density is given in Fig. 3.13

3.10 Estimating the Statistical Error

As with any statistical result, appropriate statistical errors needs to be included for it to be taken seriously. Systematic errors, that is, errors introduced due to limitations in the model, will be discussed in each method's respective section. Statistical errors, that is, the deviation from the true ensemble average due to the fact that we can never fulfill the equality in Eq. (3.59), can be estimated using several methods, some of which are *naive* in the sense that they assume the dataset to be completely *uncorrelated*.

3.10.1 The Variance and Standard Deviates

Given a set of samplings, e.g. local energies, the variance is a measure of their spread from the true mean value

$$\begin{aligned}\text{Var}(E) &= \langle (E - \langle E \rangle)^2 \rangle \\ &= \langle E^2 \rangle - 2 \underbrace{\langle E \langle E \rangle \rangle}_{\langle E \rangle \langle E \rangle} + \langle E \rangle^2 \\ &= \langle E^2 \rangle - \langle E \rangle^2 \tag{3.89} \\ &\simeq \overline{E^2} - \overline{E}^2 \tag{3.90}\end{aligned}$$

In the case of having the exact wave function, i.e $|\Psi_T\rangle = |\Psi_0\rangle$, the variance becomes zero:

$$\begin{aligned}\text{Var}(E)_{\text{Exact}} &= \langle \Psi_0 | \hat{\mathbf{H}}^2 | \Psi_0 \rangle - \langle \Psi_0 | \hat{\mathbf{H}} | \Psi_0 \rangle^2 \\ &= E_0^2 - (E_0)^2 \\ &= 0\end{aligned}$$

The variance is in other words an excellent measure of how good a fit different trial wave functions are to the system. Note however, a common misconception is to use the numerical value of the variance to compare *different* systems; for instance, if system *A* has variance equal to half of system *B*'s, one could easily conclude that system *A* has the best fit. This is not true. The variance has units (in the case of local energies) energy squared, and will thus scale with the magnitude of the energy. One can only safely use the variance as a direct measure locally in each specific system, e.g. Beryllium simulations.

Another misconception is that the variance is a direct numerical measure of the error. This can in no way be true given that the units mismatch. The *standard deviation*, σ , is the square root of the variance,

$$\sigma^2(x) = \text{Var}(x), \tag{3.91}$$

and has hence a unit equal to that of the measured value. It is therefore related to the *spread* in the sampled value; zero deviation implies perfect samples, while increasing deviation means increasing spread and statistical uncertainty. The standard deviation is in other words a useful quantity when it comes to calculating the error, i.e. the expected deviation from the exact mean $\langle E \rangle$.

3.10.2 The Covariance and correlated samples

It was briefly mentioned in the introduction that certain error estimation techniques was too naive in case of correlated samples. Two samples, x, y , are said to be correlated if their *covariance*, $\text{Cov}(x, y)$, is non-zero

$$\begin{aligned}
 \text{Cov}(x, y) &\equiv \langle (x - \langle x \rangle)(y - \langle y \rangle) \rangle \\
 &= \langle xy \rangle - \langle x \rangle \langle y \rangle - \langle x \rangle \langle y \rangle + \langle x \rangle \langle y \rangle \\
 &= \langle xy \rangle - \langle x \rangle \langle y \rangle - \underbrace{\langle y \rangle \langle x \rangle}_{0} + \underbrace{\langle x \rangle \langle y \rangle}_{0} \\
 &= \langle xy \rangle - \langle x \rangle \langle y \rangle.
 \end{aligned} \tag{3.92}$$

Notice that $\text{Cov}(x, x) = \text{Var}(x)$. Using this definition, whether or not we have correlated samples boils down to whether or not $\langle xy \rangle = \langle x \rangle \langle y \rangle$.

The consequence of ignoring correlations is an error estimate which is generally less than the true error; correlated samplings are more clustered, i.e. less spread, due to previous samplings' influence on the value of the current sample. Denoting the true standard deviation as σ_c , the above discussion can be distilled to

$$\sigma_c(x) \geq \sigma(x), \tag{3.93}$$

where σ is the deviation from Eq. (3.91).

3.10.3 The Deviate from the Exact Mean

There is an important difference between the deviate from the exact mean, and the deviate of a single sample from it's combined mean, i.e.

$$\sigma(\bar{x}) \neq \sigma(x). \tag{3.94}$$

Imagine doing a number of simulations, each resulting in a unique \bar{x} , the quantity of interest is not the deviation within a single simulation, but the deviation between all the simulations.

$$m \equiv \bar{x} = \frac{1}{n} \sum_{i=1}^n x_i \tag{3.95}$$

$$\sigma^2(m) = \langle m^2 \rangle - \langle m \rangle^2 \tag{3.96}$$

Combining the above equations yields

$$\begin{aligned}
\sigma^2(m) &= \left\langle \frac{1}{n^2} \left[\sum_{i=1}^n x_i \right]^2 \right\rangle - \left\langle \frac{1}{n} \sum_{i=1}^n x_i \right\rangle^2 \\
&= \frac{1}{n^2} \left(\left\langle \sum_{i=1}^n x_i \sum_{j=1}^n x_j \right\rangle - \left\langle \sum_{i=1}^n x_i \right\rangle \left\langle \sum_{j=1}^n x_j \right\rangle \right) \\
&= \frac{1}{n^2} \sum_{i,j=1}^n \langle x_i x_j \rangle - \langle x_i \rangle \langle x_j \rangle \\
&= \frac{1}{n^2} \sum_{i,j=1}^n \text{Cov}(x_i, x_j)
\end{aligned} \tag{3.97}$$

This result is important; the true error is given in terms of the covariance, and is, as discussed previously, only equal to the sample variance if our samples are uncorrelated. Going back to the definition of covariance in Eq. (3.92), we see that in order to calculate the covariance as in Eq. (3.97), we need to know the true mean $\langle x_i \rangle$. Using $m = \bar{x}$ as an approximation to the true mean yields

$$\begin{aligned}
\text{Cov}(x_i, x_j) &\equiv \langle (x_i - \langle x_i \rangle)(x_j - \langle x_j \rangle) \rangle \\
&\simeq \langle (x_i - m)(x_j - m) \rangle \\
&\simeq \frac{1}{n^2} \sum_{k,l=1}^n (x_k - m)(x_l - m)
\end{aligned} \tag{3.98}$$

$$\equiv \frac{1}{n} \text{Cov}(x) \tag{3.99}$$

Inserting this relation into Eq. (3.97) yields

$$\begin{aligned}
\sigma^2(m) &= \frac{1}{n^2} \sum_{i,j=1}^n \text{Cov}(x_i, x_j) \\
&\simeq \frac{1}{n^2} \sum_{i,j=1}^n \frac{1}{n} \text{Cov}(x) \\
&= \frac{1}{n^3} \text{Cov}(x) \sum_{i,j=1}^n \underbrace{\phantom{\sum_{i,j=1}^n}}_{n^2} \\
&= \frac{1}{n} \text{Cov}(x),
\end{aligned} \tag{3.100}$$

which serves as an estimate of the full error including correlations.

Explicitly computing the covariance is rarely done in Monte-Carlo simulations; if the sample size is large, it is extremely expensive. A variety of alternative methods to counter the correlations are available, the simplest of which is to define a *correlation length*, τ^7 , which defines an interval at which points from the sampling sets are used for actual averaging. In other words, only the points $x_0, x_\tau, \dots, x_{n\tau}$ are used in the calculation of \bar{x}

⁷This parameter is often referred to as the *auto-correlation time* in the literature.

$$\bar{x} = \frac{1}{n} \sum_{k=0}^n x_{k\tau} \quad (3.101)$$

This basically means that we need $n\tau$ samples in order to get the same magnitude of samples to our average as in Eq. (3.95); the *effective sample size* becomes $n_{\text{eff}} = n_{\text{tot}}/\tau$. $\tau = 1$ defines the uncorrelated case. For details regarding the derivations of τ based on the covariance, see ref. [20] and ref. [13].

3.10.4 Blocking

Introducing correlation lengths in the system solver is not an efficient option. Neither is calculating the covariance of billions of data points. However, the error is not a value vital to the simulation process, i.e. you do not need to know the error at any stage during the sampling. This means that we can post process the error calculation (given that we store the data sets).

An efficient algorithm for calculating the error of correlated data is *blocking*. This method is described in high detail in ref. [20], however, details aside, the idea itself is quite intuitive: Given a data set of N samples from a single Monte-Carlo simulation, imagine dividing the dataset into *blocks* of n samples, that is, blocks of size $n_b = N/n$. The error σ_n in each block will increase as n decrease, (see Eq. (3.100))

$$\sigma_n \propto \frac{1}{\sqrt{n}} \quad (3.102)$$

However, treating each block as an individual simulation, we have n_b averages m_n that we can use to calculate the total error in Eq. (3.96), that is, estimate the covariance

$$\overline{m_n^r} \equiv \frac{1}{n_b} \sum_{k=1}^{n_b} m_n^r \quad (3.103)$$

$$\begin{aligned} \sigma^2(m) &= \langle m^2 \rangle - \langle m \rangle^2 \\ &\simeq \overline{m_n^2} - (\overline{m_n})^2 \end{aligned} \quad (3.104)$$

The approximation should hold for a range of different block sizes, however, just as there is no a priori way of telling the correlation length, there is no a priori way of telling how many blocks is needed. What we do know however, is that if the system is correlated, there should be a range of different block sizes which fulfill Eq. (3.104) to reasonable precision. The result of a blocking analysis is therefore a series of $(n, \sigma(m))$ pairs. Plotting these pairs should in light of previous arguments result in a increasing curve which stabilizes over a certain span of block sizes. This plateau will then serve as a reasonable approximation to the covariance. See Fig. 3.14 for a demonstration of the blocking technique.

3.10.5 Variance Estimators

The standard intuitive variance estimator given by

$$\sigma^2(x) \simeq \frac{1}{n} \sum_{i=1}^n (x_i - \bar{x})^2 = \left(\frac{1}{n} \sum_{i=1}^n x_i^2 \right) - \bar{x}^2 \quad (3.105)$$

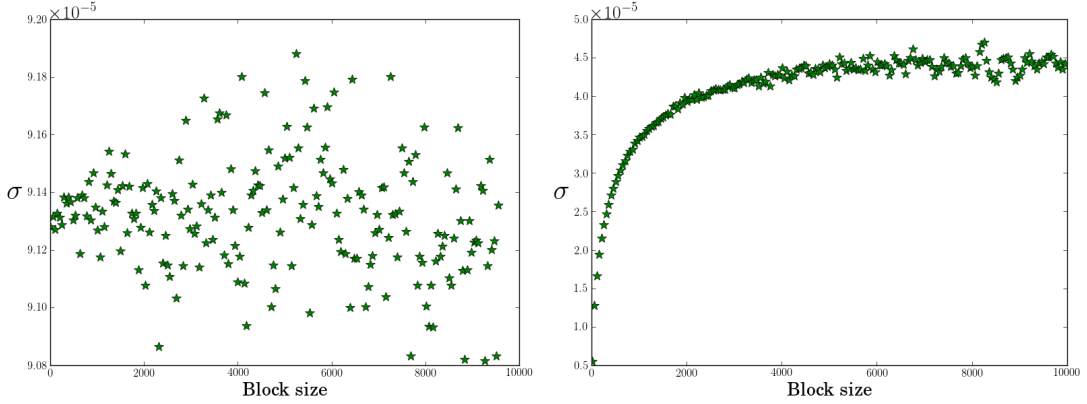


Figure 3.14: Left hand side: Blocking result of (approximately) uncorrelated data generated from a uniform Monte-Carlo integration of $\int_1^2 2x dx$ resulting in 3.00003 (exact is 3.0). This is in excellent agreement with the magnitude of the error $\sim 9 \cdot 10^{-5}$. On the right hand side we have the blocking result (DMC) for 6-particle $\omega = 0.1$ Quantum Dot, used in Table 5.3. We clearly see the plateau discussed in the blocking section, resulting in a total error in the range of $4.5 \cdot 10^{-5}$ to $5 \cdot 10^{-5}$.

is just an example of a variance estimator. A more precise estimator is

$$\sigma^2(x) \simeq \frac{1}{n-1} \sum_{i=1}^n (x_i - \bar{x})^2 = \left(\frac{1}{n-1} \sum_{i=1}^n x_i^2 \right) - \frac{n}{n-1} \bar{x}^2 \quad (3.106)$$

which is only noticeably different from Eq. (3.105) when the sample size gets small, as in blocking analysis. It is therefore standard to use Eq. (3.106) for blocking errors.

4

Generalization and Optimization

There is a big difference in strategy between writing code for a specific problem, and creating a general solver. A general Quantum Monte-Carlo solver involves several layers of complexity, such as support for different potentials, single particle bases, sampling models, etc., which may easily lead to a combinatoric disaster if the planning is not done right.

This chapter will cover the underlaying assumptions and goals in Section 4.1, the ..

4.1 Underlying Assumptions and Goals

Thousands of lines of code should be written once and for all¹. This section will cover the assumptions made and the goals set, preliminary to the coding process.

4.1.1 Assumptions

The code scheme was laid down based on the following assumptions

- (i) The constituents of the simulated systems are either pure fermionic or pure bosonic.
- (ii) A fermionic system is a two-level system described by one Slater determinant pr. spin eigenvalue^a.
- (iii) The trial wave function of a fermionic system is a single determinant.
- (iv) A bosonic system is modeled by all particles being in the same assumed single particle ground state.

^aThe actual code is developed to easily add support for n -level systems.

Other assumptions, such as the time-independence of the Hamiltonian, arise due to the QMC solver, not the specific implementation, and are hence covered in Chapter 3.

¹This, however, is rarely the case. The code used in this thesis has been completely restructured four times.

4.1.2 Generalization Goals

The implementation should be general for:

- (i) Fermions and Bosons.
- (ii) Anisotropic- and isotropic diffusion, i.e. Brute Force - or Importance sampling.
- (iii) Different minimization algorithms.
- (iv) Any Jastrow factor.
- (v) Any error estimation algorithm.
- (vi) Any single particle basis, including expanded single particle bases.
- (vii) Any combination of any potentials.

In addition, the following constraint is set on solvers:

- (viii) Full numerical support for all values involving derivatives.

The challenge is, despite the vast array of combinations, to preserve simplicity and structure as layers of complexity are added. If-testing inside the solvers in order to achieve generalization are in other words out of the question (see the next section).

4.1.3 Optimization Goals

Designed for the CPU, runtime optimizations are favored over memory optimizations. The following list may appear short, but every step brings immense amounts of complexity to the implementation

- (i) Identical values should never be re-calculated.
- (ii) Generalization should not be achieved through if-tests in repeated function calls, but rather through polymorphism (see Section 2.2.3).
- (iii) Linear scaling of runtime and number of CPUs for large simulations.

4.2 Specifics Regarding Generalization

Generalization is achieved through the use of deep object orientation, i.e. polymorphism, rather than if-testing. These concepts are described in Section 2.2. The assumptions listed in Section 4.1.1 are applied if not otherwise is stated.

For details regarding the implementation of methods, see the code in [6].

4.2.1 Generalization Goals (i)-(vii)

As discussed in Section 3.5.1, the mathematical difference between fermions and bosons (of importance to QMC) is how the many-body wave functions are constructed from the single-particle basis. In the case of fermions, the expression is given in terms of two Slater determinants, while for bosons, it is simply the product of all states.

```

1 double Fermions::get_spatial_wf(const Walker* walker) {
2     using namespace arma;
3
4     //Spin up times Spin down (determinants)
5     return det(walker->phi(span(0, n2 - 1), span())) * det(walker->phi(span(n2, n_p - 1),
6     span()));
}

```



```

1 double Bosons::get_spatial_wf(const Walker* walker) {
2
3     double wf = 1;
4
5     //Using the phi matrix as a vector in the case of bosons.
6     //Assuming all particles to occupy the same single particle state (neglecting
7     //permutations).
8     for (int i = 0; i < n_p; i++) {
9         wf *= walker->phi(i);
10    }
11
12    return wf;
13 }
```

Fermion/Boson overloaded pure virtual methods exist for all methods involving evaluation of the many body wave function, e.g. the spatial ratio and the Laplacian sum. When the QMC solver asks the `System*` object for a spatial ratio, depending on whether Fermions or Bosons are loaded run-time, the Fermion or Boson spatial ratio is evaluated.

This way of splitting the system class also takes care of optimization goal (ii) in Section 4.1.3 regarding no use of repeating if-tests.

Similar polymorphic splitting is introduced in the following classes:

- **Orbitals** Hydrogen orbitals, harmonic oscillator, etc.
- **BasisFunctions** Stand-alone single particle wave functions. Initialized by **Orbitals**.
- **Sampling** Brute force - or importance sampling.
- **Diffusion** Isotropic or Fokker-Planck. Automatically selected by **Sampling**.
- **ErrorEstimator** Simple or Blocking.
- **Jastrow** Padé Jastrow - or no Jastrow factor.
- **QMC** VMC or DMC.
- **Minimizer** ASGD. Support for adding additional minimizers.

Implementing a new Jastrow Factor done simply by creating a new subclass of **Jastrow**: Simple yet versatile. For more details, see Section 2.2. The splitting done in **QMC** is done to avoid rewriting a lot of general QMC code.

A detailed description of the generalization of potentials (point (vii)) is given in Section 2.2.3.

4.2.2 Generalization Goal (vi) and Expanded bases

An expanded single particle basis is implemented as a subclass of the **Orbitals** superclass. It is designed as a wrapper to an **Orbitals** subclass containing basis elements $\phi_\alpha(r_j)$. In addition to these elements, the class has a set of expansion coefficients $C_{\gamma\alpha}$ in which the new basis elements are constructed

$$\psi_\gamma^{\text{Exp.}}(r_j) = \sum_{\alpha=0}^{B-1} C_{\gamma\alpha} \phi_\alpha(r_j) \quad (4.1)$$

where B is the size of the expanded basis.

```

1 class ExpandedBasis : public Orbitals {
2 ...
3 ...
4 ...
5 protected:
6 ...
7     int basis_size;
8     arma::mat coeffs;
9     Orbitals* basis;
10 ...
11 //Hartree-Fock
12 void calculate_coefficients();
13 ...
14 };

```

In order to calculate the expansion coefficients, a *Hartree-Fock* solver has been implemented. For a given set of orbitals, e.g. harmonic oscillator, everything that is needed in order to obtain an expanded basis, is to implement expressions for the one-body - and two-body interaction elements.

The implementation of Eq. (4.1) are done by overloading the original **Orbitals.phi** method

```

1 double ExpandedBasis::phi(const Walker* walker, int particle, int q_num) {
2

```

```

3   double value = 0;
4
5   //Dividing basis_size by half assuming a two-level system.
6   //In case of Bosons, expanding s.p. w.f. does not make sense.
7   for (int m = 0; m < basis_size/2; m++) {
8     value += coeffs(q_num, m) * basis->phi(walker, particle, m);
9   }
10
11  return value;
12}
13

```

See Section [REF HF](#) for details regarding Hartree-Fock theory.

4.2.3 Generalization Goal (viii)

Functionality for evaluating derivatives numerically is important for two reasons; the first being debugging, the second being the cases where no closed-form expressions for the derivatives can be obtained².

As an example, `Orbitals.dell_phi`, which returns a single particle derivative, is virtual, and can be overloaded to call the numerical derivative implementation `Orbitals.num_diff`³. The same goes for the Jastrow factor and the variational derivatives in the minimizers. Similar implementations exist for the Laplacian.

The numerical implementations are finite difference schemes with error proportional to the squared step length.

4.3 Optimizations due to a Single two-level Determinant

Assumption (iii) unlocks the possibility to optimize the expressions involving the Slater-determinant dramatically. Similar optimizations for bosons due to assumption (iv) are considered trivial and will not be covered in detail. See the code in [6] for details regarding bosons.

The full trial wave function Ψ_T is given by Eq. (3.55). I will drop the function arguments to clean up the expressions. Written in terms of a spatial function $|D|$ and a Jastrow function J , we get

$$\Psi_T = |D^\uparrow||D^\downarrow|J \quad (4.2)$$

The Quantum Force becomes

$$\begin{aligned}
F_i &= 2 \frac{\nabla_i (|D^\uparrow||D^\downarrow|J)}{|D^\uparrow||D^\downarrow|J} \\
&= 2 \left(\frac{\nabla_i |D^\uparrow|}{|D^\uparrow|} + \frac{\nabla_i |D^\downarrow|}{|D^\downarrow|} + \frac{\nabla_i J}{J} \right) \\
&= 2 \left(\frac{\nabla_i |D^\alpha|}{|D^\alpha|} + \frac{\nabla_i J}{J} \right)
\end{aligned} \quad (4.3)$$

²In most cases they can, however, in some cases the expressions are so heavy that they are not practical to use.

³An alternative would be to perform the derivative on the full many-body wave function, however, this would demand another layer of polymorphism and make the code less intuitive.

where α is the spin configuration of particle i . The counterpart to α has no dependence of particle i and will hence be zero in the expression above.

Equally for the Laplacians used in the local energy, we get

$$E_L = \sum_i \frac{1}{\Psi_T} \nabla_i^2 \Psi_T + V \quad (4.4)$$

$$\begin{aligned} \frac{1}{\Psi_T} \nabla_i^2 \Psi_T &= \frac{1}{|D^\uparrow||D^\downarrow|J} \nabla_i^2 |D^\uparrow||D^\downarrow|J \\ &= \frac{\nabla_i^2 |D^\uparrow|}{|D^\uparrow|} + \frac{\nabla_i^2 |D^\downarrow|}{|D^\downarrow|} + \frac{\nabla_i^2 J}{J} \\ &\quad + 2 \frac{(\nabla_i |D^\uparrow|)(\nabla_i |D^\downarrow|)}{|D^\uparrow||D^\downarrow|} + 2 \frac{(\nabla_i |D^\uparrow|)(\nabla_i J)}{|D^\uparrow|J} + 2 \frac{(\nabla_i |D^\downarrow|)(\nabla_i J)}{|D^\downarrow|J} \\ &= \frac{\nabla_i^2 |D^\alpha|}{|D^\alpha|} + \frac{\nabla_i^2 J}{J} + 2 \frac{\nabla_i |D^\alpha|}{|D^\alpha|} \frac{\nabla_i J}{J} \end{aligned} \quad (4.5)$$

Finally, the expression for the R_ψ ratio for Metropolis is

$$\begin{aligned} R_\psi &= \frac{\Psi_T^{\text{new}}}{\Psi_T^{\text{old}}} \\ &= \frac{|D^\uparrow|^{\text{new}} |D^\downarrow|^{\text{new}} J^{\text{new}}}{|D^\uparrow|^{\text{old}} |D^\downarrow|^{\text{old}} J^{\text{old}}} \\ &= \frac{|D^\alpha|^{\text{new}} J^{\text{new}}}{|D^\alpha|^{\text{old}} J^{\text{old}}} \end{aligned} \quad (4.6)$$

where either the spin up or the spin down determinant is unchanged by the step.

From these expressions it is clear that we get a halving of the dimensionality of the system by splitting the Slater determinants. Calculation the determinant of a $N \times N$ matrix is $\mathcal{O}(N^2)$ floating point operations (flops). This implies a speedup of four in estimating the determinants alone.

4.4 Optimizations due to Single-particle Moves

Moving only one particle at the time (see the diffusion algorithm in Fig. 3.1), means changing a single row in the Slater-determinant at the time. Changes to a single row means that almost every *co-factor* remains unchanged. Since all of the expressions deduced in the previous section contains ratios of the spatial wave functions, expressing these determinants in terms of their co-factors should reveal cancellation of terms.

4.4.1 Optimizing the Slater ratios

The inverse of the Slater-matrix is given in terms of its *adjugate* by the following relation [21] (spin-configuration parameter α will be skipped for now)

$$D^{-1} = \frac{1}{|D|} \text{adj} D$$

The adjugate of a matrix is the transpose of the cofactor matrix C . Given in terms of matrix element equations, we have

$$D_{ij}^{-1} = \frac{C_{ji}}{|D|} \quad (4.7)$$

$$D_{ji} = \phi_i(r_j) \quad (4.8)$$

Moreover, the determinant can be expressed as a *cofactor expansion* around row j (Kramer's rule)

$$|D| = \sum_i D_{ji} C_{ji}. \quad (4.9)$$

The spatial part of the R_ψ ratio is then (inserting Eq. (4.9) into Eq. (4.6))

$$R_S = \frac{\sum_i D_{ji}^{\text{new}} C_{ji}^{\text{new}}}{\sum_i D_{ji}^{\text{old}} C_{ji}^{\text{old}}} \quad (4.10)$$

Let j represent the moved particle, the j 'th column of the cofactor matrix is unchanged when the particle moves (column j depends on every column but its own). In other words,

$$C_{ji}^{\text{new}} = C_{ji}^{\text{old}} = (D_{ij}^{\text{old}})^{-1} |D^{\text{old}}|, \quad (4.11)$$

where the inverse relation of Eq. (4.7) has been used. Inserting this into Eq. (4.10) yields

$$\begin{aligned} R_S &= \frac{|D^{\text{old}}| \sum_i D_{ji}^{\text{new}} (D_{ij}^{\text{old}})^{-1}}{|D^{\text{old}}| \sum_i D_{ji}^{\text{old}} (D_{ij}^{\text{old}})^{-1}} \\ &= \frac{\sum_i D_{ji}^{\text{new}} (D_{ij}^{\text{old}})^{-1}}{I_{jj}} \end{aligned}$$

The diagonal element of the identity matrix is by definition unity. Inserting this fact combined with the relation from Eq. (4.8) yields the optimized expression for the ratio

$$R_S = \sum_i \phi_i(r_j^{\text{new}}) (D_{ij}^{\text{old}})^{-1} \quad (4.12)$$

where j is the currently moved particle. The sum i spans the Slater matrix whose spin value matches that of particle j .

Similar reductions can be applied to all the Slater ratio expressions from the previous section, see refs. [9, 13]:

$$\frac{\nabla_i |D|}{|D|} = \sum_k \nabla_i \phi_k(r_i^{\text{new}}) (D_{ki}^{\text{new}})^{-1} \quad (4.13)$$

$$\frac{\nabla_i^2 |D|}{|D|} = \sum_k \nabla_i^2 \phi_k(r_i^{\text{new}}) (D_{ki}^{\text{new}})^{-1} \quad (4.14)$$

where again, k spans the Slater matrix whose spin values match that of the moved particle. Unlike for the ratio, $N/2$ of the gradients needs to be recalculated once a particle is moved (with N being the number of particles). This is due to the fact that it is the new Slater inverse that is used, and not the old.

Closed form expressions for the derivatives and Laplacians of the single particle may be implemented and accessed when calling these functions to avoid expensive numerical calculations. See Appendices **REF SYMPYGEN** for a tabulation of closed form expressions.

4.4.2 Optimizing the Inverse

One might question the efficiency of calculating inverse matrices compared to brute force estimation of the determinants. However, as for the ratio in Eq. (4.12), using co-factor expansions we can construct an updating algorithm which dramatically decreases the cost of calculating the inverse of the new Slater matrix.

Let i be the currently moved particle, the new inverse is given in terms of the old by the following expression [9, 13]

$$\tilde{I}_{ij} = \sum_l D_{il}^{\text{new}} (D_{lj}^{\text{old}})^{-1} \quad (4.15)$$

$$(D_{kj}^{\text{new}})^{-1} = (D_{kj}^{\text{old}})^{-1} - \frac{1}{R_S} (D_{ji}^{\text{old}})^{-1} \tilde{I}_{ij} \quad j \neq i \quad (4.16)$$

$$(D_{ki}^{\text{new}})^{-1} = \frac{1}{R_S} (D_{ki}^{\text{old}})^{-1} \quad \text{else} \quad (4.17)$$

This reduces the cost of calculating the inverse by an order of magnitude down to $\mathcal{O}(N^2)$.

Further optimization can be achieved by calculating the \tilde{I} vector for particle i prior to performing the loop over k and j . Again, this loop should only update the inverse Slater matrix whose spin value correspond to that of the moved particle.

4.4.3 Optimizing the Padé Jastrow factor Ratio

As for the Green's function ratio is Eq. (3.37), the ratio between two Jastrow factors are best calculating as exponentiation the logarithm

$$\log \frac{J^{\text{new}}}{J^{\text{old}}} = \sum_{k < j=1}^N \frac{a_{kj} r_{kj}^{\text{new}}}{1 + \beta r_{kj}^{\text{new}}} - \frac{a_{kj} r_{kj}^{\text{old}}}{1 + \beta r_{kj}^{\text{old}}} \quad (4.18)$$

$$\equiv \sum_{k < j=1}^N g_{kj}^{\text{new}} - g_{kj}^{\text{old}} \quad (4.19)$$

The relative distances r_{kj} behave much like the cofactors in Section 4.4.1; changing r_i only changes r_{ij} , in other words

$$r_{kj}^{\text{new}} = r_{kj}^{\text{old}} \quad k \neq i \quad (4.20)$$

which inserted into Eq. (4.19) yields

$$\begin{aligned} \log \frac{J^{\text{new}}}{J^{\text{old}}} &= \sum_{k < j \neq i} g_{kj}^{\text{old}} - g_{kj}^{\text{old}} + \sum_{j=1}^N g_{ij}^{\text{new}} - g_{ij}^{\text{old}} \\ &= \sum_{j=1}^N a_{ij} \left(\frac{r_{ij}^{\text{new}}}{1 + \beta r_{ij}^{\text{new}}} - \frac{r_{ij}^{\text{old}}}{1 + \beta r_{ij}^{\text{old}}} \right) \end{aligned} \quad (4.21)$$

Exponentiating both sides reveals the final optimized ratio

$$\frac{J^{\text{new}}}{J^{\text{old}}} = \exp \left[\sum_{j=1}^N a_{ij} \left(\frac{r_{ij}^{\text{new}}}{1 + \beta r_{ij}^{\text{new}}} - \frac{r_{ij}^{\text{old}}}{1 + \beta r_{ij}^{\text{old}}} \right) \right] \quad (4.22)$$

4.5 Optimizing the Padé Jastrow Derivative Ratios

The shape of the Padé Jastrow factor is general in the sense that its shape is independent of the system at hand. Calculating closed form expressions for the derivatives is then a process which can be done once and for all.

4.5.1 The Gradient

Using the notation of Eq. (4.19), the x component of the Padé Jastrow gradient ratio for particle i then becomes

$$\frac{1}{J} \frac{\partial J}{\partial x_i} = \frac{1}{\prod_{k < l} \exp g_{kl}} \frac{\partial}{\partial x_i} \prod_{k < l} \exp g_{kl} \quad (4.23)$$

Using the product rule, only terms with k or l equal to i survive the differentiation. In addition, the terms independent of i will cancel the corresponding terms in the denominator. In other words,

$$\begin{aligned} \frac{1}{J} \frac{\partial J}{\partial x_i} &= \sum_{k \neq i} \frac{1}{\exp g_{ik}} \frac{\partial}{\partial x_i} \exp g_{ik} \\ &= \sum_{k \neq i} \frac{1}{\exp g_{ik}} \exp g_{ik} \frac{\partial g_{ik}}{\partial x_i} \\ &= \sum_{k \neq i} \frac{\partial g_{ik}}{\partial x_i} \\ &= \sum_{k \neq i} \frac{\partial g_{ik}}{\partial r_{ik}} \frac{\partial r_{ik}}{\partial x_i} \end{aligned} \quad (4.24)$$

$$\begin{aligned}
\frac{\partial g_{ik}}{\partial r_{ik}} &= \frac{\partial}{\partial r_{ik}} \left(\frac{a_{ik}r_{ik}}{1 + \beta r_{ik}} \right) \\
&= \frac{a_{ik}}{1 + \beta r_{ik}} - \frac{a_{ik}r_{ik}}{(1 + \beta r_{ik})^2} \beta \\
&= \frac{a_{ik}(1 + \beta r_{ik}) - a_{ik}\beta r_{ik}}{(1 + \beta r_{ik})^2} \\
&= \frac{a_{ik}}{(1 + \beta r_{ik})^2}
\end{aligned} \tag{4.25}$$

$$\begin{aligned}
\frac{\partial r_{ik}}{\partial x_i} &= \frac{\partial}{\partial x_i} \sqrt{(x_i - x_k)^2 + (y_i - y_k)^2 + (z_i - z_k)^2} \\
&= \frac{1}{2} \frac{2(x_i - x_k)}{\sqrt{(x_i - x_k)^2 + (y_i - y_k)^2 + (z_i - z_k)^2}} \\
&= \frac{x_i - x_k}{r_{ik}}
\end{aligned} \tag{4.26}$$

Combining these expressions yields

$$\frac{1}{J} \frac{\partial J}{\partial x_i} = \sum_{k \neq i} \frac{a_{ik}}{r_{ik}} \frac{x_i - x_k}{(1 + \beta r_{ik})^2} \tag{4.27}$$

When changing Cartesian variable in the differentiation, the only change to the expression is that the corresponding Cartesian variable changes in the numerator of Eq. (4.27). In other words, generalizing to the full gradient is done by substituting the Cartesian difference with the position vector difference.

$$\frac{\nabla_i J}{J} = \sum_{k \neq i=1}^N \frac{a_{ik}}{r_{ik}} \frac{\vec{r}_i - \vec{r}_k}{(1 + \beta r_{ik})^2}$$

4.5.2 The Laplacian

The method of deducing the closed form expression for the Laplacian of the Padé Jastrow factor is identical to that of the gradient. The full calculation is done in ref. [13]. The expression becomes

$$\frac{\nabla_i^2 J}{J} = \left| \frac{\nabla_i J}{J} \right|^2 + \sum_{k \neq i=1}^N \left(\frac{d-1}{r_{ik}} \frac{\partial g_{ik}}{\partial r_{ik}} + \frac{\partial^2 g_{ik}}{\partial r_{ik}^2} \right) \tag{4.29}$$

where d is the number of dimensions, arising due to the fact that the Laplacian, unlike the gradient, is a summation of contributions from all dimensions. A simple differentiation of Eq. (4.25) with respect to r_{ik} yields

$$\frac{\partial^2 g_{ik}}{\partial r_{ik}^2} = -\frac{2a_{ik}\beta}{(1 + \beta r_{ik})^3} \tag{4.30}$$

Inserting Eq. (4.25) and Eq. (4.30) into Eq. (4.29) yields

$$\begin{aligned}\frac{\nabla_i^2 J}{J} &= \left| \frac{\nabla_i J}{J} \right|^2 + \sum_{k \neq i=1}^N \left(\frac{d-1}{r_{ik}} \frac{a_{ik}}{(1+\beta r_{ik})^2} - \frac{2a_{ik}\beta}{(1+\beta r_{ik})^3} \right) \\ &= \left| \frac{\nabla_i J}{J} \right|^2 + \sum_{k \neq i=1}^N a_{ik} \frac{(d-1)(1+\beta r_{ik}) - 2\beta r_{ik}}{r_{ik}(1+\beta r_{ik})^3}\end{aligned}$$

which with a little cleanup results in

$$\frac{\nabla_i^2 J}{J} = \left| \frac{\nabla_i J}{J} \right|^2 + \sum_{k \neq i} a_{ik} \frac{(d-1) + (d-3)\beta r_{ik}}{r_{ik}(1+\beta r_{ik})^3} \quad (4.31)$$

The local energy calculation needs the sum of the Laplacians for all particles (see Eq. (4.4)). In other words, the quantity of interest becomes

$$\sum_i \frac{\nabla_i^2 J}{J} = \sum_i \left| \frac{\nabla_i J}{J} \right|^2 + \sum_{i \neq k}^N a_{ik} \frac{(d-1) + (d-3)\beta r_{ik}}{r_{ik}(1+\beta r_{ik})^3} \quad (4.32)$$

However, due to the symmetry of r_{ik} , the second term count equal values twice. We can therefore optimize the calculation by only summing for $k > i$, and rather multiply the sum by two. Bringing it all together, we get

$$\sum_i \frac{\nabla_i^2 J}{J} = \sum_i \left| \frac{\nabla_i J}{J} \right|^2 + 2 \sum_{i < k}^N a_{ik} \frac{(d-1) + (d-3)\beta r_{ik}}{r_{ik}(1+\beta r_{ik})^3} \quad (4.33)$$

4.6 Tabulating Recalculated Data

The optimizations covered in this section will exclusively arise from point (i) in section 4.1.3. Avoiding recalculating expressions also include exploiting, such as was done in the Padé Jastrow Laplacian in Eq. (4.33).

rrel, r2, phimatrix, delphi, oppdatere jastrow gradient, qnum indie terms ++ a s a s d a d sd f s f s a sa
dsa sda a a ads ad gf asrfs asdf as fas a asd asd as

4.6.1 The relative distance matrix

In the discussions regarding the optimization of the Jastrow ratio, it became clear that moving one particle only changed N of the relative distances. Storing these values in a matrix, consequently updating the values corresponding to the moved particle, ensures that these values are calculated once and for all.

$$r_{rel} = r_{rel}^T = \begin{pmatrix} 0 & r_{12} & r_{13} & \cdots & r_{1N} \\ & 0 & r_{23} & \cdots & r_{2N} \\ & & \ddots & \ddots & \vdots \\ & \cdots & & 0 & r_{(N-1)N} \\ & & & & 0 \end{pmatrix}. \quad (4.34)$$

```

1 void Sampling::update_pos(const Walker* walker_pre, Walker* walker_post, int particle)
2 {
3     ...
4
5     //Updating the part of the r_rel matrix which is changed by moving the [particle]
6     for (int j = 0; j < n_p; j++) {
7         if (j != particle) {
8             walker_post->r_rel(particle, j) = walker_post->r_rel(j, particle)
9                 = walker_post->calc_r_rel(particle, j);
10        }
11    }
12
13    ...
14 }
15 }
```

Functions such as `Coulomb.get_potential_energy` and all of the evaluation functions of the Jastrow Factor can then simply access these matrix elements.

Similar storage has been done for the squared distance vector.

4.6.2 The Slater related matrices

Apart from the inverse, whose optimization was covered in Section 4.4.2, calculating the single particle wave functions and its gradients are the most expensive operations of the QMC algorithm.

Storing these function values in a matrices representing the Slater Matrix and its derivatives, will ensure that these values never gets recalculated.

$$D \equiv [D^\uparrow D^\downarrow] = \begin{bmatrix} \phi_1(r_0) & \phi_1(r_1) & \cdots & \phi_1(r_N) \\ \phi_2(r_0) & \phi_2(r_1) & \cdots & \phi_2(r_N) \\ \vdots & \vdots & & \vdots \\ \phi_{N/2}(r_0) & \phi_{N/2}(r_1) & \cdots & \phi_{N/2}(r_N) \end{bmatrix} \quad (4.35)$$

$$\nabla D \equiv \begin{bmatrix} \nabla\phi_1(r_0) & \nabla\phi_1(r_1) & \cdots & \nabla\phi_1(r_N) \\ \nabla\phi_2(r_0) & \nabla\phi_2(r_1) & \cdots & \nabla\phi_2(r_N) \\ \vdots & \vdots & & \vdots \\ \nabla\phi_{N/2}(r_0) & \nabla\phi_{N/2}(r_1) & \cdots & \nabla\phi_{N/2}(r_N) \end{bmatrix} \quad (4.36)$$

4.6.3 Avoiding spin tests

Since the slater determinant is split by spin eigenvalues, the same splitting occurs in the inverse, the Slater matrix etc. The brute force implementation is to if-test which of the matrices to access. In the case of a two-level system we get

$$\begin{aligned} i < N/2 & D^\uparrow(i) \\ i \geq N/2 & D^\downarrow(i - N/2) \end{aligned} \quad (4.37)$$

However, simply concatenating the Slater related matrices solves the entire problem. This has already been done in Eq. (4.35) and Eq. (4.36). Applying this to the inverse yields

$$D^{-1} \equiv [(D^\uparrow)^{-1} (D^\downarrow)^{-1}] \quad (4.38)$$

Leaving no if-tests required in order to sort the spin splitting. In e.g. the updating algorithm for the inverse, we must now simply keep track of which part we need to update by selecting a start and stop criteria, the rest of the code is general.

4.6.4 The Padé Jastrow gradient

Consider Eq. (4.28). Defining

$$d\vec{J}_{ik} = -d\vec{J}_{ki} \equiv \frac{a_{ik}}{r_{ik}} \frac{\vec{r}_i - \vec{r}_k}{(1 + \beta r_{ik})^2}, \quad (4.39)$$

the gradient can be written in a more compact form

$$\frac{\nabla_i J}{J} = \sum_{k \neq i=1}^N d\vec{J}_{ik}. \quad (4.40)$$

As for the relative distances, storing the elements and exploiting the symmetry properties, only half the total elements needs to be calculated.

$$d\vec{J} = -d\vec{J}^T \equiv \begin{pmatrix} 0 & d\vec{J}_{12} & d\vec{J}_{13} & \cdots & d\vec{J}_{1N} \\ 0 & d\vec{J}_{23} & \cdots & d\vec{J}_{2N} \\ \ddots & \ddots & \vdots \\ (-) & 0 & d\vec{J}_{(N-1)N} \\ & & 0 \end{pmatrix}. \quad (4.41)$$

```

1 void Pade_Jastrow::get_dJ_matrix(Walker* walker, int i) const {
2
3     //for all j != i
4     b_ij = 1.0 + beta * walker->r_rel(i, j);
5     factor = a(i, j) / (walker->r_rel(i, j) * b_ij * b_ij);
6     for (int k = 0; k < dim; k++) {
7         walker->dJ(i, j, k) = (walker->r(i, k) - walker->r(j, k)) * factor;
8         walker->dJ(j, i, k) = -walker->dJ(i, j, k);
9     }
10 }
```

Calculating the gradient is now only a matter of summing the rows of the matrix in Eq. (4.41). On a more careful notice, we can further optimize the calculation of the gradient by taking into account that we have access to the previous gradient

$$\frac{\nabla_i J^{\text{old}}}{J^{\text{old}}} = \sum_{k \neq i=1}^N d\vec{J}_{ik}^{\text{old}} \quad (4.42)$$

$$\frac{\nabla_i J^{\text{new}}}{J^{\text{new}}} = \sum_{k \neq i=1}^N d\vec{J}_{ik}^{\text{new}} \quad (4.43)$$

By moving particle p in QMC, only a single row and column of the $dvecJ$ matrix changes. Assuming that $i \neq p$, only a single term from the new matrix is required

$$\frac{\nabla_{i \neq p} J^{\text{new}}}{J^{\text{new}}} = \sum_{k \neq i \neq p} d\vec{J}_{ik}^{\text{old}} + d\vec{J}_{ip}^{\text{new}} \quad (4.44)$$

$$= \left[\sum_{k \neq i \neq p} d\vec{J}_{ik}^{\text{old}} + d\vec{J}_{ip}^{\text{old}} \right] - d\vec{J}_{ip}^{\text{old}} + d\vec{J}_{ip}^{\text{new}} \quad (4.45)$$

$$= \frac{\nabla_i J^{\text{old}}}{J^{\text{old}}} - d\vec{J}_{ip}^{\text{old}} + d\vec{J}_{ip}^{\text{new}} \quad (4.46)$$

reducing the calculation to three flops. For the case $i = p$, the entire sum as in Eq. (4.43) must be calculated.

```

1 void Pade_Jastrow::get_grad(const Walker* walker_pre, Walker* walker_post, int p) const {
2     double sum;
3
4     //i < p
5     for (int i = 0; i < p; i++) {
6         for (int k = 0; k < dim; k++) {
7             walker_post->jast_grad(i, k) = walker_pre->jast_grad(i, k)
8                 + walker_post->dJ(i, p, k) - walker_pre->dJ(i, p, k);
9         }
10    }
11
12    //i = p
13    for (int k = 0; k < dim; k++) {
14
15        sum = 0;
16        for (int j = 0; j < p; j++) {
17            sum += walker_post->dJ(p, j, k);
18        }
19
20        for (int j = p + 1; j < n_p; j++) {
21            sum += walker_post->dJ(p, j, k);
22        }
23
24        walker_post->jast_grad(p, k) = sum;
25    }
26
27    //i > p
28    for (int i = p + 1; i < n_p; i++) {
29        for (int k = 0; k < dim; k++) {
30            walker_post->jast_grad(i, k) = walker_pre->jast_grad(i, k)
31                + walker_post->dJ(i, p, k) - walker_pre->dJ(i, p, k);
32        }
33    }
34 }
35
36 }
```

This optimization scales very well with increasing number of particles.

4.6.5 The single-particle Wave Functions

A single particle wave function is defined by a position in space r and a quantum number q . A QMC walker holds the position of all particles, so in the case of QMC, the parameters defining the single particle wave function is a walker, a particle number i and of course the quantum number (for the gradient we also need the dimension).

For systems of many particles, the function call `Orbitals.phi(walker, i, qnum)` needs to figure out which expression is related to which quantum number. The brute force implementation is to simply if-test on the quantum number, and calculate the corresponding expression inside the correct if-test.

```

1 double AlphaHarmonicOscillator::phi(const Walker* walker, int particle, int q_num) {
2
3     //Ground state of the harmonic oscillator
4     if (q_num == 0){
5         return exp(-0.5*w*walker->get_r_i2(i));
6     }
7
8     ...
9
10 }
```

This is however inefficient when the number of particles numbers become large. A more efficient implementation is to implement the single particle wave function expressions as `BasisFunctions` subclasses. `BasisFunctions` has one pure virtual function, `eval`, which then only needs the particle number i and the walker. The class itself is defined by the quantum number.

The following is an example of the harmonic oscillator single particle wave function for quantum number $q = 1$.

```

1 double HarmonicOscillator_1::eval(const Walker* walker, int i) {
2
3     y = walker->r(i, 1);
4
5     //y*exp(-k^2*r^2/2)
6
7     H = y;
8     return H*exp(-0.5*w*walker->get_r_i2(i));
9
10 }
```

These objects representing single particle wave functions can be loaded into an array, such that element q corresponds to the `BasisFunctions` object representing this quantum number. The new `Orbitals` function then becomes

```

1 double Orbitals::phi(const Walker* walker, int particle, int q_num) {
2     return basis_functions[q_num]->eval(walker, particle);
3 }
```

with no if-tests required.

Other more specific optimizations can be implemented, so called *quantum number independent factors*, \bar{Q}_i . When moving particle p , as discussed previously, a single column in the Slater matrix from Eq. (4.35) needs to be updated. All these terms are calculated in the same position. This implies that terms independent of the quantum number will be equal. Looking at the single particle states for harmonic oscillator and hydrogen listed in the Appendix, their exponential form results in that an exponential factor independent of the quantum number is present in all terms.

$$\bar{Q}_i^{\text{H.O.}} = e^{-\frac{1}{2}\alpha\omega r_i^2} \quad (4.47)$$

$$\bar{Q}_i^{\text{Hyd.}} = e^{-\frac{1}{n}\alpha Z r_i} \quad (4.48)$$

For hydrogen, we have a dependence on the principle quantum number n , however, for e.g $n = 2, 20$ terms share this exponential factor. Calculating it once and for all saves 19 exponential calls pr. particle pr. walker pr. cycle etc.

The implementation is rather simple. Upon moving a particle, the virtual function

`Orbitals.set_qnum_indie_terms` is called, updating the value of e.g. an `exp_factor` pointer shared by all the loaded `BasisFunctions` objects and the `Orbitals` class.

```

1 void AlphaHarmonicOscillator::set_qnum_indie_terms(const Walker * walker, int i) {
2
3     //k2 = alpha*omega
4     *exp_factor = exp(-0.5 * (*k2) * walker->get_r_i2(i));
5 }
6
7 void hydrogenicOrbitals::set_qnum_indie_terms(const Walker* walker, int i) {
8
9     //k = alpha*z
10    *exp_factor_n1 = exp(-(*k) * walker->get_r_i(i));
11    *exp_factor_n2 = exp(-(*k) * walker->get_r_i(i) / 2);
12    ...
13 }
14 }
```

The `BasisFunctions` objects can then simply access this value instead of calculating the exponential

```

1 double HarmonicOscillator_1::eval(const Walker* walker, int i) {
2
3     y = walker->r(i, 1);
4
5     //y*exp(-k^2*r^2/2)
6
7     H = y;
8     return H*(*exp_factor);
9 }
10
11 double lapl_hydrogenic_0::eval(const Walker* walker, int i) {
12
13     //k*(k*r - 2)*exp(-k*r)/r
14
15     psi = (*k)*((*k)*walker->get_r_i(i) - 2)/walker->get_r_i(i);
16     return psi*(*exp_factor);
17 }
18 }
```

This optimization is an enormous speedup for many particle simulations.

All single particle expressions given are calculated using *SymPy*. See Appendix **REF SYMPY** for details. For Quantum Dots, 84 `BasisFunctions` objects are needed for a 42-particle simulation, reducing the number of exponential calls with 83 pr. particle pr. walker pr. cycle, which for an average DMC calculation results in $24 \cdot 10^9$ saved exponential calls.

4.7 CPU Cache Optimization

The *CPU cache* is a limited amount of memory directly connected to the CPU designed to reduce the average time to access memory. Simply speaking, standard memory is slower than the CPU cache, as bits have to travel through the motherboard before it can be fed to the CPU (a so called *bus*).

Which values are held in the CPU cache is controlled by the compiler, however, if programmed poorly, the compiler will not be able to handle the cache storage optimally. Optimization tools exist in order to work around this, however, keeping the cache in mind from the beginning of the coding process can result in a much faster code. In the case of the QMC code, the most optimal use of the cache would be to have complete walkers ready in the cache at all times.

The memory is sent to the cache as arrays, which means that storing walker data sequentially in memory is the way to go in order to make take full use of the processor cache. This is ensured by not using

pointers within the walker objects, as pointers are free to be declared in any memory address.

4.7.1 Disadvantage of Generalizing the code

The size of the matrices within the walker objects are dynamically allocated in order to handle any number of particles and dimensions. At compile-time, there is no telling how much memory each walker will demand, and thus it is harder for the compiler to optimize the cache usage.

The alternative is to statically declare, i.e. declare with a fixed size known at compile time, the matrices to be of the maximum possible simulation size. This would however waste a ton of memory, and would render most applications impossible to run at a standard computer. A second alternative would be to re-compile the code every time the system variables are changed. This is not optimal in the case of a generalized solver.

4.7.2 Consequences

The QMC code has support for both kinds of scenarios. Compiling the source code with a main file which fixes the system variables will result in a more efficient executable. For the purpose of this thesis, this was not done; all system variables are controlled via a configuration script (see `runQMC.py` in ref. [6]).

Part II

Results

Results

5.1 Optimization Results

The optimizations listed in this section has been estimated using a 30 particle Quantum Dot system with a Padé Jastrow Factor.

Profiling the code revealed that, not surprisingly, 99% of the runtime was spent in the `QMC.diffuse_walker` function for both VMC, DMC and ASGD. Optimizing the code then solely involved optimizing this function.

The profiling tool of choice was KCacheGrind, aviable at the Ubuntu Software Center. KCacheGrind lists relative time spent in functions graphically in blocks, whose size is proportional to the time spent inside the function, much like standard hard drive listing software does with files and file size.

Prior to the listed optimizations, all other optimizations mentioned in previous sections has been implemented. The reason why they are not explicitly listed is the fact that they were implemented from start, and are considered “standard optimizations”. Writing a program without them was considered pointless.

Storing the Slater Matrix

This optimization is described in detail in Section 4.6.2. In addition to storing the slater, the calculation of \tilde{I} from the Slater inverse updating algorithm in Eq. (4.16) was pre calculated outside the main loops.

The percentages listed in the following table is the total time spent inside this specific function relative to all other functions.

| <u>Orbitals.phi</u> | |
|---|--------|
| Relative time spent prior to optimization | 80.88% |
| Relative time spent after optimization | 8.2% |
| Relative speedup | 9.86 |

The speedup is not because of optimizations within the function itself, but rather due to far less calls to the function. If the calculation of \tilde{I} was done outside the main loops in the first place, the speedup would be far less.

Optimized Jastrow Gradient

The optimization described in this Section is discussed in detail in Section 4.6.4.

The percentages listed in the following table is the total time spent inside this specific function relative to all other functions.

| <code>Jastrow.get_grad + Jastrow.calc_dJ</code> | |
|---|-------|
| Relative time spent prior to optimization | 40% |
| Relative time spent after optimization | 5.24% |
| Relative speedup | 7.63 |

Exploiting the symmetries of the Padé Jastrow Gradient in addition to calculating the new gradient based on the old is in other words extremely efficient. Keep in mind however, that these results are for a high number of particles. For e.g. two particles, this optimization would not matter at all.

Storing the Orbital Derivatives

This optimization is covered in detail in Section 4.6.2. Much like for the Slater matrix, the optimization in this case comes from the fact that the function itself is called fewer times, rather than being optimized.

The percentages listed in the following table is the total time spent inside this specific function relative to all other functions.

| <code>Orbitals.dell_phi</code> | |
|---|--------|
| Relative time spent prior to optimization | 56.27% |
| Relative time spent after optimization | 7.31% |
| Relative speedup | 7.70 |

Storing the Quantum Number Independent Terms

This optimization is covered in detail in Section 4.6.5. This optimization lowers the number of exponential function calls, and hence optimizes the calculation time of single particle states, its gradients and Laplacians.

The percentages listed in the following table is the total time spent inside this specific function relative to all other functions.

| <code>Jastrow.get_grad + Jastrow.calc_dJ</code> | |
|---|-------|
| Relative time spent prior to optimization | 5.85% |
| Relative time spent after optimization | 0.13% |
| Relative speedup | 45 |

This result is not surprisingly equal to 15 quantum numbers (for 30 particles) times three. One from the orbitals, and two from their gradients. Prior to this optimization, 45 exponential calls was needed to fill a row in the Slater matrix and the derivative matrix; this has been reduced to one.

Overall Optimization

Combining all the optimizations listed in this chapter, the final runtime was reduced to 5% of the original. The final scaling was

5.2 Validating the code

5.2.1 Calculation for non-interacting particles

For non-interacting particles in a Quantum Dot, no Jastrow factor and $\alpha = 1$ provides the exact wave function. This serves as a powerful guide, since results can be benchmarked against exact solutions. In the non-interacting case, the minimization should always yield $\alpha = 1$.

Let R denote the highest filled *shell*, i.e. the maximum value of $n_x + n_y$, N_j be the number of particles in a given shell ($1 \leq j \leq R$), χ be the spin levels and $\epsilon_i = i\omega$, where $i = n_x + n_y$, is the single particle energy at shell level i . Then the non-interacting energy of a closed shell Quantum Dot is

$$E_0 = \sum_{\chi} \sum_{i=1}^R \sum_{j=1}^{N_i} \epsilon_i \quad (5.1)$$

$$= 2 \sum_{i=1}^R N_i i\omega \quad (5.2)$$

Realizing that (not counting spin) $N_i = i$ for a Quantum Dot, we get

$$E_0 = 2\omega \sum_{i=1}^R i^2 \quad (5.3)$$

$$= 2\omega \left(\frac{1}{6} R(R+1)(2R+1) \right) \quad (5.4)$$

$$= \frac{R}{3} (R+1)(2R+1)\omega \quad (5.5)$$

which tabulated for the lowest lying shells yields

| R | N | E_0/ω |
|---|----|--------------|
| 1 | 2 | 2 |
| 2 | 6 | 10 |
| 3 | 12 | 28 |
| 4 | 20 | 60 |
| 5 | 30 | 110 |
| 6 | 42 | 182 |

The first step to validating the code would be to reproduce these exact results. The minimization method should seek an α close to one, where the variational derivative should be zero. In Table 5.1, validation runs for the three lowest shells are run. Figure 5.1 shows the ASGD method finding the minima.

Similar validation can be done for atoms, and is listed in Table 5.2. The non-interaction energy is given by the following expression

$$E_0 = -\frac{N^2}{2} \sum_{i=1}^N \frac{1}{n_i^2} \quad (5.6)$$

| N | ω | E_{VMC} | E_{DMC} | α | E_0 |
|----|----------|------------------|------------------|----------|-------|
| 2 | 0.5 | 1.0 | 1.0 | 1.0 | 1 |
| | 1.0 | 2.0 | 2.0 | 1.0 | 2 |
| 6 | 0.5 | 5.0 | 5.0 | 1.0 | 5 |
| | 1.0 | 10.0 | 10.0 | 1.0 | 10 |
| 12 | 0.5 | 14.0 | 14.0 | 1.0 | 14 |
| | 1.0 | 28.0 | 28.0 | 1.0 | 28 |

Table 5.1: Validation results for Quantum Dots generated using 2000 to 3000 ASGD cycles starting from $\alpha = 0.5$. The sampled variance from DMC and VMC is of order 10^{-16} (non-zero due to small deviations in α from unity). The last column lists the exact energies. As required we have an exact match (to machine precision). Hard coding $\alpha = 1.0$ will yield zero variance.

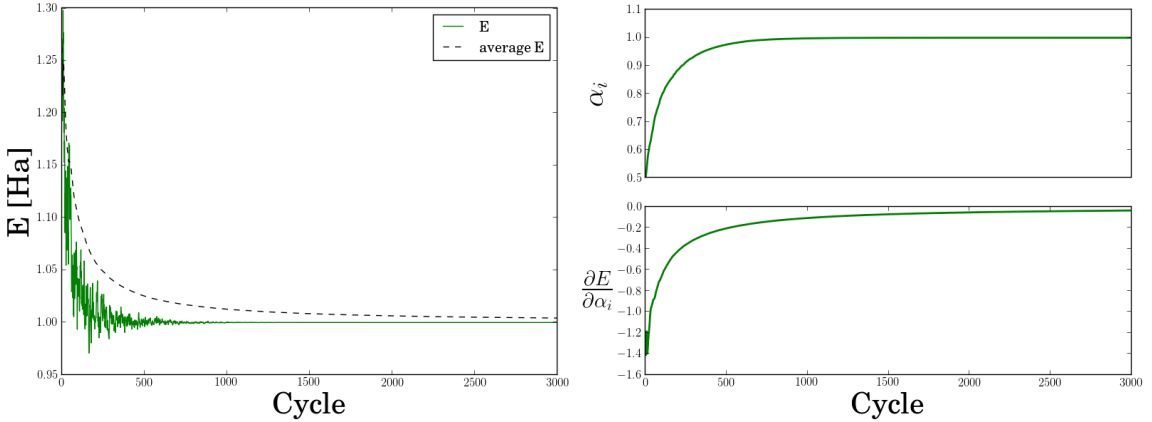


Figure 5.1: ASGD results for a non-interaction two-particle Quantum Dot with $\omega = 0.5$. The exact energy of $E_0 = 1$ is reached after approximately 1000 cycles, where α has converged close to unity. Due to enormous fluctuations, the variational derivative is plotted as an accumulated average, and is in practice dead zero after 1000 cycles. The variational principle described in Section 3.5.5 is governing the trend of the energy convergence, however, a lot of statistical noise is present in the first 1000 cycles due to high variance and few samples.

| N | E_{VMC} | E_{DMC} | α | E_0 |
|----|------------------|------------------|----------|-------|
| 2 | -4.0 | -4.0 | 1.0 | -4 |
| 4 | -20.0 | -20.0 | 1.0 | -20 |
| 10 | -200.0 | -200.0 | 1.0 | -200 |

Table 5.2: Validation results for Atoms generated in a similar way to the Quantum Dots results in Table 5.1.

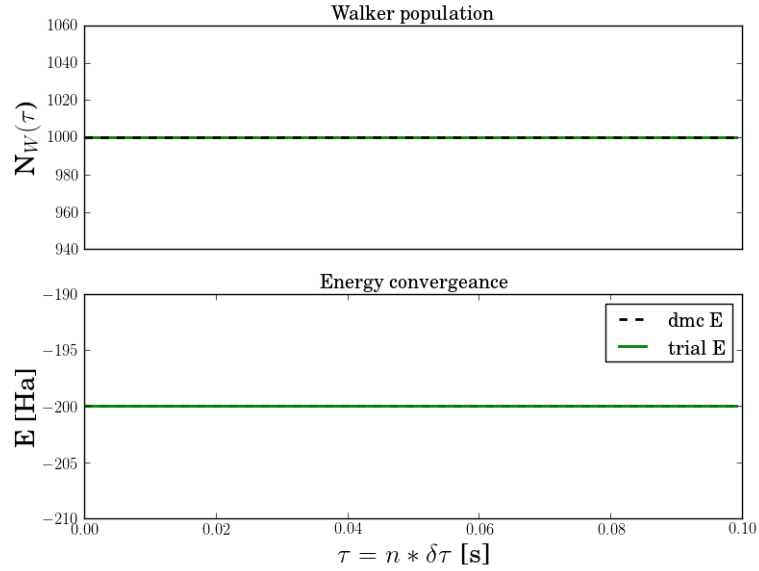


Figure 5.2: DMC convergence for the Neon result listed in Table 5.2. The trial energy is fixed at the exact ground state energy as expected. The number of walkers are constant, implying a approximatly zero variance.

The DMC method in case of an exact wave function should do nothing. The trial energy should equal the ground state energy through all time steps and zero fluctuations in the number of walkers should occur. This trend is shown for Neon in Fig. 5.2.

A final non-interacting case to run is the case of DMC without the exact wave function. As discussed in Chapter 3, DMC should result in a better estimate of the ground state energy than VMC in case of a trial wave function different from the exact grounds state. A test-case is presented in Fig. 5.3.

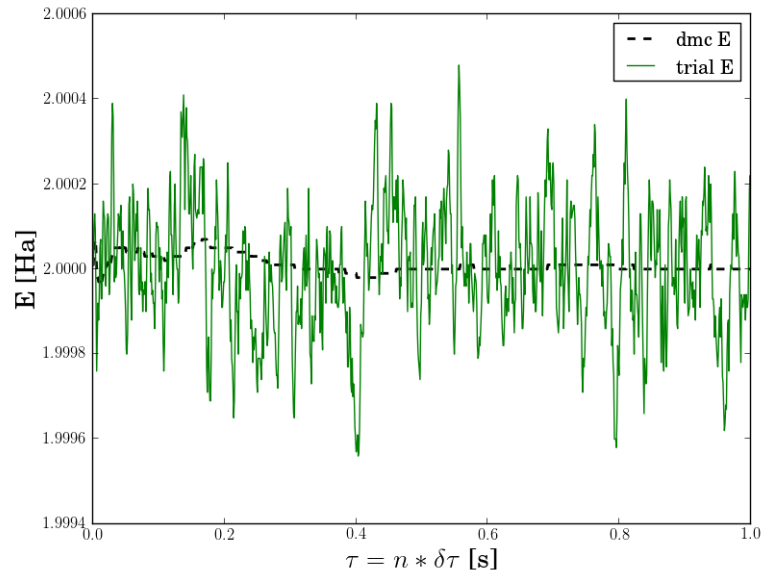


Figure 5.3: DMC convergence for a non-interacting two-particle Quantum Dot with $\omega = 1$. Calculations are done with $\alpha = 0.75$, where the exact wave function is given for $\alpha = 1$. Unlike the case with the exact wave function, the trial energy oscillates around the exact value. The final result (with blocking) reveals a DMC energy of 2.00000(2), where the original VMC energy was 2.0042(3). This illustrates the power of DMC over VMC in the interesting cases with an unknown exact wave function. The calculation were done with 10000 walkers.

5.3 Results for Quantum Dots

5.3.1 FIXED NODE TESTS

blah blah

| N | ω | E _{VMC} | E _{DMC} | $E_{\text{ref}}^{(a)}$ | $E_{\text{ref}}^{(b)}$ | $E_{\text{ref}}^{(c)}$ | $E_{\text{ref}}^{(d)}$ |
|----|----------|------------------|------------------|------------------------|------------------------|------------------------|------------------------|
| 2 | 0.01 | 0.07406(5) | 0.073839(2) | - | - | 0.0738 {23} | 0.07383505 {19} |
| | 0.1 | 0.44130(5) | 0.44079(1) | - | - | 0.4408 {23} | 0.44079191 {19} |
| | 0.28 | 1.02215(5) | 1.02164(1) | - | 0.99263 {19} | 1.0217 {23} | 1.0216441 {19} |
| | 0.5 | 1.66021(5) | 1.65977(1) | 1.65975(2) | 1.643871 {19} | 1.6599 {23} | 1.6597723 {19} |
| | 1.0 | 3.00030(5) | 3.00000(1) | 3.00000(3) | 2.9902683 {19} | 3.0002 {23} | 3.0000001 {19} |
| 6 | 0.1 | 3.5690(3) | 3.55385(5) | - | 3.49991 {18} | 3.5805 {22} | 3.551776 {9} |
| | 0.28 | 7.6216(4) | 7.60019(6) | 7.6001(1) | 7.56972 {18} | 7.6254 {22} | 7.599579 {6} |
| | 0.5 | 11.8103(4) | 11.78484(6) | 11.7888(2) | 11.76228 {18} | 11.8055 {22} | 11.785915 {6} |
| | 1.0 | 20.1902(4) | 20.15932(8) | 20.1597(2) | 20.14393 {18} | 20.1734 {22} | 20.160472 {8} |
| 12 | 0.1 | 12.3162(5) | 12.26984(8) | - | 12.2253 {17} | 12.3497 {21} | 12.850344 {3} |
| | 0.28 | 25.7015(6) | 25.63577(9) | - | 25.61084 {17} | 25.7095 {21} | 26.482570 {2} |
| | 0.5 | 39.2343(6) | 39.1596(1) | 39.159(1) | 39.13899 {17} | 39.2194 {21} | 39.922693 {2} |
| | 1.0 | 65.7905(7) | 65.7001(1) | 65.700(1) | 65.68304 {17} | 65.7399 {21} | 66.076116 {3} |
| 20 | 0.1 | 30.0729(8) | 29.9779(1) | - | 29.95345 {16} | 30.2700 {8} | 34.204867 {1} |
| | 0.28 | 62.0543(8) | 61.9268(1) | 61.922(2) | 61.91368 {16} | 62.0676 {20} | 67.767987 {1} |
| | 0.5 | 94.0236(9) | 93.8752(1) | 93.867(3) | 93.86145 {16} | 93.9889 {20} | 100.93607 {1} |
| | 1.0 | 156.062(1) | 155.8822(1) | 155.868(6) | 155.8665 {16} | 155.9569 {20} | 164.61280 {1} |
| 30 | 0.1 | 60.584(1) | 60.4205(2) | - | 60.43000 {15} | 61.3827 {9} | - |
| | 0.28 | 124.181(1) | 123.9683(2) | - | 123.9733 {15} | 124.2111 {9} | - |
| | 0.5 | 187.294(1) | 187.0426(2) | - | 187.0408 {15} | 187.2231 {19} | - |
| | 1.0 | 308.858(1) | 308.5627(2) | - | 308.5536 {15} | 308.6810 {19} | - |
| 42 | 0.1 | 107.881(1) | 107.6389(2) | - | - | 111.7170 {8} | - |
| | 0.28 | 220.161(1) | 219.8426(2) | - | 219.8836 {14} | 222.1401 {8} | - |
| | 0.5 | 331.002(1) | 330.6306(2) | - | 330.6485 {14} | 331.8901 {8} | - |
| | 1.0 | 544.2(8) | 542.9428(8) | - | 542.9528 {14} | 543.1155 {18} | - |
| 56 | 0.1 | 176.269(2) | 175.9553(7) | - | - | 186.1034 {9} | - |
| | 0.28 | 358.594(2) | 358.145(2) | - | - | 363.2048 {9} | - |
| | 0.5 | 538.5(6) | 537.353(2) | - | - | 540.3430 {9} | - |
| | 1 | 880.2(7) | 879.3986(6) | - | - | 879.6386 {17} | - |

Table 5.3: Results for Quantum Dots with fixed node approximation calculated on the cluster Abel using 10^8 VMC cycles, 64000 walkers, with 2000 DMC cycles on 128 cores. Ref: (a): F. Pederiva [22] (DMC), b: S. Reimann [23] (SRG), c: C. Hirth [24] (CCSD), d: V. K. B. Olsen [25] (FCI). The numbers inside curly brackets denote the number of shells used above *Fermi-level* to construct the basis for the calculation.

| N | ω | E_{DMC} | $E_{\text{DMC}}^{\text{F.N.}}$ | $\epsilon_{\text{DMC}}^{\text{F.N.}}/\bar{\sigma}$ |
|----|----------|------------------|--------------------------------|--|
| 2 | 0.1 | 0.44079(1) | 0.44079(1) | 0 |
| | 0.28 | 1.02164(1) | 1.02164(1) | 0 |
| | 0.5 | 1.65977(1) | 1.65977(1) | 0 |
| | 1.0 | 3.00000(1) | 3.00000(1) | 0 |
| 6 | 0.1 | 3.55385(5) | 3.55374(5) | 2.2 |
| | 0.28 | 7.60019(6) | 7.60016(5) | 0.54 |
| | 0.5 | 11.78484(6) | 11.78489(6) | 0.83 |
| | 1.0 | 20.15932(8) | 20.15945(7) | 1.73 |
| 12 | 0.1 | 12.26984(8) | 12.26986(8) | 0.25 |
| | 0.28 | 25.63577(9) | 25.6358(1) | 0.32 |
| | 0.5 | 39.1596(1) | 39.1594(1) | 2 |
| | 1.0 | 65.7001(1) | 65.7000(1) | 1 |
| 20 | 0.1 | 29.9779(1) | 29.9779(2) | 0 |
| | 0.28 | 61.9268(1) | 61.9265(2) | 2 |
| | 0.5 | 93.8752(1) | 93.8752(2) | 0 |
| | 1.0 | 155.8822(1) | 155.8821(2) | 0.66 |
| 30 | 0.1 | 60.4205(2) | 60.4207(2) | 1 |
| | 0.28 | 123.9683(2) | 123.9682(2) | 0.5 |
| | 0.5 | 187.0426(2) | 187.0430(2) | 2 |
| | 1.0 | 308.5627(2) | 308.5626(2) | 0.5 |
| 42 | 0.1 | 107.6389(2) | 107.638(2) | 0.81 |
| | 0.28 | 219.8426(2) | 219.8426(3) | 0 |
| | 0.5 | 330.6306(2) | 330.6307(2) | 0.5 |
| | 1.0 | 542.9428(8) | - | - |

Table 5.4: Results for Quantum Dots without fixed node approximation calculated on the cluster Abel using 2000 DMC cycles on 128 cores. $\epsilon_{\text{DMC}}^{\text{F.N.}} = |E_{\text{DMC}} - E_{\text{DMC}}^{\text{F.N.}}|$. $\bar{\sigma} = \frac{1}{2}(\sigma_{\text{DMC}} + \sigma_{\text{DMC}}^{\text{F.N.}})$. The last column serves as an indicator of how many average standard deviations the results differ. For two particles, where the fixed node approximation does not affect the system, the results are as expected exactly the same. For all other system sizes, the difference is mostly within one deviation. This indicates that the effect due to the fixed node approximation for closed shell Quantum Dots are very small.

5.3.2 One-body Densities

The one-body densities have been calculated using the methods described in Section 3.9.

From figure 5.6 it is clear that the particle distribution of Quantum Dots follows a clear trend: Odd number of closed shells ($N = 2, 12, 30$) are all similar in shape; the $N = 2$ case can be viewed as a zoom-in of the $N = 12$ top, which in turn can be viewed as a zoom-in of the $N = 30$ top. A metaphoric example would be the density “rising from the ground” as the number of particles increase. The same trend is clearly visible for the even numbered shells ($N = 6, 20, 42$). The density for $N = 56$ (not included) further demonstrates this trend.

5.3.3 Lowering the frequency

Viewing the one-body densities for lower values of ω (Fig. 5.7) in light of the corresponding densities for $\omega = 1$ (Fig. 5.6), it is clear that there is little to no change in the density profile of $\omega = 1$ to $\omega = 0.28$. This is further verified by $\omega = 0.5$ densities (not presented).

This implies that the oscillator frequency merely scales the extent of the wave function and leaves the general density profile unchanged. However, going below $\omega = 0.28$ reveals an interesting scenario where all of a sudden the densities change form. This is illustrated in figure 5.8: At $\omega = 0.1$ the changes become visible, yet the density is still comparable with that of higher frequencies. Going further down to $\omega = 0.01$, the profile is entirely different, and will not collapse onto high frequency densities.

The ground state density represents the most energy efficient state of the particles given a potential, and it is therefore implied that the sudden change in the density profile at lower frequencies must be induced by a shift in the system’s priorities between the different potential sources. In the case of Quantum Dots, these sources are the oscillator well and the Coulomb interaction. The amount of kinetic energy is also of interest.

It is tempting to state that the impact of the oscillator potential goes down proportional to the frequency squared (remember $V(\vec{r}) = \frac{1}{2}\omega^2 r^2$), however, this view is in fact too naive, as the Coulomb interaction and the kinetic energy is dependent of the distribution of particles which in turn is dependent on the oscillator frequency. What is true, however, is that in the limit $\omega \rightarrow 0$, the effect of the oscillator potential is gone.

Imagine an extremely narrow oscillator well: All the particles would favor stacking up in the center, as r^2 (oscillator) decrease quicker than r^{-1} (Coulomb) increase. For lower frequencies we have the different situation where the particles would favor being very far apart, since the coefficient ω^2 scaling the oscillator is very small. However, at a certain level, there comes a point where climbing the well further would cause the oscillator energy to increase more than Coulomb decrease. In other words, there is a balance - the oscillator will impact the particles even at very small frequencies. This is illustrated in Fig.

The question then becomes: Why do we get a change in the distribution below $\omega = 0.28$ if a balance is always present between the oscillator and Coulomb? The answer is

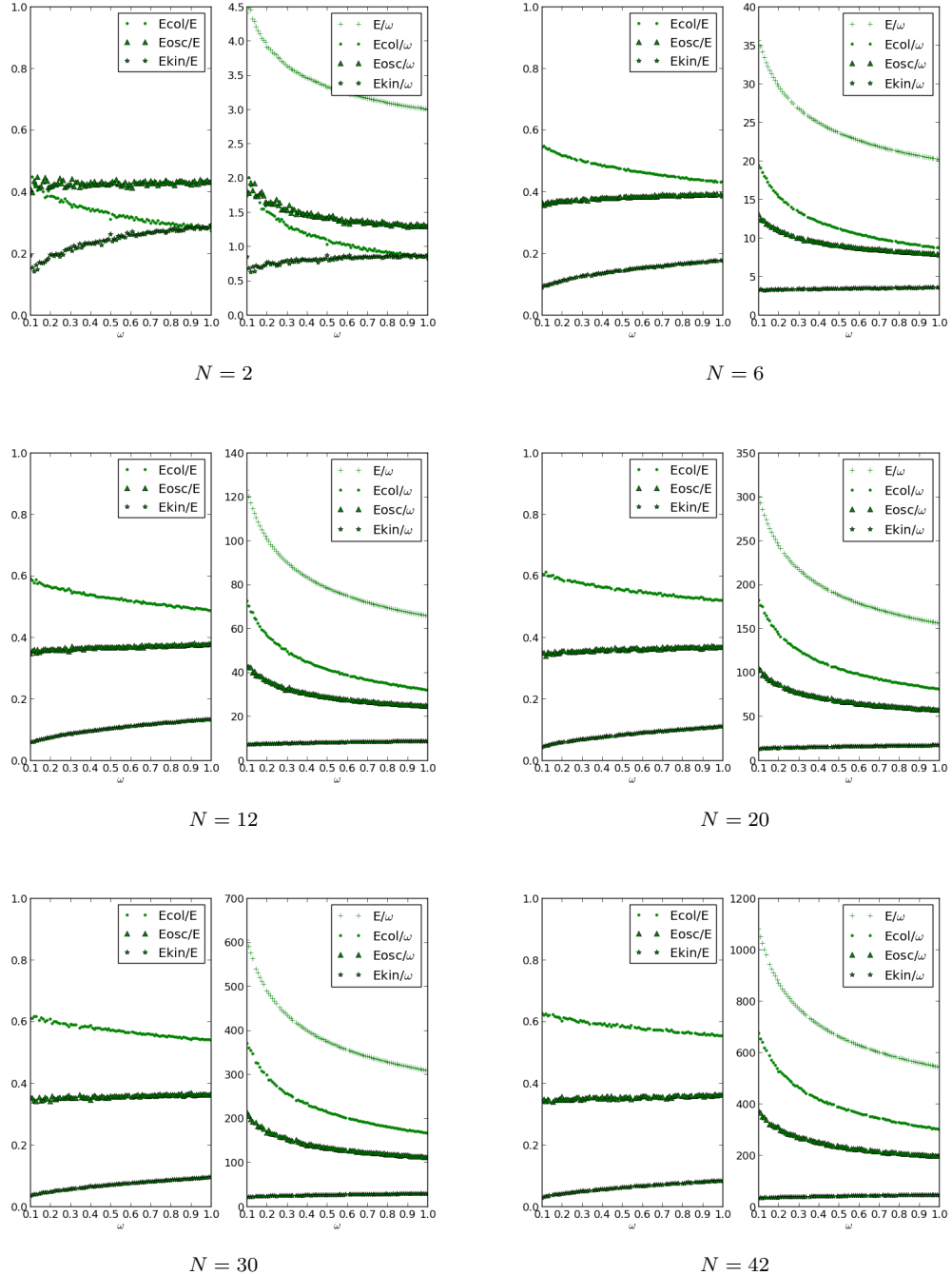


Figure 5.4

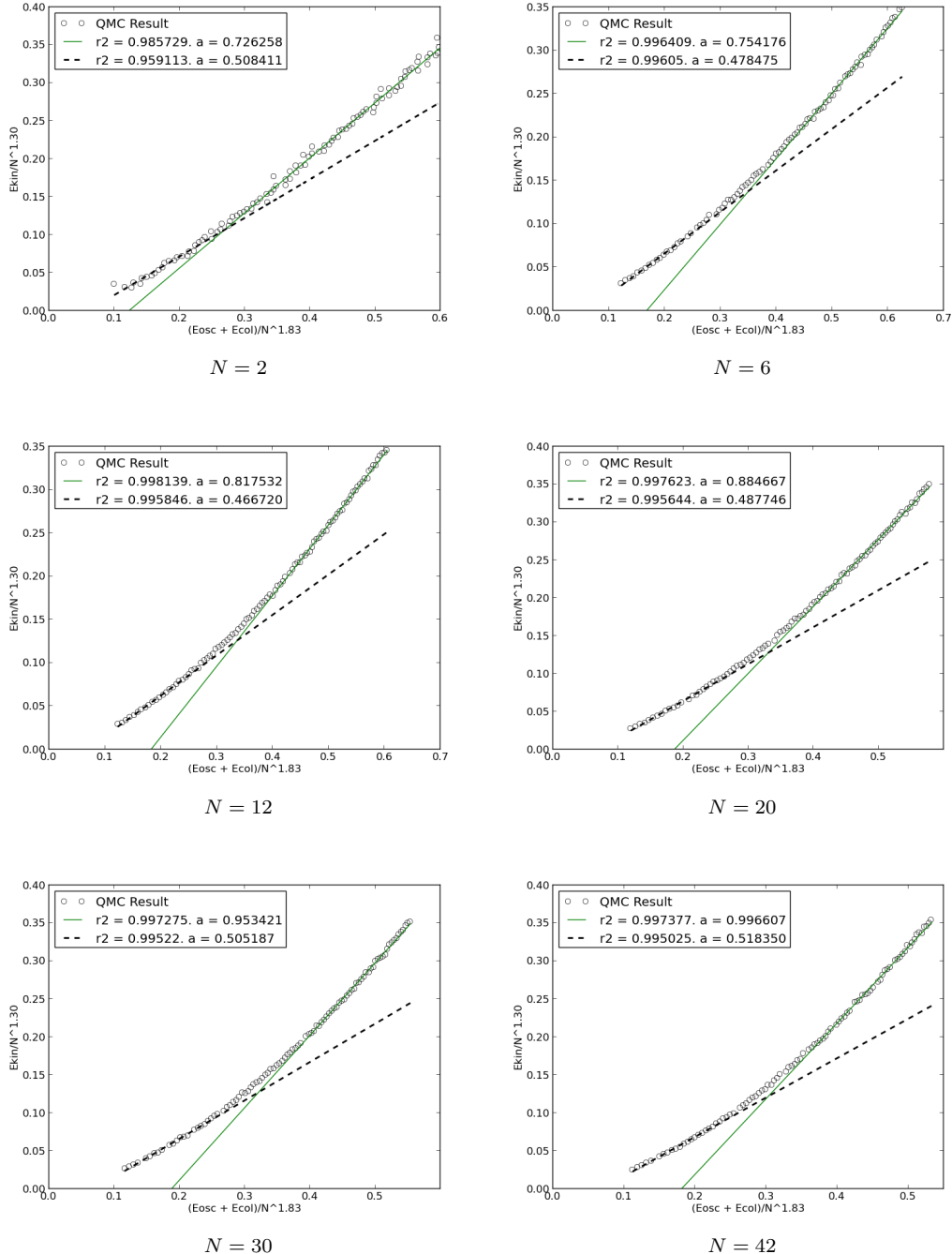


Figure 5.5

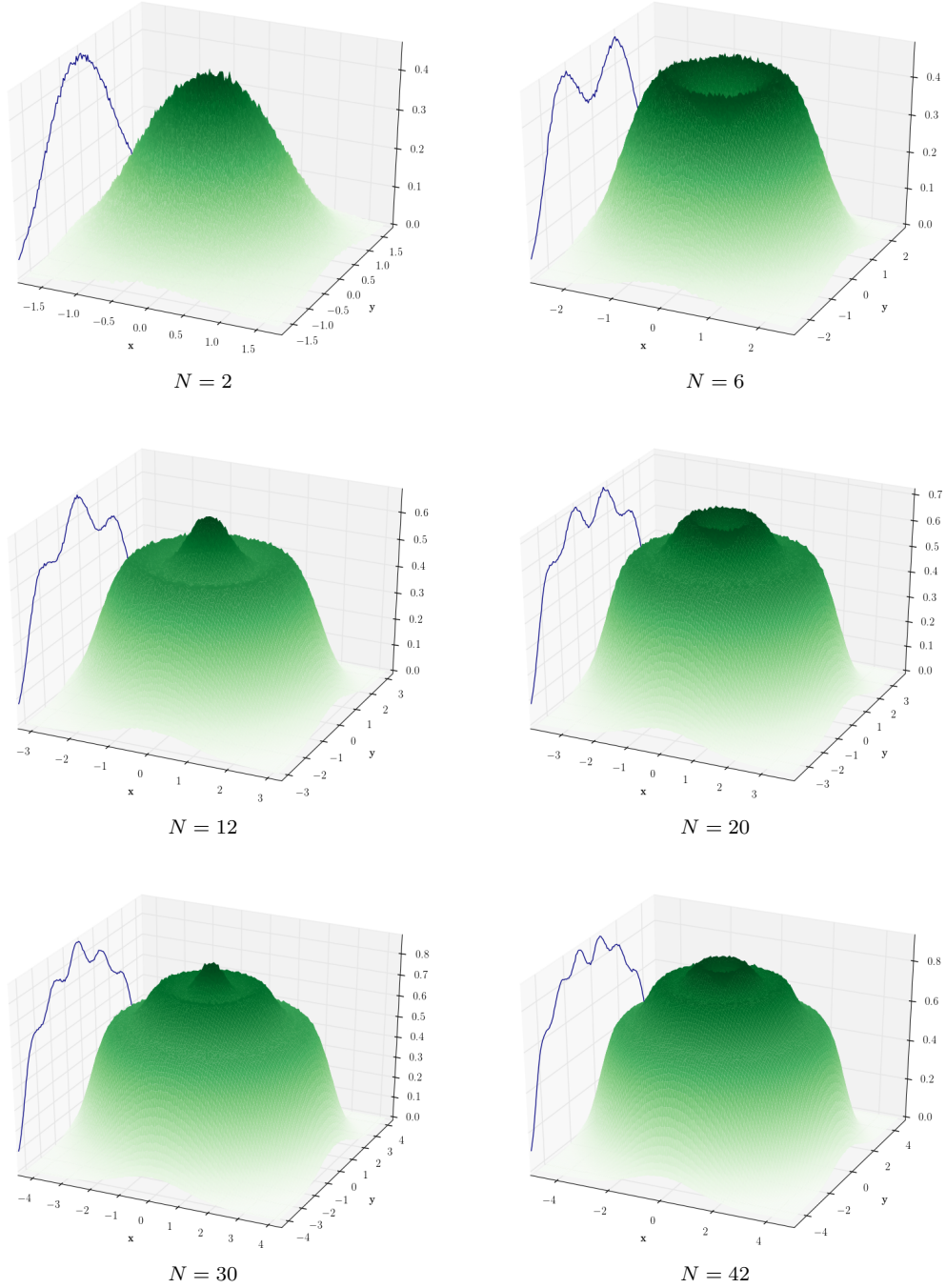


Figure 5.6: DMC one-body densities for Quantum Dots with frequency $\omega = 1$. The number of particles N are listed below each density. The density for 56 particles are calculated, however, it brings little new insights as it follows the clear trend demonstrated in the current figure.

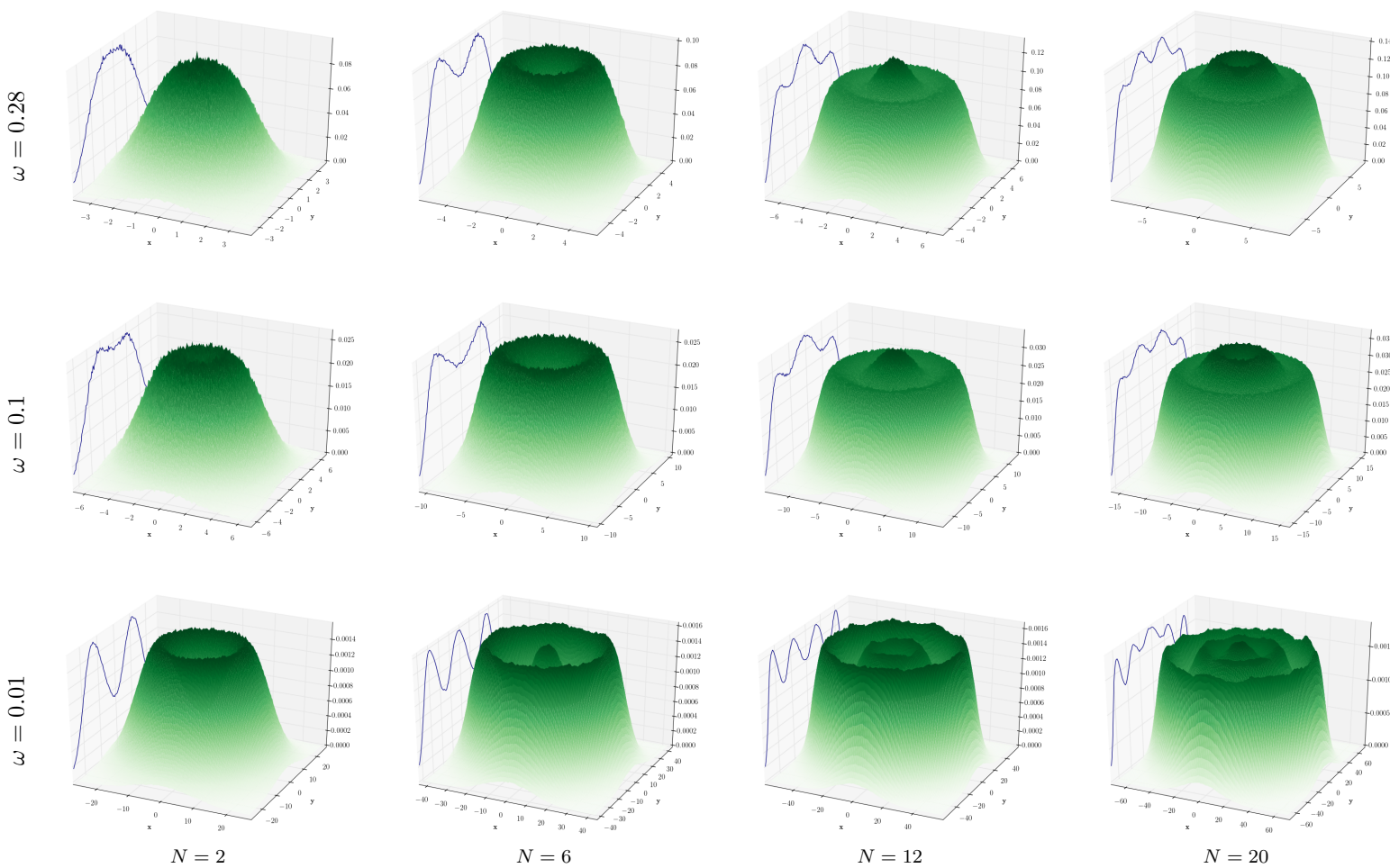


Figure 5.7: DMC One-body densities for Quantum Dots for decreasing oscillator frequencies ω and increasing number of particles N . Each row represents a given ω , and each column represents a given N . Notice that the densities for $\omega = 1$ (from figure 5.6) are indistinguishable from those of $\omega = 0.28$ except for their radial extent. This trend has been verified in the case of $N = 30, 42$ and 56 electrons as well as for $\omega = 0.5$, however, for the sake of transparency, these results are left out of the current figure. Results for $N = 30, 42$ and 56 particles for $\omega = 0.01$ has too wide radial extent to converge with the computational resources available at the present time and has thus not been computed.

blah blah something clever.

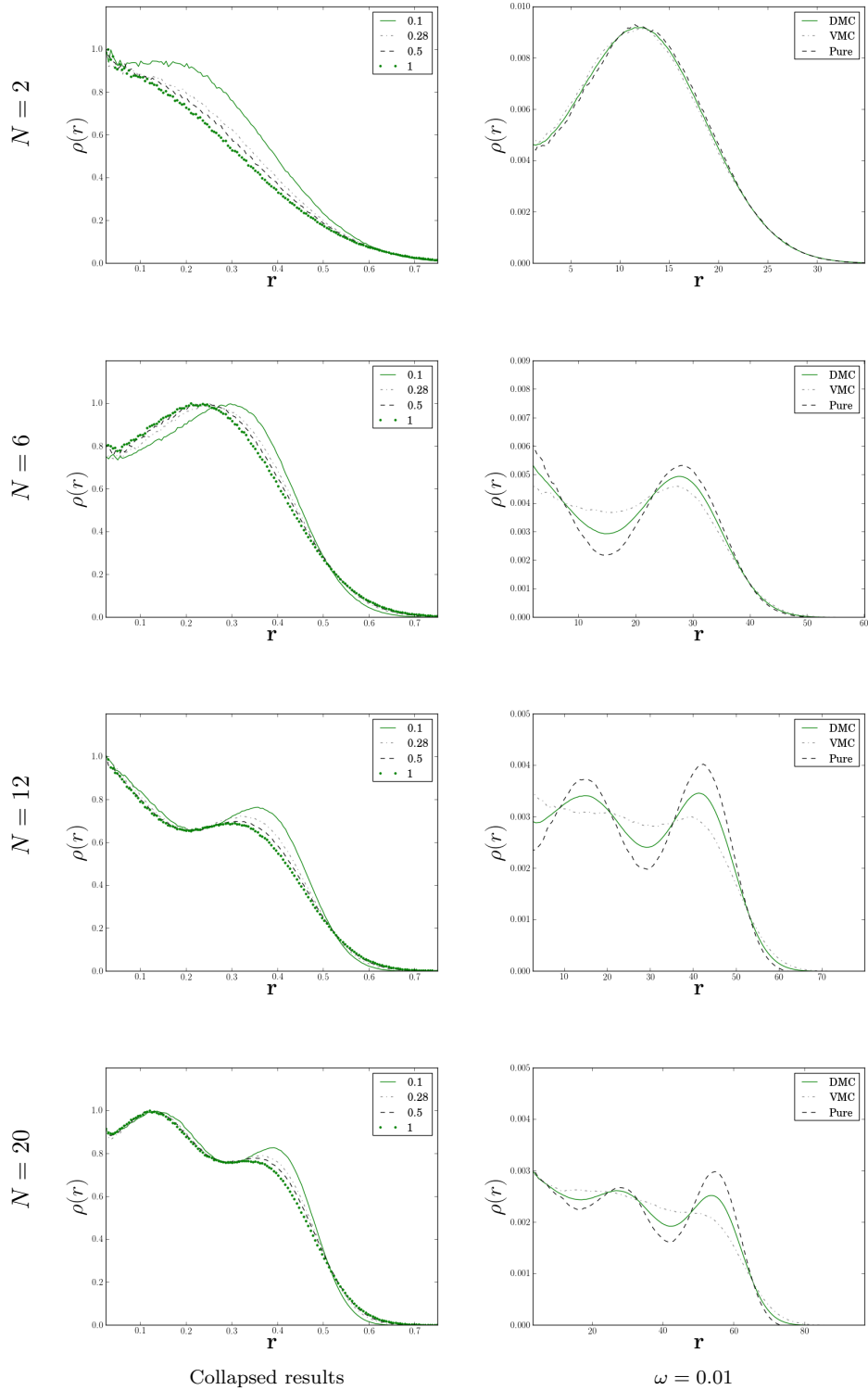


Figure 5.8: Right column: Radial one-body densities for high frequencies (see specific legends)

Table 5.5: Ground state energies for Atoms calculated using Variational - and Diffusion Monte-Carlo. Experimental energies are listed in the last column. As we see, DMC is rather close to the experimental energy. $\epsilon_{\text{rel}} = |E_{\text{DMC}} - \text{Expt.}| / |\text{Expt.}|$

| Atom | E_{VMC} | E_{DMC} | Expt. | ϵ_{rel} |
|------|------------------|------------------|--------------------------|-------------------------|
| He | -2.8903(2) | -2.9036(2) | -2.9037 ^a | $3.44 \cdot 10^{-5}$ |
| Be | -14.145(2) | -14.657(2) | -14.6674 ^a | $7.10 \cdot 10^{-4}$ |
| Ne | -127.853(2) | -128.765(4) | -128.9383 ^a | $1.34 \cdot 10^{-3}$ |
| Mg | -197.269(3) | -199.904(8) | -200.054 ^a | $7.50 \cdot 10^{-4}$ |
| Ar | -524.16(7) | -527.30(4) | -527.544 ^a | $4.63 \cdot 10^{-4}$ |
| Kr | -2700(5) | -2749.9(2) | -2752.05498 ^b | $7.83 \cdot 10^{-4}$ |

5.4 Results for Atoms

5.4.1 Ground State Energies

5.4.2 The Noble-Gases

blah blah

nuclear interaction extremely dominating. One-body densities utterly boring; exponential decay from core.

Interesting still: angular averaged radial one-body density.

More dispersed = More chemically unstable.

As expected Krypton is most stable.

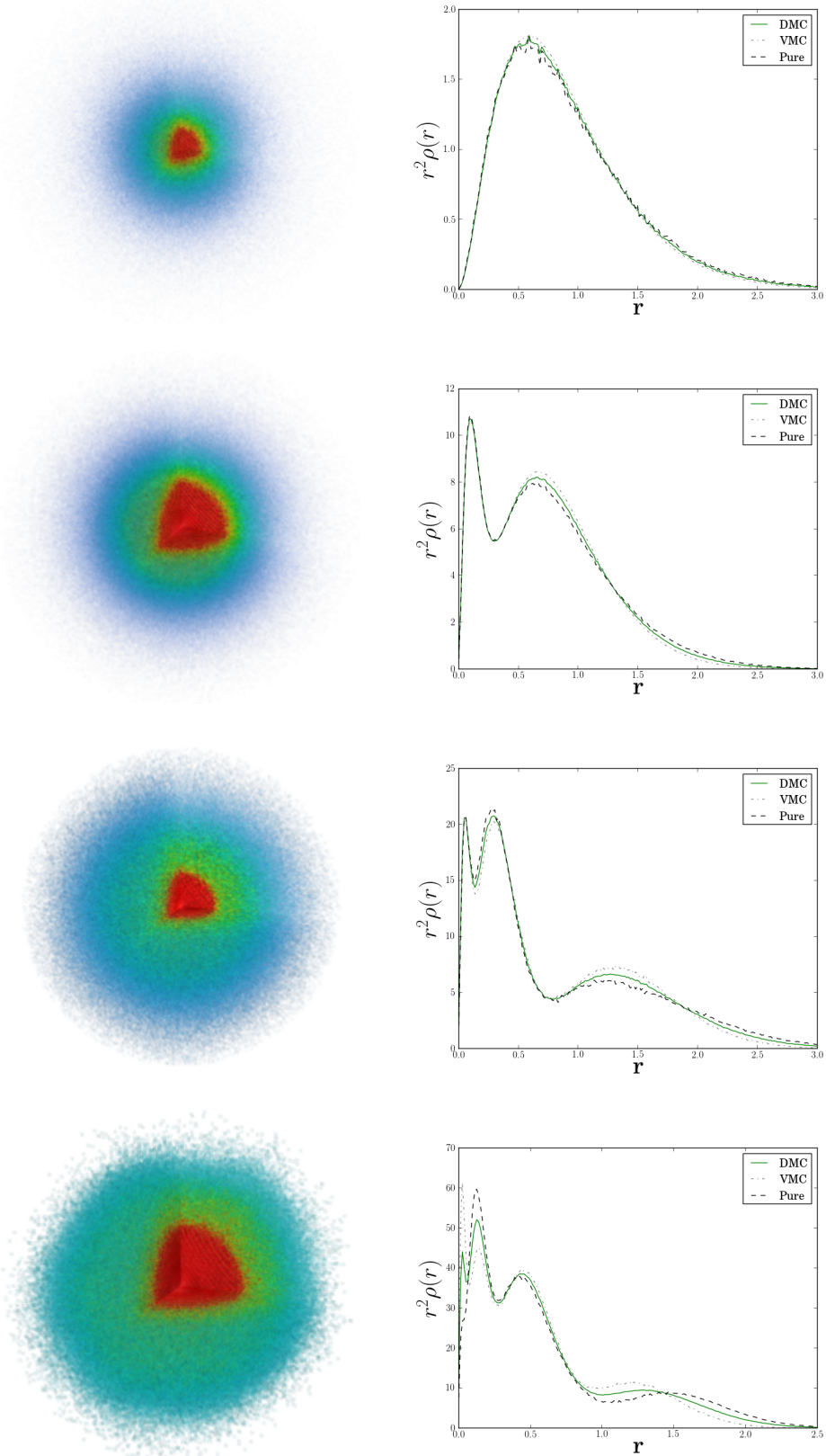


Figure 5.9: Counting top to bottom: Helium, Neon, Argon and Krypton. See Fig. 5.10 for descriptions.

5.4.3 Alkaline Earth Metals

blah blah good approximation with one determinant - \downarrow calculations possible.

More smushed out; missing contribution from higher $-m_l$ since the shell is not closed.

DMC still are able to span out a more correct wave function. This is backed up by experimental data comparisons.

The densities are similar to their close noble-gas relative, however, the two additional particles creates a disperse probability cloud. The noble gases have more well-defined (sharp) shell structures.

Another interesting fact: VMC distribution and the estimated pure DMC distribution is more different for the alkaline earth metals than for the noble gases. This is expected since M=0 S=0 ground state is major contributions from 3p 2p states.

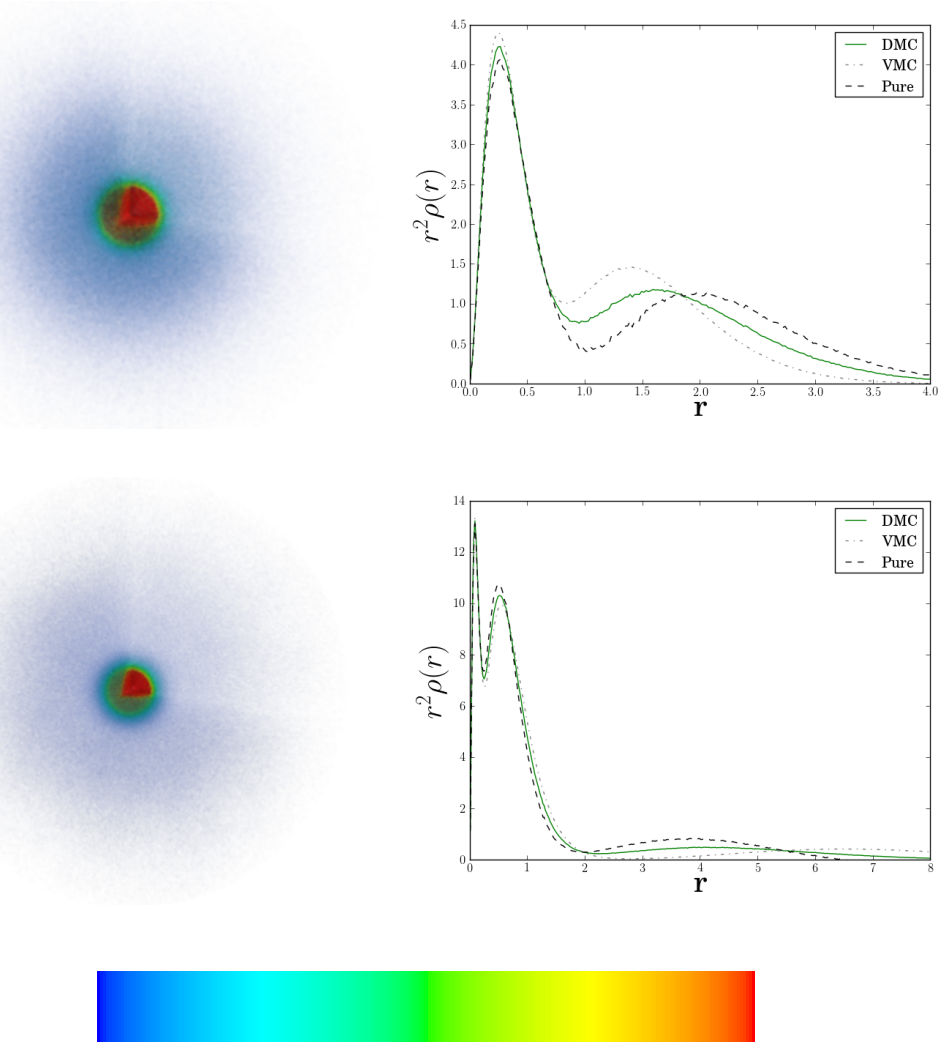


Figure 5.10: Three dimensional one-body density (left column) and angular averaged radii (right column) for alkaline earth metals; Beryllium (top) and Magnesium (bottom). The color bar shows increasing values from left to right. Notice that it is not the radial one-body density (which is too steep to reveal characteristics) in the right column, but the electron . Compared to the noble gases in Fig. 5.9, the alkaline earth metals have a surrounding dispersed probability cloud due to the broken closed shell symmetry. The element is thus more unstable and potent for chemical reactions and molecular formations through covalent bonds.

Appendices

A

Dirac Notation

Due to the orthogonal nature of Hermitian operators' eigenfunctions¹, the inner product between two states constructed from them will result in a lot of integrals being zero, one, or eigenvalues for that matter. Writing the integrals in their full form then feels like a waste of space and time. Even specifying e.g. a position basis is obsolete. Abstracting the wave functions from a given parameter space (e.g. \mathbb{C}^n) into a *Hilbert space*² is what is called the *Dirac notation*, or the *Bra-ket notation*.

The basic idea is that since the coordinate representation of a wave function is the projection of an abstract state on the position basis through an inner product, we can separate the different pieces of the inner product:

$$\psi(\vec{r}) = \langle r, \psi_j \rangle \equiv \langle r | \psi_j \rangle = \langle r | \times | \psi_j \rangle .$$

The notation is designed to be simple. The right hand side of the inner product is called a *ket*, while the left hand side is called a *bra*. Combining both of them leaves you with an inner product bracket, hence the names. Let us look at an example where this notation is extremely powerful. Imagine a coupled two-particle spin- $\frac{1}{2}$ system in the following state

$$|\psi\rangle = N \left[|\uparrow\downarrow\rangle - i |\downarrow\uparrow\rangle \right] \quad (\text{A.1})$$

$$\langle\psi| = N \left[\langle\uparrow\downarrow| + i \langle\downarrow\uparrow| \right] \quad (\text{A.2})$$

Using the fact that both the full two-particle state and the two-level spin states should be orthonormal, we can with this notation calculate the normalization factor without explicitly calculating anything.

$$\begin{aligned} \langle\psi|\psi\rangle &= N^2 \left[\langle\uparrow\downarrow| + i \langle\downarrow\uparrow| \right] \left[|\uparrow\downarrow\rangle - i |\downarrow\uparrow\rangle \right] \\ &= N^2 \left[\langle\uparrow\downarrow|\uparrow\downarrow\rangle + i \langle\downarrow\uparrow|\uparrow\downarrow\rangle - i \langle\uparrow\downarrow|\downarrow\uparrow\rangle + \langle\downarrow\uparrow|\downarrow\uparrow\rangle \right] \\ &= N^2 \left[1 + 0 - 0 + 1 \right] \\ &= 2N^2 \end{aligned}$$

¹Eigenfunctions of a Hermitian operator always make up a complete orthogonal set.

²A Hilbert space is an inner product space spanned by the different states. For every state, there exists a complementary state which is the Hermitian conjugate of the original[7].

This implies as we expected $N = 1/\sqrt{2}$. With this powerful notation at hand, we can easily show properties such as the *completeness relation* of a set. We start by expanding one state $|\phi\rangle$ in a complete set of different states $|\psi_i\rangle$:

$$\begin{aligned} |\phi\rangle &= \sum_i c_i |\psi_i\rangle \\ \langle\psi_k|\phi\rangle &= \sum_i c_i \langle\psi_k|\psi_i\rangle \\ &= c_k \\ |\phi\rangle &= \sum_i \langle\psi_i|\phi\rangle |\psi_i\rangle \\ &= \left[\sum_i |\psi_i\rangle \langle\psi_i| \right] |\phi\rangle, \end{aligned}$$

which implies that

$$\sum_i |\psi_i\rangle \langle\psi_i| = \mathbb{1} \quad (\text{A.3})$$

for any complete set of orthonormal states $|\psi_i\rangle$. For a continuous basis like e.g. the position basis we have a similar relation:

$$\int |\psi(x)|^2 dx = 1 \quad (\text{A.4})$$

$$\begin{aligned} \int |\psi(x)|^2 dx &= \int \psi^*(x)\psi(x)dx \\ &= \int \langle\psi|x\rangle \langle x|\psi\rangle dx \\ &= \langle\psi| \left[\int |x\rangle \langle x| dx \right] |\psi\rangle. \end{aligned} \quad (\text{A.5})$$

Combining eq. A.4 and eq. A.5 with the fact that $\langle\psi|\psi\rangle = 1$ yields the identity

$$\int |x\rangle \langle x| dx = \mathbb{1}. \quad (\text{A.6})$$

B

DCViz: Visualization of Data

With an increasingly massive code framework comes the increased need of data analysis tools. Data analysis usually involves visualization of the data; there is only so much information a single number can hold. To supplement the QMC code, a visualization tool has been developed.

The tool DCViz (Dynamic Column data Visualizer) is a Python based visualization tool designed to plot data stored in columns. The plot library used is *Matplotlib*. The data can be plotted dynamically at a specified interval, and is hence designed to run parallel to the main application, e.g. DMC. The convergence of the DMC method is much better represented by a trailing energy graph than simply a stream of numbers. The same goes for the minimization process.

B.1 Basic Usage

Just like for the `orbitalsGenerator` tool (see Appendix C), specific implementations come in the shape of subclasses of the DCViz superclass. All the functionality regarding setting up figures, re-plotting dynamically, clearing figures to avoid random crashes if used repeatedly, etc. is inherited from the superclass. The necessary elements to implement is

| | |
|-------------------------------|--|
| <code>figMap</code> | A dictionary representing the names and structure of the plotted figures. <code>figMap = {"fig1": ["subFig1", "subFig2", "subFig3"], "fig2": ["subFig4"]}</code> Will create two figures, where the first is split into three sub-figures. In class member functions, <code>self.subFig1</code> will be available as the figure representing the first sub-figure of <code>self.fig1</code> . |
| <code>nametag</code> | A string, e.g. <code>nametag = "DMC_out_\d+\.dat"</code> , representing the name of the output files associated with the given implementation (subclass). Full regular expressions support. Used in order to automatically detect which subclass to load for a specific file. |
| <code>plot(self, data)</code> | The loaded file will be loaded into a <code>data</code> object, which is an iterator where each elements represents a column in the data file. Designed such that expressions like <code>col1, col2 = data</code> is possible (and fast). To access the raw data as a matrix, use <code>data.data</code> In the plot function, the sub-figures introduced in <code>figMap</code> should be loaded with data through e.g. <code>self.subFig1.plot(col1, col2)</code> . |

An example implementation would be

```

1 #DCViz_classes.py
2
3 from DCViz_sup import DCVizPlotter
4
5 class myTestClass(DCVizPlotter):
6     nametag = 'testcase\d\.dat' #filename with regex support
7
8     #1 figure with 1 subfigure
9     figMap = {'fig1': ['subfig1']}
10
11     #skip first row.
12     skipRows = 1
13
14     def plot(self, data):
15         column1 = data[0]
16
17         self.subfig1.set_title('I have $\\LaTeX$ support!')
18
19         self.subfig1.set_ylim([-1,1])
20
21         self.subfig1.plot(column1)

```

Additional Support

Additional parameters can be overloaded for additional functionality

| | |
|-----------------------|--|
| <code>nCols</code> | The number of columns present in the file. Will be automatically detected unless the data is stored in binary format. |
| <code>skipRows</code> | The number of initial rows to skip. Will be automatically detected unless the data is stores as a single column. |
| <code>skipCols</code> | The number of initial columns to skip. Defaults to zero. |
| <code>armaBin</code> | Boolean flag. If set to true, the data is assumed to be stored in Armadillo's binary format (doubles). Number of columns and rows will be read from the file header. |
| <code>fileBin</code> | Boolean flag. If set to true, the data is assumed to be stores in binary format. The number of columns must be specified. |

The L^AT_EXsupport is enabled if the correct packages is installed.

Families

A specific implementation can be flagged to belong to a family by setting the class member variable `isFamilyMember` to true. If this flag is true, the folder where the originally data was loaded will be scanned for additional matches, all of which will be loaded into the `data` input to the `plot` function. In this case each element of the `data` list would be a column iterator as explained previously.

To keep track of which file a given data-set was loaded from, a list `self.familyFileNames` is created, where element *i* is the filename corresponding to `data[i]`.

A class member string `familyName` can be overridden to display a more general name in the auto-detection feedback. An example implementation using data file families would be

```

1 #DCViz_classes.py
2
3 from DCViz_sup import DCVizPlotter
4

```

```

5 class myTestClassFamily(DCVizPlotter):
6     nametag = 'testcaseFamily\d\.dat' #filename with regex support
7
8     #1 figure with 3 subfigures
9     figMap = {'fig1': ['subfig1', 'subfig2', 'subfig3']}
10
11    #skip first row of each data file.
12    skipRows = 1
13
14    #Using this flag will read all the files matching the nametag
15    #(in the same folder.) and make them aviable in the data arg
16    isFamilyMember = True
17    familyName = "testcase"
18
19    def plot(self, data):
20
21        #figures[0] is 'fig1' figures. the 0'th element is the
22        #self.fig1 itself. Subfigures are always index [1:]
23        mainFig = self.figures[0][0]
24        mainFig.suptitle('I have $\\LaTeX$ support!')
25        subfigs = self.figures[0][1:]
26
27        #Notice we plot fileData.data (In order to get the numpy object)
28        #and not fileData alone, as fileData is a 'dataGenerator' instance
29        #used to speed up file reading. Alternatively, we could send data[:,]
30        for subfig, fileData in zip(subfigs, data):
31            subfig.plot(fileData.data)
32            subfig.set_ylim([-1,1])

```

loading e.g. `testcaseFamily0.dat` would automatically load `testcaseFamily1.dat` etc. as well.

The Application Programming Interface (API)

The DCViz library has been developed to interface nicely with any Python script¹. Given a path to the data file, all that is needed in order to visualize it is

```

1 import DCVizWrapper as viz
2 dynamicMode = False #or true
3
4 ...
5 #Perform some calculations and store these in the file myDataFile (including path)
6
7 #DCVizWrapper.main() automatically detects the subclass implementation
8 #matching the specified file. Thread safe and easily interruptable.
9 viz.main(path=myDataFile, dynamic=dynamicMode)

```

The Terminal Client

The `DCVizWrapper.py` script can also be called directly from a terminal using the path as first command line argument. If the option `-d` is supplied, dynamic mode is activated.

The GUI

The script `DCVizGUI.py` sets up a GUI for visualizing data using DCViz. The GUI is implemented using pyside (python wrapper for Qt), and is designed to be simple. Data files are loaded from an open-file

¹DCViz can also be called through C++, however, no header has been implemented for this. Typically one would use the std::system or std::thread to start the script in the background.

dialog, and will appear in a drop-down menu once loaded. The play button executes the main loop of the currently selected data file. Dynamic mode is selected though a check-box, and the refresh interval is set by a slider (from zero to ten seconds). Warnings can be disabled through the configuration file.

The GUI can be opened from any Python script by calling the `main` function (should be threaded if used as part of another application). If a path is supplied to the function, this path will be default in all file dialogues. Defaults to the current working directory.

The following is a tiny script executing the GUI for a QMC application. If no path is supplied at the command line, the default path is set to the scratch path.

```

1 import sys, os
2 from pyLibQMC import paths #contains all files specific to the QMC library
3
4 #Adds DCVizGUI to the Python path
5 sys.path.append(os.path.join(paths.toolsPath, "DCViz", "GUI"))
6
7 import DCVizGUI
8
9 if __name__ == "__main__":
10
11     if len(sys.argv) > 1:
12         path = sys.argv[1]
13     else:
14         path = paths.scratchPath
15
16     sys.exit(DCVizGUI.main(path))

```

Alternatively, `DCVizGUI.py` can be executed directly from the terminal with an optional default path as first command line argument.

The following is the terminal feedback supplied from opening the GUI

```

~/.../DCViz/GUI$ python DCVizGUI.py
[ Detector ]: Found subclasses 'myTestClass', 'myTestClassFamily', 'EnergyTrail',
'Blocking', 'DMC_OUT', 'radial_out', 'dist_out', 'testBinFile', 'MIN_OUT'
[ GUI      ]: Data reset.

```

Selecting a folder from the open-folder dialog initializes the detector on all file content

```

[ Detector ]: matched [ DMC_out.dat ] with [      DMC_OUT      ]
[ Detector ]: matched [ ASGD_out.dat ] with [      MIN_OUT      ]
[ Detector ]: matched [blocking_DMC_out.dat] with [      Blocking    ]
[ Detector ]: 'blocking_MIN_out0_RAWDATA.arma' does not match any DCViz class
[ Detector ]: 'blocking_DMC_out_RAWDATA.arma' does not match any DCViz class
[ Detector ]: matched [blocking_VMC_out.dat] with [      Blocking    ]

```

All matched files will be listed in the drop-down menu. Selecting a file, and pressing the play button initializes a job. Pressing the stop button (replacing the play in case of dynamic mode), will end the job. All jobs are threaded, hence several non-dynamic jobs can be ran at once. The limit is set to one dynamic job pr. application.

```

[   Job     ]: Starting.
[   Job     ]: Stoping... Stopped.

```

Screen-shots of the GUI taken in the process listed previously is given in Fig. B.1.

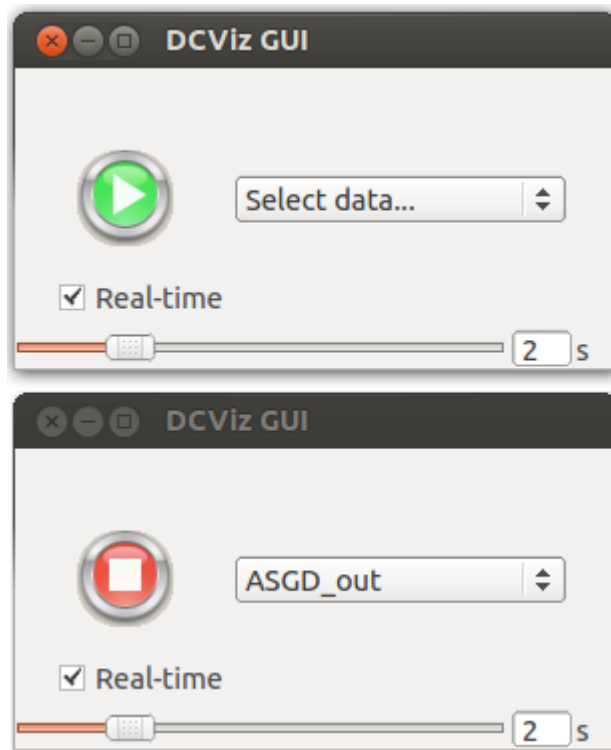


Figure B.1: Two consequent screen shots of the GUI. The first (top) is taken directly after the detector is finished loading files into the drop-down menu. The second is taken directly after the job is started.

The terminal tracker can be silenced through to configuration file to not interfere with the standard output of an application. Alternatively, the GUI thread can redirect its standard output to file.

C

Auto-generation with SymPy

“SymPy is a Python library for symbolic mathematics. It aims to become a full-featured computer algebra system (CAS) while keeping the code as simple as possible in order to be comprehensible and easily extensible. SymPy is written entirely in Python and does not require any external libraries.” - The SymPy Home Page

The focus on this appendix will be on using SymPy to calculate closed form expressions for single particle wave functions needed to optimize the calculations of the Slater gradient and Laplacian. For systems of many particles, it is crucial to optimize to have these expressions in order for the code to remain efficient.

Calculating these expressions by hand is out of the question, given that the complexity of the expressions is proportional to the magnitude of the quantum number, which again scales with the number of particles. In the case of a 42 particle Quantum Dot, the number of unique derivatives involved in the simulation is 84.

C.1 Usage

SymPy is, as described in the introductory quote, designed to be simple to use. This section will cover the basics needed to calculate gradients and Laplacians, auto-generating C++ - and Latex code.

C.1.1 Doing Symbolic Algebra

In order for SymPy to recognize e.g. `x` as a symbol, that is, a *mathematical variable*. In contrast to programming variables, symbols are not initialized to a value. Initializing symbols can be done in several ways, the two most common are listed below

```
1 In [1]: from sympy import Symbol, symbols
2
3 In [2]: x = Symbol('x')
4
5 In [3]: y, z = symbols('y z')
6
7 In [7]: x*x+y
8 Out[7]: 'x**2 + y'
```

The `Symbol` function handles single symbols, while `symbols` can initialize several symbols simultaneously. The string argument might seem redundant, however, this represents the *label* displayed using print functions. In addition, key word arguments can be sent to the symbol functions, flagging variables as e.g. positive, real, etc.

```

1 In [1]: from sympy import Symbol, symbols, im
2
3 In [2]: x2 = Symbol('x^2', real=True, positive=True) #Flagged as real. Note the label.
4
5 In [3]: y, z = symbols('y z') #Not flagged as real
6
7 In [7]: x2+y #x2 is printed more nicely given a describing label
8 Out[7]: 'x^2 + y'
9
10 In [8]: im(z) #Imaginary part cannot be assumed to be anything.
11 Out[8]: 'im(z)'
12
13 In [9]: im(x2) #Flagged as real, the imaginary part is zero.
14 Out[9]: 0

```

C.1.2 Exporting C++ and Latex Code

Exporting code is extremely simple. Consider the following example

```

1 In [1]: from sympy import symbols, printing, exp
2
3 In [2]: x, x2 = symbols('x x^2')
4
5 In [3]: printing.ccode(x*x*x*x*exp(-x2*x))
6 Out[3]: 'pow(x, 4)*exp(-x*x^2)'
7
8 In [4]: printing.ccode(x*x*x*x)
9 Out[4]: 'pow(x, 4)'
10
11 In [5]: print printing.latex(x*x*x*x*exp(-x2))
12 \frac{x^{ 4} }{e^{x^2} }

```

The following expression is the direct output from line five compiled in Latex

$$\frac{x^4}{e^{x^2}}$$

C.1.3 Calculating Derivatives

As an example for this section, let's look at the $2s$ orbital from hydrogen (not normalized)

$$\phi_{2s}(\vec{r}) = (Zr - 2)e^{-\frac{1}{2}Zr} \quad (C.1)$$

$$r^2 = x^2 + y^2 + z^2 \quad (C.2)$$

Calculating the gradients and Laplacian is very simply by using the `diff` function

```

1 In [1]: from sympy import symbols, diff, exp, sqrt
2
3 In [2]: x, y, z, Z = symbols('x y z Z')
4
5 In [3]: r = sqrt(x*x + y*y + z*z)
6

```

```

7 In [4]: r
8 Out[4]: '(x**2 + y**2 + z**2)**(1/2)'
9
10 In [5]: phi = (Z*r - 2)*exp(-Z*r/2)
11
12 In [6]: phi
13 Out[6]: '(Z*(x**2 + y**2 + z**2)**(1/2) - 2)*exp(-Z*(x**2 + y**2 + z**2)**(1/2)/2)'
14
15 In [7]: diff(phi, x)
16 Out[7]: '-Z*x*(Z*(x**2 + y**2 + z**2)**(1/2) - 2)*exp(-Z*(x**2 + y**2 + z**2)**(1/2)/2)
17     /(2*(x**2 + y**2 + z**2)**(1/2)) + Z*x*exp(-Z*(x**2 + y**2 + z**2)**(1/2)/2)/(x**2 +
y**2 + z**2)**(1/2)',
```

Now, this looks like a nightmare. However, SymPy has great support for simplifying expressions. The following code demonstrated this quite nicely

```

1 ...
2
3 In [6]: phi
4 Out[6]: '(Z*(x**2 + y**2 + z**2)**(1/2) - 2)*exp(-Z*(x**2 + y**2 + z**2)**(1/2)/2)'
5
6 In [7]: from sympy import factor, Symbol, printing
7
8 In [8]: R = Symbol('r') #Creates a symbolic equivalent of the mathematical r
9
10 In [9]: diff(phi, x).factor() #Gathers all the terms nicely
11 Out[9]: '-Z*x*(Z*(x**2 + y**2 + z**2)**(1/2) - 4)*exp(-Z*(x**2 + y**2 + z**2)**(1/2)/2)
12     /(2*(x**2 + y**2 + z**2)**(1/2))'
13
14 In [10]: diff(phi, x).factor().subs(r, R) #replaces (x^2 + y^2 + z^2)^(1/2) with r
15 Out[10]: '-Z*x*(Z*r - 4)*exp(-Z*r/2)/(2*r)'
16
17 In [11]: print printing.latex(diff(phi, x).factor().subs(r, R))
- \frac{Z x \left(Z r - 4\right)}{2 r e^{\frac{1}{2} Z r}}
```

This version of the expression is much more satisfying to the eye. Result:

$$-\frac{Zx(Zr - 4)}{2re^{\frac{1}{2}Zr}}$$

Estimating the Laplacian is just a matter of summing double derivatives

```

1 ...
2
3 In [12]: (diff(diff(phi, x), x) +
4     ....: diff(diff(phi, y), y) +
5     ....: diff(diff(phi, z), z)).factor().subs(r, R)
6 Out[12]: 'Z*(Z**2*x**2 + Z**2*y**2 + Z**2*z**2 - 10*Z*r + 16)*exp(-Z*r/2)/(4*r)'
7
8 In [13]: (diff(diff(phi, x), x) + #Not quite satisfying.
9     ....: diff(diff(phi, y), y) + #Let's collect the 'Z' terms.
10    ....: diff(diff(phi, z), z)).factor().collect(Z).subs(r, R)
11 Out[13]: 'Z*(Z**2*(x**2 + y**2 + z**2) - 10*Z*r + 16)*exp(-Z*r/2)/(4*r)'
12
13 In [14]: (diff(diff(phi, x), x) + #Still not satisfying.
14     ....: diff(diff(phi, y), y) + #The r^2 terms needs to be substituted as well.
15     ....: diff(diff(phi, z), z)).factor().collect(Z).subs(r, R).subs(r**2, R**2)
16 Out[14]: 'Z*(Z**2*r**2 - 10*Z*r + 16)*exp(-Z*r/2)/(4*r)'
17
18 In [15]: (diff(diff(phi, x), x) + #Let's try to factorize once more.
19     ....: diff(diff(phi, y), y) +
20     ....: diff(diff(phi, z), z)).factor().collect(Z).subs(r, R).subs(r**2, R**2).factor()
21 Out[15]: 'Z*(Z*r - 8)*(Z*r - 2)*exp(-Z*r/2)/(4*r)'
```

Getting the right factorization may come across as tricky, but with minimal training this poses no real problems.

C.2 Using the auto-generation Script

The Python superclass `orbitalsGenerator` (the generator) aims to serve as a interface with the C++ `BasisFunctions` class, automatically generating the C++ code containing all the implementations of the derivatives for the given single particle states. The single particle states are implemented in the generator by subclasses overloading system specific virtual functions:

| | |
|------------------------------|--|
| <code>constructor</code> | Takes argument <code>M</code> equal to the number of orbitals to compute, should directly be set by <code>self.setMax(M)</code> . |
| | Second argument <code>doInit</code> defaults to <code>True</code> . Should be sent to superclass constructor. If false, does not initialize the construction of expression, latex file, etc. |
| | Third argument <code>toCPP</code> defaults to <code>False</code> . Should be sent to superclass constructor. If true, C++ files will be generated. |
| <code>makeStateMap</code> | Setup the <code>self.stateMap</code> list, where index i represents a set of quantum numbers. Auto-generated L ^A T _E Xtables will then include quantum numbers. Ensured correct quantum number - expression pairs sent to simplification functions etc. |
| <code>setupOrbitals</code> | Fill the <code>self.orbitals</code> list with SymPy expressions representing the single particle wave functions. Must be functions of the x , y and z SymPy Symbols. Used to calculate the gradients and Laplacians. Element i will represent quantum number i . |
| <code>simplifyLocal</code> | Implement the factorization of the raw expressions. E.g. $kxe^{-x} + ke^{-x} \rightarrow k(x + 1)e^{-x}$. Quantum numbers are supplied in the argument in case they are needed, e.g. in the n -dependent exponential factor of the hydrogenic orbitals. |
| <code>genericFactor</code> | Defaults to unity. In case all expressions share a common factor, e.g. $\exp(-\frac{1}{2}\alpha\omega r^2)$ in the case of Quantum Dots, this can be implemented as a generic factor, cleaning up the Latex table. May also dramatically clean up the simplification code. |
| <code>extraToFile</code> | Returns a string which will be set as an introductory text to the Latex output. |
| <code>initCPPbasis</code> | Set up the C++ class names, constructor arguments, member variables. See e.g. the <code>H0.py</code> file for examples. |
| <code>getCPRe</code> | Given an expression and a its index i as input, set up the C++ pre-return calculation. E.g. <code>H = printing.ccode(expr/self.genericFactor(i))</code> ; |
| <code>getCreturn</code> | Given an expression and a its index i as input, set up the C++ return value. E.g. <code>return H*(exp_factor)</code> ; |
| <code>makeOrbConstArg</code> | Used to set up the constructor input in the generated <code>Orbitals</code> constructor. Defaults to sending names equal to those used in the declaration, however, in e.g. the case of hydrogenic orbitals, different basis functions need different exponential factors. See <code>hydrogenic.py</code> for an example. |

Implementing these functions will generate a Latex file listing the calculated expressions (see Appendix D and E), the constructor needed by the `Orbitals` subclass holding the generated orbitals and C++ header and source files containing the `BasisFunctions` implementation. In the code used in this thesis, 6000 lines of C++ code was auto-generated using SymPy.

D

Harmonic Oscillator Orbitals

Orbitals are constructed in the following fashion:

$$\phi(\vec{r})_{n_x, n_y} = H_{n_x}(kx)H_{n_y}(ky)e^{-\frac{1}{2}k^2 r^2}$$

where $k = \sqrt{(\omega\alpha)}$, with ω being the oscillator frequency and α being the variational parameter.

| | |
|-----------|--|
| $H_0(kx)$ | 1 |
| $H_1(kx)$ | $2kx$ |
| $H_2(kx)$ | $4k^2x^2 - 2$ |
| $H_3(kx)$ | $8k^3x^3 - 12kx$ |
| $H_4(kx)$ | $16k^4x^4 - 48k^2x^2 + 12$ |
| $H_5(kx)$ | $32k^5x^5 - 160k^3x^3 + 120kx$ |
| $H_6(kx)$ | $64k^6x^6 - 480k^4x^4 + 720k^2x^2 - 120$ |
| $H_0(ky)$ | 1 |
| $H_1(ky)$ | $2ky$ |
| $H_2(ky)$ | $4k^2y^2 - 2$ |
| $H_3(ky)$ | $8k^3y^3 - 12ky$ |
| $H_4(ky)$ | $16k^4y^4 - 48k^2y^2 + 12$ |
| $H_5(ky)$ | $32k^5y^5 - 160k^3y^3 + 120ky$ |
| $H_6(ky)$ | $64k^6y^6 - 480k^4y^4 + 720k^2y^2 - 120$ |

Table D.1: Hermite polynomials used to construct orbital functions

| $\phi_0 \rightarrow \phi_{0,0}$ | |
|--------------------------------------|---------------------|
| $\phi(\vec{r})$ | 1 |
| $\vec{i} \cdot \nabla \phi(\vec{r})$ | $-k^2 x$ |
| $\vec{j} \cdot \nabla \phi(\vec{r})$ | $-k^2 y$ |
| $\nabla^2 \phi(\vec{r})$ | $k^2 (k^2 r^2 - 2)$ |

Table D.2: Orbital expressions HOOrbitals : 0, 0. Factor $e^{-\frac{1}{2}k^2r^2}$ is omitted.

| $\phi_1 \rightarrow \phi_{0,1}$ | |
|--------------------------------------|-----------------------|
| $\phi(\vec{r})$ | y |
| $\vec{i} \cdot \nabla \phi(\vec{r})$ | $-k^2 xy$ |
| $\vec{j} \cdot \nabla \phi(\vec{r})$ | $-(ky - 1)(ky + 1)$ |
| $\nabla^2 \phi(\vec{r})$ | $k^2 y (k^2 r^2 - 4)$ |

Table D.3: Orbital expressions HOOrbitals : 0, 1. Factor $e^{-\frac{1}{2}k^2r^2}$ is omitted.

| $\phi_2 \rightarrow \phi_{1,0}$ | |
|--------------------------------------|-----------------------|
| $\phi(\vec{r})$ | x |
| $\vec{i} \cdot \nabla \phi(\vec{r})$ | $-(kx - 1)(kx + 1)$ |
| $\vec{j} \cdot \nabla \phi(\vec{r})$ | $-k^2 xy$ |
| $\nabla^2 \phi(\vec{r})$ | $k^2 x (k^2 r^2 - 4)$ |

Table D.4: Orbital expressions HOOrbitals : 1, 0. Factor $e^{-\frac{1}{2}k^2r^2}$ is omitted.

| $\phi_3 \rightarrow \phi_{0,2}$ | |
|--------------------------------------|------------------------------------|
| $\phi(\vec{r})$ | $2k^2 y^2 - 1$ |
| $\vec{i} \cdot \nabla \phi(\vec{r})$ | $-k^2 x (2k^2 y^2 - 1)$ |
| $\vec{j} \cdot \nabla \phi(\vec{r})$ | $-k^2 y (2k^2 y^2 - 5)$ |
| $\nabla^2 \phi(\vec{r})$ | $k^2 (k^2 r^2 - 6) (2k^2 y^2 - 1)$ |

Table D.5: Orbital expressions HOOrbitals : 0, 2. Factor $e^{-\frac{1}{2}k^2r^2}$ is omitted.

| $\phi_4 \rightarrow \phi_{1,1}$ | |
|--------------------------------------|------------------------|
| $\phi(\vec{r})$ | xy |
| $\vec{i} \cdot \nabla \phi(\vec{r})$ | $-y (kx - 1)(kx + 1)$ |
| $\vec{j} \cdot \nabla \phi(\vec{r})$ | $-x (ky - 1)(ky + 1)$ |
| $\nabla^2 \phi(\vec{r})$ | $k^2 xy (k^2 r^2 - 6)$ |

Table D.6: Orbital expressions HOOrbitals : 1, 1. Factor $e^{-\frac{1}{2}k^2r^2}$ is omitted.

| | |
|--------------------------------------|--------------------------------|
| $\phi_5 \rightarrow \phi_{2,0}$ | |
| $\phi(\vec{r})$ | $2k^2x^2 - 1$ |
| $\vec{i} \cdot \nabla \phi(\vec{r})$ | $-k^2x(2k^2x^2 - 5)$ |
| $\vec{j} \cdot \nabla \phi(\vec{r})$ | $-k^2y(2k^2x^2 - 1)$ |
| $\nabla^2 \phi(\vec{r})$ | $k^2(k^2r^2 - 6)(2k^2x^2 - 1)$ |

Table D.7: Orbital expressions HOOrbitals : 2, 0. Factor $e^{-\frac{1}{2}k^2r^2}$ is omitted.

| | |
|--------------------------------------|---------------------------------|
| $\phi_6 \rightarrow \phi_{0,3}$ | |
| $\phi(\vec{r})$ | $y(2k^2y^2 - 3)$ |
| $\vec{i} \cdot \nabla \phi(\vec{r})$ | $-k^2xy(2k^2y^2 - 3)$ |
| $\vec{j} \cdot \nabla \phi(\vec{r})$ | $-2k^4y^4 + 9k^2y^2 - 3$ |
| $\nabla^2 \phi(\vec{r})$ | $k^2y(k^2r^2 - 8)(2k^2y^2 - 3)$ |

Table D.8: Orbital expressions HOOrbitals : 0, 3. Factor $e^{-\frac{1}{2}k^2r^2}$ is omitted.

| | |
|--------------------------------------|----------------------------------|
| $\phi_7 \rightarrow \phi_{1,2}$ | |
| $\phi(\vec{r})$ | $x(2k^2y^2 - 1)$ |
| $\vec{i} \cdot \nabla \phi(\vec{r})$ | $-(kx - 1)(kx + 1)(2k^2y^2 - 1)$ |
| $\vec{j} \cdot \nabla \phi(\vec{r})$ | $-k^2xy(2k^2y^2 - 5)$ |
| $\nabla^2 \phi(\vec{r})$ | $k^2x(k^2r^2 - 8)(2k^2y^2 - 1)$ |

Table D.9: Orbital expressions HOOrbitals : 1, 2. Factor $e^{-\frac{1}{2}k^2r^2}$ is omitted.

| | |
|--------------------------------------|----------------------------------|
| $\phi_8 \rightarrow \phi_{2,1}$ | |
| $\phi(\vec{r})$ | $y(2k^2x^2 - 1)$ |
| $\vec{i} \cdot \nabla \phi(\vec{r})$ | $-k^2xy(2k^2x^2 - 5)$ |
| $\vec{j} \cdot \nabla \phi(\vec{r})$ | $-(ky - 1)(ky + 1)(2k^2x^2 - 1)$ |
| $\nabla^2 \phi(\vec{r})$ | $k^2y(k^2r^2 - 8)(2k^2x^2 - 1)$ |

Table D.10: Orbital expressions HOOrbitals : 2, 1. Factor $e^{-\frac{1}{2}k^2r^2}$ is omitted.

| | |
|--------------------------------------|---------------------------------|
| $\phi_9 \rightarrow \phi_{3,0}$ | |
| $\phi(\vec{r})$ | $x(2k^2x^2 - 3)$ |
| $\vec{i} \cdot \nabla \phi(\vec{r})$ | $-2k^4x^4 + 9k^2x^2 - 3$ |
| $\vec{j} \cdot \nabla \phi(\vec{r})$ | $-k^2xy(2k^2x^2 - 3)$ |
| $\nabla^2 \phi(\vec{r})$ | $k^2x(k^2r^2 - 8)(2k^2x^2 - 3)$ |

Table D.11: Orbital expressions HOOrbitals : 3, 0. Factor $e^{-\frac{1}{2}k^2r^2}$ is omitted.

| $\phi_{10} \rightarrow \phi_{0,4}$ | |
|--------------------------------------|--|
| $\phi(\vec{r})$ | $4k^4y^4 - 12k^2y^2 + 3$ |
| $\vec{i} \cdot \nabla \phi(\vec{r})$ | $-k^2x(4k^4y^4 - 12k^2y^2 + 3)$ |
| $\vec{j} \cdot \nabla \phi(\vec{r})$ | $-k^2y(4k^4y^4 - 28k^2y^2 + 27)$ |
| $\nabla^2 \phi(\vec{r})$ | $k^2(k^2r^2 - 10)(4k^4y^4 - 12k^2y^2 + 3)$ |

Table D.12: Orbital expressions HOOrbitals : 0, 4. Factor $e^{-\frac{1}{2}k^2r^2}$ is omitted.

| $\phi_{11} \rightarrow \phi_{1,3}$ | |
|--------------------------------------|-----------------------------------|
| $\phi(\vec{r})$ | $xy(2k^2y^2 - 3)$ |
| $\vec{i} \cdot \nabla \phi(\vec{r})$ | $-y(kx - 1)(kx + 1)(2k^2y^2 - 3)$ |
| $\vec{j} \cdot \nabla \phi(\vec{r})$ | $-x(2k^4y^4 - 9k^2y^2 + 3)$ |
| $\nabla^2 \phi(\vec{r})$ | $k^2xy(k^2r^2 - 10)(2k^2y^2 - 3)$ |

Table D.13: Orbital expressions HOOrbitals : 1, 3. Factor $e^{-\frac{1}{2}k^2r^2}$ is omitted.

| $\phi_{12} \rightarrow \phi_{2,2}$ | |
|--------------------------------------|--|
| $\phi(\vec{r})$ | $(2k^2x^2 - 1)(2k^2y^2 - 1)$ |
| $\vec{i} \cdot \nabla \phi(\vec{r})$ | $-k^2x(2k^2x^2 - 5)(2k^2y^2 - 1)$ |
| $\vec{j} \cdot \nabla \phi(\vec{r})$ | $-k^2y(2k^2x^2 - 1)(2k^2y^2 - 5)$ |
| $\nabla^2 \phi(\vec{r})$ | $k^2(k^2r^2 - 10)(2k^2x^2 - 1)(2k^2y^2 - 1)$ |

Table D.14: Orbital expressions HOOrbitals : 2, 2. Factor $e^{-\frac{1}{2}k^2r^2}$ is omitted.

| $\phi_{13} \rightarrow \phi_{3,1}$ | |
|--------------------------------------|-----------------------------------|
| $\phi(\vec{r})$ | $xy(2k^2x^2 - 3)$ |
| $\vec{i} \cdot \nabla \phi(\vec{r})$ | $-y(2k^4x^4 - 9k^2x^2 + 3)$ |
| $\vec{j} \cdot \nabla \phi(\vec{r})$ | $-x(ky - 1)(ky + 1)(2k^2x^2 - 3)$ |
| $\nabla^2 \phi(\vec{r})$ | $k^2xy(k^2r^2 - 10)(2k^2x^2 - 3)$ |

Table D.15: Orbital expressions HOOrbitals : 3, 1. Factor $e^{-\frac{1}{2}k^2r^2}$ is omitted.

| $\phi_{14} \rightarrow \phi_{4,0}$ | |
|--------------------------------------|--|
| $\phi(\vec{r})$ | $4k^4x^4 - 12k^2x^2 + 3$ |
| $\vec{i} \cdot \nabla \phi(\vec{r})$ | $-k^2x(4k^4x^4 - 28k^2x^2 + 27)$ |
| $\vec{j} \cdot \nabla \phi(\vec{r})$ | $-k^2y(4k^4x^4 - 12k^2x^2 + 3)$ |
| $\nabla^2 \phi(\vec{r})$ | $k^2(k^2r^2 - 10)(4k^4x^4 - 12k^2x^2 + 3)$ |

Table D.16: Orbital expressions HOOrbitals : 4, 0. Factor $e^{-\frac{1}{2}k^2r^2}$ is omitted.

| $\phi_{15} \rightarrow \phi_{0,5}$ | |
|--------------------------------------|--|
| $\phi(\vec{r})$ | $y(4k^4y^4 - 20k^2y^2 + 15)$ |
| $\vec{i} \cdot \nabla \phi(\vec{r})$ | $-k^2xy(4k^4y^4 - 20k^2y^2 + 15)$ |
| $\vec{j} \cdot \nabla \phi(\vec{r})$ | $-4k^6y^6 + 40k^4y^4 - 75k^2y^2 + 15$ |
| $\nabla^2 \phi(\vec{r})$ | $k^2y(k^2r^2 - 12)(4k^4y^4 - 20k^2y^2 + 15)$ |

Table D.17: Orbital expressions HOOrbitals : 0, 5. Factor $e^{-\frac{1}{2}k^2r^2}$ is omitted.

| $\phi_{16} \rightarrow \phi_{1,4}$ | |
|--------------------------------------|---|
| $\phi(\vec{r})$ | $x(4k^4y^4 - 12k^2y^2 + 3)$ |
| $\vec{i} \cdot \nabla \phi(\vec{r})$ | $-(kx - 1)(kx + 1)(4k^4y^4 - 12k^2y^2 + 3)$ |
| $\vec{j} \cdot \nabla \phi(\vec{r})$ | $-k^2xy(4k^4y^4 - 28k^2y^2 + 27)$ |
| $\nabla^2 \phi(\vec{r})$ | $k^2x(k^2r^2 - 12)(4k^4y^4 - 12k^2y^2 + 3)$ |

Table D.18: Orbital expressions HOOrbitals : 1, 4. Factor $e^{-\frac{1}{2}k^2r^2}$ is omitted.

| $\phi_{17} \rightarrow \phi_{2,3}$ | |
|--------------------------------------|---|
| $\phi(\vec{r})$ | $y(2k^2x^2 - 1)(2k^2y^2 - 3)$ |
| $\vec{i} \cdot \nabla \phi(\vec{r})$ | $-k^2xy(2k^2x^2 - 5)(2k^2y^2 - 3)$ |
| $\vec{j} \cdot \nabla \phi(\vec{r})$ | $-(2k^2x^2 - 1)(2k^4y^4 - 9k^2y^2 + 3)$ |
| $\nabla^2 \phi(\vec{r})$ | $k^2y(k^2r^2 - 12)(2k^2x^2 - 1)(2k^2y^2 - 3)$ |

Table D.19: Orbital expressions HOOrbitals : 2, 3. Factor $e^{-\frac{1}{2}k^2r^2}$ is omitted.

| $\phi_{18} \rightarrow \phi_{3,2}$ | |
|--------------------------------------|---|
| $\phi(\vec{r})$ | $x(2k^2x^2 - 3)(2k^2y^2 - 1)$ |
| $\vec{i} \cdot \nabla \phi(\vec{r})$ | $-(2k^2y^2 - 1)(2k^4x^4 - 9k^2x^2 + 3)$ |
| $\vec{j} \cdot \nabla \phi(\vec{r})$ | $-k^2xy(2k^2x^2 - 3)(2k^2y^2 - 5)$ |
| $\nabla^2 \phi(\vec{r})$ | $k^2x(k^2r^2 - 12)(2k^2x^2 - 3)(2k^2y^2 - 1)$ |

Table D.20: Orbital expressions HOOrbitals : 3, 2. Factor $e^{-\frac{1}{2}k^2r^2}$ is omitted.

| $\phi_{19} \rightarrow \phi_{4,1}$ | |
|--------------------------------------|---|
| $\phi(\vec{r})$ | $y(4k^4x^4 - 12k^2x^2 + 3)$ |
| $\vec{i} \cdot \nabla \phi(\vec{r})$ | $-k^2xy(4k^4x^4 - 28k^2x^2 + 27)$ |
| $\vec{j} \cdot \nabla \phi(\vec{r})$ | $-(ky - 1)(ky + 1)(4k^4x^4 - 12k^2x^2 + 3)$ |
| $\nabla^2 \phi(\vec{r})$ | $k^2y(k^2r^2 - 12)(4k^4x^4 - 12k^2x^2 + 3)$ |

Table D.21: Orbital expressions HOOrbitals : 4, 1. Factor $e^{-\frac{1}{2}k^2r^2}$ is omitted.

| $\phi_{20} \rightarrow \phi_{5,0}$ | |
|--------------------------------------|--|
| $\phi(\vec{r})$ | $x(4k^4x^4 - 20k^2x^2 + 15)$ |
| $\vec{i} \cdot \nabla \phi(\vec{r})$ | $-4k^6x^6 + 40k^4x^4 - 75k^2x^2 + 15$ |
| $\vec{j} \cdot \nabla \phi(\vec{r})$ | $-k^2xy(4k^4x^4 - 20k^2x^2 + 15)$ |
| $\nabla^2 \phi(\vec{r})$ | $k^2x(k^2r^2 - 12)(4k^4x^4 - 20k^2x^2 + 15)$ |

Table D.22: Orbital expressions HOOrbitals : 5, 0. Factor $e^{-\frac{1}{2}k^2r^2}$ is omitted.

| $\phi_{21} \rightarrow \phi_{0,6}$ | |
|--------------------------------------|--|
| $\phi(\vec{r})$ | $8k^6y^6 - 60k^4y^4 + 90k^2y^2 - 15$ |
| $\vec{i} \cdot \nabla \phi(\vec{r})$ | $-k^2x(8k^6y^6 - 60k^4y^4 + 90k^2y^2 - 15)$ |
| $\vec{j} \cdot \nabla \phi(\vec{r})$ | $-k^2y(8k^6y^6 - 108k^4y^4 + 330k^2y^2 - 195)$ |
| $\nabla^2 \phi(\vec{r})$ | $k^2(k^2r^2 - 14)(8k^6y^6 - 60k^4y^4 + 90k^2y^2 - 15)$ |

Table D.23: Orbital expressions HOOrbitals : 0, 6. Factor $e^{-\frac{1}{2}k^2r^2}$ is omitted.

| $\phi_{22} \rightarrow \phi_{1,5}$ | |
|--------------------------------------|---|
| $\phi(\vec{r})$ | $xy(4k^4y^4 - 20k^2y^2 + 15)$ |
| $\vec{i} \cdot \nabla \phi(\vec{r})$ | $-y(kx - 1)(kx + 1)(4k^4y^4 - 20k^2y^2 + 15)$ |
| $\vec{j} \cdot \nabla \phi(\vec{r})$ | $-x(4k^6y^6 - 40k^4y^4 + 75k^2y^2 - 15)$ |
| $\nabla^2 \phi(\vec{r})$ | $k^2xy(k^2r^2 - 14)(4k^4y^4 - 20k^2y^2 + 15)$ |

Table D.24: Orbital expressions HOOrbitals : 1, 5. Factor $e^{-\frac{1}{2}k^2r^2}$ is omitted.

| $\phi_{23} \rightarrow \phi_{2,4}$ | |
|--------------------------------------|---|
| $\phi(\vec{r})$ | $(2k^2x^2 - 1)(4k^4y^4 - 12k^2y^2 + 3)$ |
| $\vec{i} \cdot \nabla \phi(\vec{r})$ | $-k^2x(2k^2x^2 - 5)(4k^4y^4 - 12k^2y^2 + 3)$ |
| $\vec{j} \cdot \nabla \phi(\vec{r})$ | $-k^2y(2k^2x^2 - 1)(4k^4y^4 - 28k^2y^2 + 27)$ |
| $\nabla^2 \phi(\vec{r})$ | $k^2(k^2r^2 - 14)(2k^2x^2 - 1)(4k^4y^4 - 12k^2y^2 + 3)$ |

Table D.25: Orbital expressions HOOrbitals : 2, 4. Factor $e^{-\frac{1}{2}k^2r^2}$ is omitted.

| $\phi_{24} \rightarrow \phi_{3,3}$ | |
|--------------------------------------|--|
| $\phi(\vec{r})$ | $xy(2k^2x^2 - 3)(2k^2y^2 - 3)$ |
| $\vec{i} \cdot \nabla \phi(\vec{r})$ | $-y(2k^2y^2 - 3)(2k^4x^4 - 9k^2x^2 + 3)$ |
| $\vec{j} \cdot \nabla \phi(\vec{r})$ | $-x(2k^2x^2 - 3)(2k^4y^4 - 9k^2y^2 + 3)$ |
| $\nabla^2 \phi(\vec{r})$ | $k^2xy(k^2r^2 - 14)(2k^2x^2 - 3)(2k^2y^2 - 3)$ |

Table D.26: Orbital expressions HOOrbitals : 3, 3. Factor $e^{-\frac{1}{2}k^2r^2}$ is omitted.

| $\phi_{25} \rightarrow \phi_{4,2}$ | |
|--------------------------------------|---|
| $\phi(\vec{r})$ | $(2k^2y^2 - 1)(4k^4x^4 - 12k^2x^2 + 3)$ |
| $\vec{i} \cdot \nabla \phi(\vec{r})$ | $-k^2x(2k^2y^2 - 1)(4k^4x^4 - 28k^2x^2 + 27)$ |
| $\vec{j} \cdot \nabla \phi(\vec{r})$ | $-k^2y(2k^2y^2 - 5)(4k^4x^4 - 12k^2x^2 + 3)$ |
| $\nabla^2 \phi(\vec{r})$ | $k^2(k^2r^2 - 14)(2k^2y^2 - 1)(4k^4x^4 - 12k^2x^2 + 3)$ |

Table D.27: Orbital expressions HOOrbitals : 4, 2. Factor $e^{-\frac{1}{2}k^2r^2}$ is omitted.

| $\phi_{26} \rightarrow \phi_{5,1}$ | |
|--------------------------------------|---|
| $\phi(\vec{r})$ | $xy(4k^4x^4 - 20k^2x^2 + 15)$ |
| $\vec{i} \cdot \nabla \phi(\vec{r})$ | $-y(4k^6x^6 - 40k^4x^4 + 75k^2x^2 - 15)$ |
| $\vec{j} \cdot \nabla \phi(\vec{r})$ | $-x(ky - 1)(ky + 1)(4k^4x^4 - 20k^2x^2 + 15)$ |
| $\nabla^2 \phi(\vec{r})$ | $k^2xy(k^2r^2 - 14)(4k^4x^4 - 20k^2x^2 + 15)$ |

Table D.28: Orbital expressions HOOrbitals : 5, 1. Factor $e^{-\frac{1}{2}k^2r^2}$ is omitted.

| $\phi_{27} \rightarrow \phi_{6,0}$ | |
|--------------------------------------|--|
| $\phi(\vec{r})$ | $8k^6x^6 - 60k^4x^4 + 90k^2x^2 - 15$ |
| $\vec{i} \cdot \nabla \phi(\vec{r})$ | $-k^2x(8k^6x^6 - 108k^4x^4 + 330k^2x^2 - 195)$ |
| $\vec{j} \cdot \nabla \phi(\vec{r})$ | $-k^2y(8k^6x^6 - 60k^4x^4 + 90k^2x^2 - 15)$ |
| $\nabla^2 \phi(\vec{r})$ | $k^2(k^2r^2 - 14)(8k^6x^6 - 60k^4x^4 + 90k^2x^2 - 15)$ |

Table D.29: Orbital expressions HOOrbitals : 6, 0. Factor $e^{-\frac{1}{2}k^2r^2}$ is omitted.

E

Hydrogen Orbitals

Orbitals are constructed in the following fashion:

$$\phi(\vec{r})_{n,l,m} = L_{n-l-1}^{2l+1}\left(\frac{2r}{n}k\right)S_l^m(\vec{r})e^{-\frac{r}{n}k}$$

where n is the principal quantum number, $k = \alpha Z$ with Z being the nucleus charge and α being the variational parameter.

$$l = 0, 1, \dots, (n - 1)$$

$$m = -l, (-l + 1), \dots, (l - 1), l$$

| $\phi_0 \rightarrow \phi_{1,0,0}$ | |
|--------------------------------------|---------------------|
| $\phi(\vec{r})$ | 1 |
| $\vec{i} \cdot \nabla \phi(\vec{r})$ | $-\frac{kx}{r}$ |
| $\vec{j} \cdot \nabla \phi(\vec{r})$ | $-\frac{ky}{r}$ |
| $\vec{k} \cdot \nabla \phi(\vec{r})$ | $-\frac{kz}{r}$ |
| $\nabla^2 \phi(\vec{r})$ | $\frac{k(kr-2)}{r}$ |

Table E.1: Orbital expressions hydrogenicOrbitals : 1, 0, 0. Factor e^{-kr} is omitted.

| $\phi_1 \rightarrow \phi_{2,0,0}$ | |
|--------------------------------------|----------------------------|
| $\phi(\vec{r})$ | $kr - 2$ |
| $\vec{i} \cdot \nabla \phi(\vec{r})$ | $-\frac{kx(kr-4)}{2r}$ |
| $\vec{j} \cdot \nabla \phi(\vec{r})$ | $-\frac{ky(kr-4)}{2r}$ |
| $\vec{k} \cdot \nabla \phi(\vec{r})$ | $-\frac{kz(kr-4)}{2r}$ |
| $\nabla^2 \phi(\vec{r})$ | $\frac{k(kr-8)(kr-2)}{4r}$ |

Table E.2: Orbital expressions hydrogenicOrbitals : 2, 0, 0. Factor $e^{-\frac{1}{2}kr}$ is omitted.

| $\phi_2 \rightarrow \phi_{2,1,0}$ | |
|--------------------------------------|-----------------------|
| $\phi(\vec{r})$ | z |
| $\vec{i} \cdot \nabla \phi(\vec{r})$ | $-\frac{kxz}{2r}$ |
| $\vec{j} \cdot \nabla \phi(\vec{r})$ | $-\frac{kyz}{2r}$ |
| $\vec{k} \cdot \nabla \phi(\vec{r})$ | $\frac{-kz^2+2r}{2r}$ |
| $\nabla^2 \phi(\vec{r})$ | $\frac{kz(kr-8)}{4r}$ |

Table E.3: Orbital expressions hydrogenicOrbitals : 2, 1, 0. Factor $e^{-\frac{1}{2}kr}$ is omitted.

| $\phi_3 \rightarrow \phi_{2,1,1}$ | |
|--------------------------------------|-----------------------|
| $\phi(\vec{r})$ | x |
| $\vec{i} \cdot \nabla \phi(\vec{r})$ | $-\frac{kx^2+2r}{2r}$ |
| $\vec{j} \cdot \nabla \phi(\vec{r})$ | $-\frac{kxy}{2r}$ |
| $\vec{k} \cdot \nabla \phi(\vec{r})$ | $-\frac{kxz}{2r}$ |
| $\nabla^2 \phi(\vec{r})$ | $\frac{kx(kr-8)}{4r}$ |

Table E.4: Orbital expressions hydrogenicOrbitals : 2, 1, 1. Factor $e^{-\frac{1}{2}kr}$ is omitted.

| $\phi_4 \rightarrow \phi_{2,1,-1}$ | |
|--------------------------------------|-----------------------|
| $\phi(\vec{r})$ | y |
| $\vec{i} \cdot \nabla \phi(\vec{r})$ | $-\frac{kxy}{2r}$ |
| $\vec{j} \cdot \nabla \phi(\vec{r})$ | $-\frac{ky^2+2r}{2r}$ |
| $\vec{k} \cdot \nabla \phi(\vec{r})$ | $-\frac{kyz}{2r}$ |
| $\nabla^2 \phi(\vec{r})$ | $\frac{ky(kr-8)}{4r}$ |

Table E.5: Orbital expressions hydrogenicOrbitals : 2, 1, -1. Factor $e^{-\frac{1}{2}kr}$ is omitted.

| $\phi_5 \rightarrow \phi_{3,0,0}$ | |
|--------------------------------------|--|
| $\phi(\vec{r})$ | $2k^2r^2 - 18kr + 27$ |
| $\vec{i} \cdot \nabla \phi(\vec{r})$ | $-\frac{kx(2k^2r^2-30kr+81)}{3r}$ |
| $\vec{j} \cdot \nabla \phi(\vec{r})$ | $-\frac{ky(2k^2r^2-30kr+81)}{3r}$ |
| $\vec{k} \cdot \nabla \phi(\vec{r})$ | $-\frac{kz(2k^2r^2-30kr+81)}{3r}$ |
| $\nabla^2 \phi(\vec{r})$ | $\frac{k(kr-18)(2k^2r^2-18kr+27)}{9r}$ |

Table E.6: Orbital expressions hydrogenicOrbitals : 3, 0, 0. Factor $e^{-\frac{1}{3}kr}$ is omitted.

| $\phi_6 \rightarrow \phi_{3,1,0}$ | |
|--------------------------------------|-----------------------------------|
| $\phi(\vec{r})$ | $z(kr-6)$ |
| $\vec{i} \cdot \nabla \phi(\vec{r})$ | $-\frac{kxz(kr-9)}{3r}$ |
| $\vec{j} \cdot \nabla \phi(\vec{r})$ | $-\frac{kyz(kr-9)}{3r}$ |
| $\vec{k} \cdot \nabla \phi(\vec{r})$ | $\frac{3kr^2-kz^2(kr-9)-18r}{3r}$ |
| $\nabla^2 \phi(\vec{r})$ | $\frac{kz(kr-18)(kr-6)}{9r}$ |

Table E.7: Orbital expressions hydrogenicOrbitals : 3, 1, 0. Factor $e^{-\frac{1}{3}kr}$ is omitted.

| $\phi_7 \rightarrow \phi_{3,1,1}$ | |
|--------------------------------------|-----------------------------------|
| $\phi(\vec{r})$ | $x(kr-6)$ |
| $\vec{i} \cdot \nabla \phi(\vec{r})$ | $\frac{3kr^2-kx^2(kr-9)-18r}{3r}$ |
| $\vec{j} \cdot \nabla \phi(\vec{r})$ | $-\frac{kxy(kr-9)}{3r}$ |
| $\vec{k} \cdot \nabla \phi(\vec{r})$ | $-\frac{kxz(kr-9)}{3r}$ |
| $\nabla^2 \phi(\vec{r})$ | $\frac{kx(kr-18)(kr-6)}{9r}$ |

Table E.8: Orbital expressions hydrogenicOrbitals : 3, 1, 1. Factor $e^{-\frac{1}{3}kr}$ is omitted.

| $\phi_8 \rightarrow \phi_{3,1,-1}$ | |
|--------------------------------------|---------------------------------------|
| $\phi(\vec{r})$ | $y(kr - 6)$ |
| $\vec{i} \cdot \nabla \phi(\vec{r})$ | $-\frac{kxy(kr-9)}{3r}$ |
| $\vec{j} \cdot \nabla \phi(\vec{r})$ | $\frac{3kr^2 - ky^2(kr-9) - 18r}{3r}$ |
| $\vec{k} \cdot \nabla \phi(\vec{r})$ | $-\frac{kyz(kr-9)}{3r}$ |
| $\nabla^2 \phi(\vec{r})$ | $\frac{ky(kr-18)(kr-6)}{9r}$ |

Table E.9: Orbital expressions hydrogenOrbitals : 3, 1, -1. Factor $e^{-\frac{1}{3}kr}$ is omitted.

| $\phi_9 \rightarrow \phi_{3,2,0}$ | |
|--------------------------------------|-----------------------------------|
| $\phi(\vec{r})$ | $-r^2 + 3z^2$ |
| $\vec{i} \cdot \nabla \phi(\vec{r})$ | $-\frac{x(k(-r^2+3z^2)+6r)}{3r}$ |
| $\vec{j} \cdot \nabla \phi(\vec{r})$ | $-\frac{y(k(-r^2+3z^2)+6r)}{3r}$ |
| $\vec{k} \cdot \nabla \phi(\vec{r})$ | $-\frac{z(k(-r^2+3z^2)-12r)}{3r}$ |
| $\nabla^2 \phi(\vec{r})$ | $\frac{k(-r^2+3z^2)(kr-18)}{9r}$ |

Table E.10: Orbital expressions hydrogenOrbitals : 3, 2, 0. Factor $e^{-\frac{1}{3}kr}$ is omitted.

| $\phi_{10} \rightarrow \phi_{3,2,1}$ | |
|--------------------------------------|--------------------------|
| $\phi(\vec{r})$ | xz |
| $\vec{i} \cdot \nabla \phi(\vec{r})$ | $-\frac{z(kx^2-3r)}{3r}$ |
| $\vec{j} \cdot \nabla \phi(\vec{r})$ | $-\frac{kxyz}{3r}$ |
| $\vec{k} \cdot \nabla \phi(\vec{r})$ | $-\frac{x(kz^2-3r)}{3r}$ |
| $\nabla^2 \phi(\vec{r})$ | $\frac{kxz(kr-18)}{9r}$ |

Table E.11: Orbital expressions hydrogenOrbitals : 3, 2, 1. Factor $e^{-\frac{1}{3}kr}$ is omitted.

| $\phi_{11} \rightarrow \phi_{3,2,-1}$ | |
|---------------------------------------|--------------------------|
| $\phi(\vec{r})$ | yz |
| $\vec{i} \cdot \nabla \phi(\vec{r})$ | $-\frac{kxyz}{3r}$ |
| $\vec{j} \cdot \nabla \phi(\vec{r})$ | $-\frac{z(ky^2-3r)}{3r}$ |
| $\vec{k} \cdot \nabla \phi(\vec{r})$ | $-\frac{y(kz^2-3r)}{3r}$ |
| $\nabla^2 \phi(\vec{r})$ | $\frac{kyz(kr-18)}{9r}$ |

Table E.12: Orbital expressions hydrogenOrbitals : 3, 2, -1. Factor $e^{-\frac{1}{3}kr}$ is omitted.

| $\phi_{12} \rightarrow \phi_{3,2,2}$ | |
|--------------------------------------|--------------------------------|
| $\phi(\vec{r})$ | $x^2 - y^2$ |
| $\vec{i} \cdot \nabla \phi(\vec{r})$ | $-\frac{x(k(x^2-y^2)-6r)}{3r}$ |
| $\vec{j} \cdot \nabla \phi(\vec{r})$ | $-\frac{y(k(x^2-y^2)+6r)}{3r}$ |
| $\vec{k} \cdot \nabla \phi(\vec{r})$ | $-\frac{kz(x^2-y^2)}{3r}$ |
| $\nabla^2 \phi(\vec{r})$ | $\frac{k(x^2-y^2)(kr-18)}{9r}$ |

Table E.13: Orbital expressions hydrogenicOrbitals : 3, 2, 2. Factor $e^{-\frac{1}{3}kr}$ is omitted.

| $\phi_{13} \rightarrow \phi_{3,2,-2}$ | |
|---------------------------------------|--------------------------|
| $\phi(\vec{r})$ | xy |
| $\vec{i} \cdot \nabla \phi(\vec{r})$ | $-\frac{y(kx^2-3r)}{3r}$ |
| $\vec{j} \cdot \nabla \phi(\vec{r})$ | $-\frac{x(ky^2-3r)}{3r}$ |
| $\vec{k} \cdot \nabla \phi(\vec{r})$ | $-\frac{kxyz}{3r}$ |
| $\nabla^2 \phi(\vec{r})$ | $\frac{kxy(kr-18)}{9r}$ |

Table E.14: Orbital expressions hydrogenicOrbitals : 3, 2, -2. Factor $e^{-\frac{1}{3}kr}$ is omitted.

| $\phi_{14} \rightarrow \phi_{4,0,0}$ | |
|--------------------------------------|---|
| $\phi(\vec{r})$ | $k^3 r^3 - 24k^2 r^2 + 144kr - 192$ |
| $\vec{i} \cdot \nabla \phi(\vec{r})$ | $-\frac{kx(k^3 r^3 - 36k^2 r^2 + 336kr - 768)}{4r}$ |
| $\vec{j} \cdot \nabla \phi(\vec{r})$ | $-\frac{ky(k^3 r^3 - 36k^2 r^2 + 336kr - 768)}{4r}$ |
| $\vec{k} \cdot \nabla \phi(\vec{r})$ | $-\frac{kz(k^3 r^3 - 36k^2 r^2 + 336kr - 768)}{4r}$ |
| $\nabla^2 \phi(\vec{r})$ | $\frac{k(kr-32)(k^3 r^3 - 24k^2 r^2 + 144kr - 192)}{16r}$ |

Table E.15: Orbital expressions hydrogenicOrbitals : 4, 0, 0. Factor $e^{-\frac{1}{4}kr}$ is omitted.

| $\phi_{15} \rightarrow \phi_{4,1,0}$ | |
|--------------------------------------|---|
| $\phi(\vec{r})$ | $z(k^2 r^2 - 20kr + 80)$ |
| $\vec{i} \cdot \nabla \phi(\vec{r})$ | $-\frac{kxz(kr-20)(kr-8)}{4r}$ |
| $\vec{j} \cdot \nabla \phi(\vec{r})$ | $-\frac{kyz(kr-20)(kr-8)}{4r}$ |
| $\vec{k} \cdot \nabla \phi(\vec{r})$ | $\frac{4k^2 r^3 - 80kr^2 - kz^2(kr-20)(kr-8) + 320r}{4r}$ |
| $\nabla^2 \phi(\vec{r})$ | $\frac{kz(kr-32)(k^2 r^2 - 20kr + 80)}{16r}$ |

Table E.16: Orbital expressions hydrogenicOrbitals : 4, 1, 0. Factor $e^{-\frac{1}{4}kr}$ is omitted.

| $\phi_{16} \rightarrow \phi_{4,1,1}$ | |
|--------------------------------------|--|
| $\phi(\vec{r})$ | $x(k^2r^2 - 20kr + 80)$ |
| $\vec{i} \cdot \nabla \phi(\vec{r})$ | $\frac{4k^2r^3 - 80kr^2 - kx^2(kr-20)(kr-8) + 320r}{4r}$ |
| $\vec{j} \cdot \nabla \phi(\vec{r})$ | $-\frac{kxy(kr-20)(kr-8)}{4r}$ |
| $\vec{k} \cdot \nabla \phi(\vec{r})$ | $-\frac{kxz(kr-20)(kr-8)}{4r}$ |
| $\nabla^2 \phi(\vec{r})$ | $\frac{kx(kr-32)(k^2r^2 - 20kr + 80)}{16r}$ |

Table E.17: Orbital expressions hydrogenOrbitals : 4, 1, 1. Factor $e^{-\frac{1}{4}kr}$ is omitted.

| $\phi_{17} \rightarrow \phi_{4,1,-1}$ | |
|---------------------------------------|--|
| $\phi(\vec{r})$ | $y(k^2r^2 - 20kr + 80)$ |
| $\vec{i} \cdot \nabla \phi(\vec{r})$ | $-\frac{kxy(kr-20)(kr-8)}{4r}$ |
| $\vec{j} \cdot \nabla \phi(\vec{r})$ | $\frac{4k^2r^3 - 80kr^2 - ky^2(kr-20)(kr-8) + 320r}{4r}$ |
| $\vec{k} \cdot \nabla \phi(\vec{r})$ | $-\frac{kyz(kr-20)(kr-8)}{4r}$ |
| $\nabla^2 \phi(\vec{r})$ | $\frac{ky(kr-32)(k^2r^2 - 20kr + 80)}{16r}$ |

Table E.18: Orbital expressions hydrogenOrbitals : 4, 1, -1. Factor $e^{-\frac{1}{4}kr}$ is omitted.

Bibliography

- [1] C. J. Murray, *The SUPERMEN*. New York: Wiley, 1997.
- [2] H. P. Langtangen, *Python Scripting for Computational Science*, 3rd ed. Springer, 2008. [Online]. Available: <http://www.bibsonomy.org/bibtex/240eb1bb4f4f80d745c3df06a8e882392/hake>
- [3] M. Lutz, *Programming Python - powerful object-oriented programming* (3. ed.). O'Reilly, 2006. [Online]. Available: <http://www.oreilly.de/catalog/python3/index.html;http://www.bibsonomy.org/bibtex/2b34de9c149a4962403c89fe6360cd3b7/dblp>
- [4] H. P. Langtangen, *A primer on scientific programming with Python*. Berlin; Heidelberg; New York: Springer, 2011. [Online]. Available: <http://www.worldcat.org/search?qt=worldcat.org.all&q=9783642183652>
- [5] G. O'Regan, *A Brief History of Computing, Second Edition*. Springer, 2012. [Online]. Available: <http://dx.doi.org/10.1007/978-1-4471-2359-0>
- [6] J. Høgberget, *Git Repository: LibBorealis*, 2013. [Online]. Available: <http://www.github.com/jorgehog/QMC2>
- [7] D. Griffiths, *Introduction to Quantum Mechanics*, 2nd ed. Pearson, 2005.
- [8] J. M. Leinaas, "Non-Relativistic Quantum Mechanics," lecture notes FYS4110.
- [9] B. Hammond, J. W. A. Lester, and P. J. Reynolds, *Monte Carlo Methods in Ab Initio Quantum Chemistry*, S. Lin, Ed. World Scientific Publishing Co., 1994.
- [10] C. W. Gardiner, *Handbook of stochastic methods for physics, chemistry, and the natural sciences*, 3rd ed. Berlin: Springer-Verlag, 2004. [Online]. Available: <http://www.loc.gov/catdir/enhancements/fy0818/2004043676-d.html>
- [11] H. Risken and H. Haken, *The Fokker-Planck Equation: Methods of Solution and Applications Second Edition*. Springer, 1989.

- [12] W. T. Coffey, Y. P. Kalmykov, and J. T. Waldron, *The Langevin Equation: With Applications to Stochastic Problems in Physics, Chemistry, and Electrical Engineering.* . World Scientific, Singapore, 2004.
- [13] M. Hjorth-Jensen, “Computational Physics,” 2010.
- [14] J. J. Sakurai, *Modern Quantum Mechanics*, Revised ed ed. New York: Addison-Wesley, 1994.
- [15] I. Shavitt and R. J. Bartlett, *Many-Body Methods in Chemistry and Physics*. Cambridge: Cambridge University Press, 2009.
- [16] D. A. Nissenbaum, “The stochastic gradient approximation: an application to li nanoclusters,” Ph.D. dissertation, Northeastern University, 2008. [Online]. Available: <http://hdl.handle.net/2047/d10016466>
- [17] G. Golub and C. Van Loan, *Matrix computations*. Johns Hopkins Univ Press, 1996, vol. 3.
- [18] A. Harju, B. Barbiellini, S. Siljamäki, R. M. Nieminen, and G. Ortiz, “Stochastic Gradient Approximation: An Efficient Method to Optimize Many-Body Wave Functions,” *Physical Review Letters*, vol. 79, pp. 1173–1177, Aug. 1997.
- [19] S. Klein, J. P. W. Pluim, M. Staring, and M. A. Viergever, “Adaptive Stochastic Gradient Descent Optimisation for Image Registration.” *International Journal of Computer Vision*, vol. 81, no. 3, pp. 227–239, 2009. [Online]. Available: <http://dx.doi.org/10.1007/s11263-008-0168-y>
- [20] H. Flyvbjerg and H. G. Petersen, “Error estimates on averages of correlated data,” *The Journal of Chemical Physics*, vol. 91, no. 1, pp. 461–466, 1989. [Online]. Available: <http://link.aip.org/link/?JCP/91/461/1>
- [21] D. C. Lay, *Linear Algebra and its Applications*, 4th ed. Pearson, 2012.
- [22] M. Pedersen Lohne, G. Hagen, M. Hjorth-Jensen, S. Kvaal, and F. Pederiva, “*Ab initio* computation of the energies of circular quantum dots,” *Phys. Rev. B*, vol. 84, p. 115302, Sep 2011. [Online]. Available: <http://link.aps.org/doi/10.1103/PhysRevB.84.115302>
- [23] S. Reimann, “SRG Title,” Master’s thesis, University of Oslo, 2013.
- [24] C. Hirth, “Studies of quantum dots: Ab initio coupled-cluster analysis using OpenCL and GPU programming,” Master’s thesis, University of Oslo, 2012.
- [25] V. K. B. Olsen, “Full Configuration Interaction Simulation of Quantum Dots,” Master’s thesis, University of Oslo, 2012.